# Power System Harmonics Analysis of High Power Variable Speed Drives

Michael Scheidiger


KTH Electrical Engineering

Degree project in
Power Electronics

Stockholm, Sweden 2013

XR-EE-E2C 2013:009


ROYAL INSTITUTE
OF TECHNOLOGY

# Power System Harmonics Analysis of High Power Variable Speed Drives

Harmonic Distortion Fundamentals, Analysis and Mitigation Techniques applied to High Power Passive Front-End Variable Speed Drives

MICHAEL SCHEIDIGER

Master's Thesis at Electric Energy Conversion Department
Supervisor: Dipl. Ing. Alexander Oswald (ILF Consulting Engineers )
Examiner: Dr. Prof. Hans-Peter Nee (KTH Royal Institute of Technology)

TRITA XR-EE-E2C 2013:009

**Abstract**

Power system harmonics are a topic of significant concern when considering power quality issues in systems containing Variable Speed Drives. The extent to which grid-connected power electronics based motor drives affect power quality is tightly enforced through standards, and must be adhered to. To ensure compliance, harmonic models of Variable Speed Drives and relevant components of the connected power system are evaluated. When necessary, analysis results can be used to aid the design of additional harmonic mitigation measures. Harmonic assessments are most commonly carried out using time-domain models.

This thesis details the fundamentals of harmonic assessment and mitigation measure design. Matlab implementations of those fundamentals are discussed, with comments regarding the accuracy and limitations of each. State of the art analytical harmonic models for Voltage Source Variable Speed Drives are analyzed and compared, from which a new model for 3-level inverter Variable Speed Drives is proposed. The new model can be implemented in any numerical computing environment and is thought to generate a harmonic current spectrum for an approximate judgement of harmonic compliance based on the current injection method.

**Sammanfattning**

Övertoner i kraftsystem innehållande frekvensomriktare är ett viktigt ämne när el-kvalité behandlas. Den grad nätanslutna elektroniska motorsystem påverkar el-kvalitén är noggrant upprätthållen av standarder och måste följas därefter. För att säkerställa att standarder upprätthålls utvärderas modeller för frekvensomriktare och relevanta komponenter. När det anses nödvändigt kan resultaten vara vägledande för design av ytterligare övertonsminskande åtgärder. Utvärdering av övertoner görs i allmänhet med hjälp av modeller i tidsdomän.

Denna uppsats går igenom grunderna för bedömning av övertoner och design av övertonsminskande åtgärder. Matlab-modeller av dessa diskuteras i termer av precision och begränsningar. De främsta analytiska modeller for frekvensomriktare undersöks och jämförs, varefter en ny modell av en växelriktare med 3 nivåer föreslås. Denna modell kan med enkelhet implementeras i numeriska datormiljöer och framställer ett frekvensspektrum av strömmen för en approximativ bedömning av el-kvalité baserad på ströminmatningsmetoden.

# Acknowledgment

First of all, I would like to thank Prof.Dr.Hans-Peter Nee, head of the Electric Conversion Department (E2C) at the Royal Institute of Technology for enabling me to write my thesis in industry. In spite of all his other tasks, I could rely on his support and established knowledge.

Moreover, many thanks go to my supervisor, Alexander Oswald, who supported me as much as his busy schedule allowed and who inspired me to set myself high goals.

Furthermore, I would like to thank Daniel Hubbauer, head of the Electric Power Engineering Department at ILF Consulting Engineers for providing me with the opportunity to write my thesis at ILF Consulting Engineers and for his generous support in problems of all kind.

Many thanks to Dr.Bernd Walther from Maschinenfabrik Reinhausen and André Wegener from GE Energy Management for their technical consultancy.

Finally, I am very grateful to my family for enabling my education and for their kind support all along my studies. I am especially thankful to my twin brother, Christoph Scheidiger, who supported me technically during this work and was - as many times before - a great help in overcoming obstacles.

Michael Scheidiger

Munich and Stockholm, November 2013

# Contents

# List of Figures

# List of Tables

# List of Abbreviations

**VSD** Variable Speed Drive

**HVDC** High Voltage Direct Current

**DC** Direct Current

**VSC** Voltage Source Converter

**RMS** Root Mean Square

**THD** Total Harmonic Distortion

**TIHD** Total Interharmonic Distortion

**PF** Power Factor

**DPF** Displacement Power Factor

**PCC** Point of Common Coupling

**STF** Single-Tuned Filter

**HPF2nd** 2nd order High-Pass Filter

**MV** Medium Voltage

**LV** Low Voltage

**HV** High Voltage

**SCC** Short Circuit Capacity

**LCI** Line Commutated Inverter

**NPC** Neutral-Point-Clamped

**PWM** Pulse-Width-Modulated

**PD** Phase Disposition

**FFT** Fast Fourier Transform

# Chapter 1

# Introduction

Non-linear system elements are sources of distorted waveforms in power system applications. Common examples include Variable Speed Drives (VSD), frequency converters in wind and solar plants, High Voltage Direct Current (HVDC). The resulting non-sinusoidal periodical waveform consists of a fundamental component and unwanted harmonic components which can disturb the power system severely. Due to the great increase in power electronics application, harmonics and their limitation have been a major concern and topic of research during the last decades.

This thesis focuses on the analysis of power system harmonics introduced by high power VSDs. While harmonics are present on both line- and load-side of any VSD, the interest of this work lies on harmonics at the line-side terminal. It is from here that harmonics penetrate the power system, and may introduce undesirable performance. In the case of power systems harmonics, standards are used to place limitations on harmonic content . A grid-connected VSD - regardless of application - must comply with all applicable standards to be approved for operations. Machine, or load-side, harmonics, on the other hand, are determined and limited through a loss/cost optimization between converter and machine–not by standards. Although this work focuses primarily on the analysis of line-side harmonics, due to the harmonic coupling across a shared DC link, analysis of line- and load-side harmonics can not be treated independently.

Power system harmonic analysis is an extensive task , and involves the modeling of harmonic sources (VSDs in this work) and the nearby power system. Past work on power system harmonics has resulted in the development of numerous analysis techniques, most of which differ greatly in complexity and accuracy. The analysis methods span from simple spreadsheet calculations to those that require sophisticated computational software. The models of harmonic sources differ extensively too. Some models, very often frequency-domain models, are based on assumptions that greatly simplify the situation. On the other end of the complexity spectrum, there are sophisticated models in the time-domain that require many details of converter design parameters as input data.

In general, this thesis aims to investigate the means needed to perform a harmonic study in an arbitrary numerical computation environment, based on the desire of ILF Consulting Engineers [1] to quantitatively cross-check the detailed power system harmonic analysis and filter design proposals provided by third parties. This implies the need to find appropriate analysis techniques and models. An extensive part of this thesis is thus literature research and presentation. The report should further serve as introduction and reference for engineers at ILF when confronted with harmonic analysis and filter design.

In order to achieve the above mentioned goals, the thesis in hand is structured in three parts:

*I*) **Power System Harmonic Fundamentals**

In this part, all relevant basics, including harmonic representation, classifica-

[1] ILF Consulting Engineers is a global technical consultancy company founded in 1967. Together with ILF Business Consulting it forms the ILF Group. Currently, ILF Consulting Engineers has 1810 employees covering civil, mechanical and electrical engineering services at various office locations in 30 countries. ILF's four main business areas are Oil & Gas, Energy & Climate Protection, Water & Environment, Transport & Structures. At the company headquarters in Munich - home to the Oil & Gas and Energy & Climate Protection business units - about 800 people are employed.

tion and standards, are discussed.

*II*) **Harmonic Compliance**

This part presents an overview on how harmonic compliance is assessed and achieved by introducing harmonic studies and harmonic mitigation measures.

*III*) **Harmonic Modeling of Variable Speed Drives**

In this part a liturate review of harmonic VSD models is presented based on which a detailed modeling approach for a Voltage Source Converter (VSC) VSD harmonic spectrum is proposed.

# Part I

# Power System Harmonics Fundamentals

# Chapter 2

# Harmonic Fundamentals

In this chapter harmonic voltage and current distortion and problems associated with it are discussed. It first introduces a mathematical representation of harmonics, shows how a phase sequence can be assigned to each harmonic order and how triplen harmonics are canceled in line-to-line voltages of balanced three-phase systems. It also addresses harmonic causes. In the second section, a harmonic classification is proposed. Thirdly, it discuses the power factor index for non-sinusoidal quantities for a six-pulse rectifier, the main building block of the front-end of most high power VSDs.

## 2.1 Harmonic Voltage and Current Distortion

Both current and voltage distortion are commonly encountered in power systems. In most cases, current distortion causes voltage distortion. In case of a strong grid, i.e. low short circuit impedance, current distortion leads to a small voltage distortion and may be neglected. Assuming a strong grid, and thus a pure sinusoidal voltage at the fundamental frequency, the supply voltage can be expressed following the notation of [1] as

$$v_s = \sqrt{2} V_s \sin \omega_1 t. \tag{2.1}$$

A distorted line current, $i_s$, is shown in Figure 2.1 and can be described as

$$i_s = i_{s1} + \sum_{h=2}^{\infty} i_{sh} \quad . \tag{2.2}$$

Here, $i_{s1}$ is the fundamental component while $i_{sh}$ is the sum of all harmonic compo-

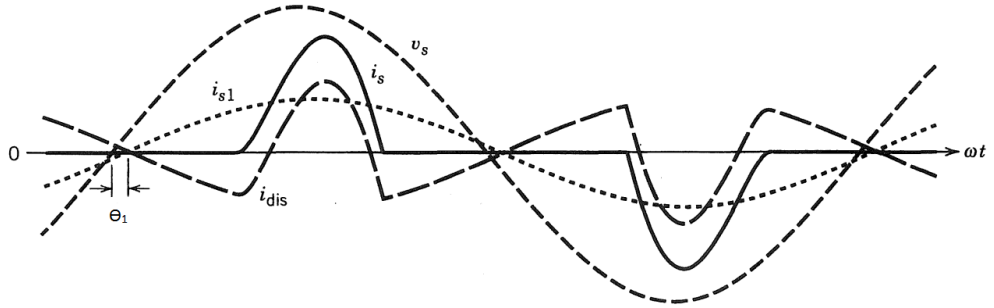


Figure 2.1: Line-current distortion [1].

nents. The subscript $h$ stands for the harmonic order and is defined as $h = 2, ..., \infty$. Equation 2.2 can be expressed as

$$i_s = \sqrt{2} I_{s1} \sin(\omega_1 t + \theta_1) + \sum_{h=2}^{\infty} I_{sh} \sin(\omega_h t + \theta_h) \tag{2.3}$$

where $\theta_1$ is the phase angle of the supply voltage, as depicted in Figure 2.1, and $\theta_h$ is the phase angle of the supply voltage at the frequency $f = h \cdot f_1$.

The RMS value of the current is calculated by

$$I_s = \sqrt{\frac{1}{T_1} \int_0^{T_1} i_s^2(t) dt} \tag{2.4}$$

and can also be expressed in terms of its Fourier components as

$$I_s = \sqrt{I_{s1}^2 + \sum_{h=2}^{\infty} I_{sh}^2} \quad . \tag{2.5}$$

The distortion component of the current is the sum of its harmonics and can be written as

$$i_{dis} = i_s - i_{s1} = \sum_{h \neq 1} i_{sh} \tag{2.6}$$

or in terms of RMS values as

$$I_{dis} = \sqrt{I_s^2 - I_{s1}^2} = \sqrt{\sum_{h\neq 1} I_{sh}^2} \quad . \tag{2.7}$$

This leads to the commonly used distortion index called total harmonic distortion (THD) which is defined as

$$\begin{aligned} THD\% &= 100 \times \frac{I_{dis}}{I_{s1}} \\ &= 100 \times \frac{\sqrt{I_s^2 - I_{s1}^2}}{I_{s1}} \\ &= 100 \times \sqrt{\sum_{h\neq 1} \left(\frac{I_{sh}}{I_{s1}}\right)^2} \quad . \end{aligned} \tag{2.8}$$

The phase currents ($i_a$, $i_b$, $i_c$) in a balance three-phase system may be expressed as:

$$\begin{aligned} i_a &= \sum_{h=1} I_h \sin(h\omega_1 t + \theta_h) \\ i_b &= \sum_{h=1} I_h \sin(h\omega_1 t + \theta_h - h\frac{2\pi}{3}) \\ i_c &= \sum_{h=1} I_h \sin(h\omega_1 t + \theta_h + h\frac{2\pi}{3}) \quad . \end{aligned} \tag{2.9}$$

Limited to the fundamental and first two harmonics (h=1,2,3) Equation 2.9 can be expanded to

$$\begin{aligned} i_a &= I_1 \sin(\omega_1 t + \theta_1) + I_2 \sin(2\omega_1 t + \theta_2) + I_3 \sin(3\omega_1 t + \theta_3) \\ i_b &= I_1 \sin(\omega_1 t + \theta_1 - \frac{2\pi}{3}) + I_2 \sin(2\omega_1 t + \theta_2 - \frac{4\pi}{3}) + I_3 \sin(3\omega_1 t + \theta_3 - \frac{6\pi}{3}) \\ &= I_1 \sin(\omega_1 t + \theta_1 - \frac{2\pi}{3}) + I_2 \sin(2\omega_1 t + \theta_2 + \frac{2\pi}{3}) + I_3 \sin(3\omega_1 + \theta_3 - 0) \\ i_c &= I_1 \sin(\omega_1 t + \theta_1 + \frac{2\pi}{3}) + I_2 \sin(2\omega_1 t + \theta_2 + \frac{4\pi}{3}) + I_3 \sin(3\omega_1 t + \theta_3 + \frac{6\pi}{3}) \\ &= I_1 \sin(\omega_1 t + \theta_1 + \frac{2\pi}{3}) + I_2 \sin(2\omega_1 t + \theta_2 - \frac{2\pi}{3}) + I_3 \sin(3\omega_1 + \theta_3 + 0) \quad . \end{aligned} \tag{2.10}$$

From Equation 2.10 it can be concluded that the fundamental component has positive (a-b-c), the $1^{st}$ harmonic, negative (a-c-b) and the $2^{nd}$ harmonic, zero sequence character. The $3^{rd}$, $4^{th}$ and $5^{th}$ harmonics are positive, negative and zero-sequences

again, respectively. This pattern repeats as the order increases.

In the next step, the assumption of an infinitely strong grid is relaxed, which consequently results in a distorted voltage across the finite system impedance, caused by the harmonic current described in Equation 2.10. If one assumes balanced conditions, this harmonic voltage distortion, at any point upwards the power system, can be described as

$$\begin{aligned} v_a(t) = {} & V_1 \cos(\omega_1 t) + V_2 \cos(2\omega_1 t) \\ & + V_3 \cos(3\omega_1 t) + V_4 \cos(4\omega_1 t) \\ & + V_5 \cos(5\omega_1 t) + V_6 \cos(6\omega_1 t) + V_7 \cos(7\omega_1 t) + ... \end{aligned} \tag{2.11a}$$

$$\begin{aligned} v_b(t) = {} & V_1 \cos(\omega_1 t - \frac{2\pi}{3})) + V_2 \cos(2\omega_1 t - \frac{4\pi}{3})) \\ & + V_3 \cos(3\omega_1 t - 2\pi) + V_4 \cos(4\omega_1 t - \frac{8\pi}{3})) \\ & + V_5 \cos(5\omega_1 t - \frac{10\pi}{3})) + V_6 \cos(6\omega_1 t - 4\pi) \\ & + V_7 \cos(7\omega_1 t - \frac{14\pi}{3})) + ... \\ = {} & V_1 \cos(\omega_1 t - \frac{2\pi}{3})) + V_2 \cos(2\omega_1 t + \frac{2\pi}{3})) \\ & + V_3 \cos(3\omega_1 t) + V_4 \cos(4\omega_1 t - \frac{2\pi}{3})) \\ & + V_5 \cos(5\omega_1 t + \frac{2\pi}{3})) + V_6 \cos(6\omega_1 t) \\ & + V_7 \cos(7\omega_1 t - \frac{2\pi}{3})) + ... \end{aligned} \tag{2.11b}$$

$$
\begin{aligned}
v_c(t) &= V_1\cos(\omega_1 t + \frac{2\pi}{3})) + V_2\cos(2\omega_1 t + \frac{4\pi}{3})) \\
&\quad + V_3\cos(3\omega_1 t + 2\pi) + V_4\cos(4\omega_1 t + \frac{8\pi}{3})) \\
&\quad + V_5\cos(5\omega_1 t + \frac{10\pi}{3})) + V_6\cos(6\omega_1 t + 4\pi) \\
&\quad + V_7\cos(7\omega_1 t + \frac{14\pi}{3})) + ... \\
&= V_1\cos(\omega_1 t + \frac{2\pi}{3})) + V_2\cos(2\omega_1 t - \frac{2\pi}{3})) \\
&\quad + V_3\cos(3\omega_1 t) + V_4\cos(4\omega_1 t + \frac{2\pi}{3})) \\
&\quad + V_5\cos(5\omega_1 t - \frac{2\pi}{3})) + V_6\cos(6\omega_1 t) \\
&\quad + V_7\cos(7\omega_1 t + \frac{2\pi}{3})) + ... \quad . \qquad (2.11c)
\end{aligned}
$$

It becomes evident that the sequence assignments hold true for voltage harmonics in the same manner as for current harmonics. In the case of a Y-connection, the line-to-line voltage can be expressed as

$$
\begin{aligned}
v_{ab}(t) &= v_a(t) - v_b(t) \\
&= \sqrt{3}(V_1\cos(\omega_1 t + \frac{\pi}{6})) + V_2\cos(2\omega_1 t - \frac{\pi}{6})) \\
&\quad + V_4\cos(4\omega_1 t + \frac{\pi}{6})) + V_5\cos(5\omega_1 t - \frac{\pi}{6})) \\
&\quad + V_7\cos(7\omega_1 t + \frac{\pi}{6}))), \qquad (2.12)
\end{aligned}
$$

illustrating that there are no line-line voltage triplen harmonics.

Harmonic distortion leads to several undesired effects. In the case of electromagnetical devices, e.g. electrical machines and transformers, harmonics are the source of additional losses. In electric machines, for example, hysteresis losses are proportional to frequency while eddy current losses follow a quadratic relationship with frequency. Thus in the presence of harmonics, electromagnetical devices have to be overrated to be able to dissipate the additional losses. Additionally, harmonics may also cause shaft vibrations that, which under resonace conditions, can damage the electric machine [16]. Another potential danger of harmonics is the occurrence of

parallel or series impedance resonance in the power system. The resulting current and voltage amplification are a danger for components in the system. Furthermore, at high harmonic content power factor compensation capacitors can be overloaded as their impedance declines inversely proportional to the frequency. The above mentioned causes are only some examples of the many undesired effects of harmonics [17].

## 2.2 Harmonic Classification

Harmonics can be subdivided into characteristic-, non-characteristic-, and interharmonics. Characteristic harmonics are odd, none triple harmonics. For a p-pulse rectifier - discussed in detail in Section 5.1 - for example, the characteristic harmonics are defined as [17]

$$h = np \pm 1 \quad n = 1, 2, 3, .... \tag{2.13}$$

Because of the half-wave symmetry characteristic of most power system components even harmonics rarely occur. Triple harmonics have zero-sequence character and can be neglected when looking at the harmonic spectrum of a VSD with ungrounded wye-wye transformers. Even and triple harmonics are thus referred to as non-characteristic harmonics. Interharmoncis are harmonics at non-integer multiples of the fundamental frequency. Interharmonics also include harmonics with frequencies lower than the fundamental one and are caused by certain power electronics devices, e.g. current source converter driven synchronous machines and fractional-slot concentrated-winding synchronous machines as well as certain loads such as arc furnaces [16].

Although interharmonics are not currently regulated via standards, many publications consider them to be extremely important, especially because of the danger of resonance excitation with filter or power factor compensation capacitors [18–20]. Because of this ambivalence, interharmonics often cause confusion and are thus addressed in the following paragraphs.

Interharmonics can be caused by [16]:

- **Arc-furnaces and other similar arc-based processes in industry**
  The reason for interharmonic generation lies in the physical process of the devices.

- **Power electronic converters with active front-end**
  The modulation of the active front-end can result in currents at any arbitrary frequency.

- **Power electronic converters with a DC link**
  Interharmonics are generated by unintentional coupling of two circuits with different frequencies (front-end and load-end).

Interhamonics cause [16]:

- **Flicker and other peak voltage dependent distortion**
  Caused by superposition of the periodic power system voltage with the non-periodic phenomenon of interharmonics affecting the peak voltage.

- **Failure of ripple control**
  Ripple control works based on modulated pulses in the frequency range of 110 to 2000 Hz. Interharmonics may lay in this range and thus cause noise which can lead to ripple control failure.

- **Resonance**
  In certain applications, e.g. a motor driven by a current source converter, the interharmonic spectrum generated during start-up is almost continuous. This goes along with the danger of resonance excitation.

Interharmonics can be limited by an increased DC link filter or additional front-end filters. Active filter are an attractive solution as they are adaptive, however, they are still expensive and rarely used in high power applications [21].

## 2.3 Power and displacement factor for non-sinusoidal quantities

Power factor (PF) is an important measure in the field of power quality and part of the input data for the harmonic filter design process and thus shortly introduced at this point. The following discussion is based on [1].

Time-averaged electric power may be expressed as:

$$P = \frac{1}{T_1}\int_0^{T_1} p(t)dt = \frac{1}{T_1}\int_0^{T_1} v_s(t)i_s(t)dt \quad . \tag{2.14}$$

As all the integrals of two different frequencies are eaual to zero, it follows

$$P = \frac{1}{T_1}\int_0^{T_1} \sqrt{2}V_s \sin\omega_1 t \cdot \sqrt{2}I_{s1}\sin(\omega t - \theta_1)dt = V_s I_{s1}\cos\theta_1 \quad , \tag{2.15}$$

where only the fundamental component of both voltage and current contribute to the time-averaged real power.

Power factor, PF, is generally defined as

$$PF = \frac{P}{S} \quad , \tag{2.16}$$

where apparent power, $S$, is expressed as:

$$S = V_s I_s \quad . \tag{2.17}$$

Power factor can thus alternatively be formulated as

$$PF = \frac{V_s I_{s1}\cos\theta_1}{V_s I_s} = \frac{I_{s1}}{I_s}\cos\theta_1 \quad . \tag{2.18}$$

In linear circuits with sinusoidal waveforms $\frac{I_{s1}}{I_s} = 1$,

$$PF = \cos\theta_1 = DPF \tag{2.19}$$

where $DPF$ is the displacement power factor. For non-sinusoidal waveforms Equation 2.18 can be rewritten as

$$PF = \frac{I_{s1}}{I_s}DPF \quad . \tag{2.20}$$

Here, an inverse relationship between harmonic distortion and power factor is formed. A large harmonic distortion causes $\frac{I_{s1}}{I_s}$ to decrease, causing the power factor to fall for a given load angle.

PF and DPF of passive six-pulse rectifiers are now investigated. Six pulse rectifiers are the building blocks of p-pulse passive front-ends, which are commonly used in high power VSDs, and thus are of great importance for this thesis. With a constant DC link voltage and neglected commutation (supply inductance $L_s = 0$) $I_s$ and $I_{s1}$ are defined as [1]

$$I_s = \sqrt{\frac{2}{3}} I_d \tag{2.21}$$

$$I_{s1} = \frac{1}{\pi}\sqrt{6} I_d = 0.78 I_d \quad . \tag{2.22}$$

where $I_d$ is the DC bus current. As voltage and the fundamental current are in phase,

$$DPF = 1 \quad . \tag{2.23}$$

The power factor is thus given by

$$PF = \frac{\frac{1}{\pi}\sqrt{6}}{\frac{2}{3}} = 0.9549 \quad . \tag{2.24}$$

Figure 2.2 shows $DPF$,$PF$ and $THD_i$, if commutation is taken into account, but the DC link voltage is still assumed to be constant. The DC link current is normalized by the short circuit current

$$I_{shortcircuit} = \frac{V_s}{\omega_1 L_s} \quad . \tag{2.25}$$

Note that the power factor depends on the rectifier loading. After a certain load, it almost reaches the calculated 0.95.

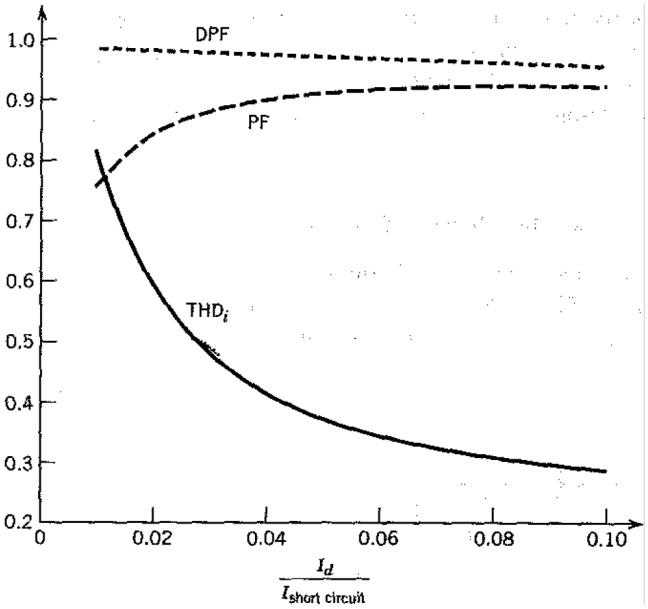


Figure 2.2: $DPF$,$PF$ and $THD_i$ as function of normalized DC current. [1]

# Chapter 3

# Harmonic Standards

Harmonic standards specify the allowed voltage and/or current distortion. IEC's[1] 61000 series on power quality is on of the most utilized harmonic standards. Another widely recognized document is the recommended practice 519 of IEEE[2], which provides guidelines on harmonic control. Additionally, many countries establish their own standards (based primarily on the IEC and IEEE documents) to better suit their nation's power system. The harmonic situation in a system such as in Sweden, where generation and load are geographically spread and interconnected with long transmissions lines, differs from a dense system like the UK, where generation is located close to consumers. Long transmission lines increase the harmonic vulnerability [17]. Harmonic standards are expected to evolve with more experience and improved measurement techniques. Furthermore, IEC is planing to address the issues of interharmonics in future versions of their standard. Currently only guiding values can be found in the appendix of [12].

In this chapter the following standards are briefly discussed:

- IEC 61000-2-4 [12], specifies compliance levels for industrial distribution systems at voltages up to 35 kV and frequencies of 50 Hz or 60 Hz. The voltage limits are summarized in Table 3.1.

[1] International Electrotechnical Commission, `http://www.iec.ch/`

[2] Institute of Electrical and Electronics Engineers, `http://www.ieee.org/`

- IEEE 519 [13], is a recommended practice for harmonic control in electric power system and also specifies compliance levels. The voltage limits are summarized in Table 3.2.
- EN 50160 [14], describes the voltage quality a consumer can expect at the point of coupling. Besides other voltage quality measures, it specifies harmonic levels which, however, should not be seen as strict limits. They are summarized in Table 3.3.

ILF's gas compressor stations, for example, have to fulfill the harmonic levels defined in [12] at the point of connection, also referred to as point of common coupling (PCC). For detailed information on the three standards the reader is referred to the original documents.

Table 3.1: IEC61000-2-4 harmonic voltage distortion limits, pages 16-18 of [12].

| Odd Harmonics | | Even Harmonics | | Triplen Harmonics | | THD [%] |
|---|---|---|---|---|---|---|
| h | $V_h$ | h | $V_h$ | h | $V_h$ | 8 |
| 5 | 6 | 2 | 2 | 3 | 5 | |
| 7 | 5 | 4 | 1 | 9 | 1.5 | |
| 11 | 3.5 | 6 | 0.5 | 15 | 0.4 | |
| 13 | 3 | 8 | 0.5 | 21 | 0.3 | |
| 17 | 2 | 10 | 0.5 | $21 < h \leq 45$ | 0.2 | |
| $17 < h \leq 29$ | x | $10 < h \leq 50$ | x | | | |
| x=2.27·(17/h)-0.27 | | x=0.25·(10/h)+0.25 | | | | |

Table 3.2: IEEE 519-1992 harmonic voltage distortion limits, page 85 of [13]

| Bus voltage | Individual $V_h$ [%] | THD [%] |
|---|---|---|
| $V < 69kV$ | 3 | 5 |
| $69 \leq V < 161kV$ | 1.5 | 2.5 |
| $V \geq 161kV$ | 1 | 1.5 |

Table 3.3: EN 50160 harmonic voltage distortion levels, page 13 of [14]

| Odd Harmonics | | Even Harmonics | | Triplen Harmonics | | THD* [%] |
|---|---|---|---|---|---|---|
| h | $V_h$ | h | $V_h$ | h | $V_h$ | 8 |
| 5 | 6 | 2 | 2 | 3 | 5 | |
| 7 | 5 | 4 | 1 | 9 | 1.5 | |
| 11 | 3.5 | 6 | 0.5 | 15 | 0.5 | |
| 13 | 3 | | | 21 | 0.5 | |
| 17 | 2 | | | | | |
| 19 | 1.5 | | | | | |
| 23 | 1.5 | | | | | |
| 25 | 1.5 | | | | | |

* including all harmonics up to h=40

# Part II

# Harmonic Compliance

# Chapter 4

# Harmonic Studies

Harmonic studies are used to investigate industrial plant's harmonic compliance and to design harmonic mitigation measures if needed. A harmonic study analyzes the penetration of harmonic currents from its source into the power system and determines the resulting harmonic voltage distortion. The present chapter explains these studies. After a general introduction to the topic, an example of a detailed harmonic study is presented. In a third part, an implementation of an impedance scan in Matlab is presented and discussed.

At minimum, a harmonic study consists of the following two analyses:

I **Impedance scan**

Displays the impedance magnitude, as seen from the harmonic source, as a function of frequency. It is represented in an impedance versus frequency plot, or in a frequency response locus, and is used to detect parallel and series resonance. Series resonance is encountered when the system impedance is predominantly resistive and tends towards its minimum (according to resonance in a series L-R-C circuit, where inductive and capacitive impedance compensate). Parallel resonance, on the other hand, results in a maximum impedance, also predominantly resistive (according to resonance in a parallel resonance R-L-C circuit). If a certain harmonic current lays at or close to series resonance, a low voltage distortion results. If, however, a current lays at

parallel resonance, the current causes a high voltage distortion. The frequency scan thus gives important information on where harmonic amplification may result and serves as a important input for harmonic filter design (see Chapter 6 ).

II **Harmonic voltage distortion**

The harmonic voltage distortion at a certain point, most commonly at PCC, is represented in from of a harmonic spectrum. It allows one to see if the harmonic requirements are fulfilled.

Harmonic studies range in complexity from simple hand-calculations for small, straightforward systems with a single harmonic source, to computer simulations for complex networks with several harmonic sources. The complexity greatly depends on the location of the harmonic sources. If there is only one harmonic source or if all harmonic sources can be lumped into a single source, the network - up to the PCC - can be represented as an equivalent impedance. The harmonic distortion at PCC can then be easily calculated based on the harmonic current injection method. More complex situations with multiple network branches and harmonic sources in several of those branches, may require sophisticated software tools such as DIgSILENT[1] or SKM HI WAVE[2]. For this thesis the current injection method is chosen and further analyzed.

The current injection method requires the network and all loads to be combined in an equivalent impedance as seen from the harmonic source. The main challenge in finding this impedance is to decide which components should be included and which neglected. In general, all buses from the harmonic source level up to the PCC should be considered. Branches other than load branches must only be included if a power quality compensation capacitor is utilized. Reactances of cables exceeding 150 meters need to be included as well [22]. If the transmission system lays within the network of interest, line capacitances and inductances should be included [23].

[1] `http://www.digsilent.de`

[2] `http://www.skm.com/hiWave.html`

After the identification of the all relevant network components, and their transformation into a common p.u. system, the equivalent impedance $Z_{eq,h}$ as seen from the harmonic source can be calculated. The evaluation of this impedance as a function of frequency results in the impedance scan plot. The only way to find out if the network was modeled accurately enough is to see if a more accurate model leads to significantly different results.

If the harmonic current spectrum, $I_h$, of a VSD is known, the harmonic voltage distortion can be calculated, according the current injection method, as

$$V_h = Z_{eq,h} \cdot I_h \tag{4.1}$$

and thus the harmonic voltage distortion is found.

Another important fact which has to be considered is the harmonic content of the supply system. The supply itself can be a major source of harmonic distortion which has to be added on top of the harmonics generated by the devices in consideration. The only way to quantify the girds inherent harmonic content is through measurements [23].

## 4.1 Example Study

This section presents some selected results of the harmonic study for the compressor station in Egtved, Denmark [2].

The simplified single line diagram which was used in the study is provided in Figure 4.1. Two 60/10 kV transformers are available for mains feed, used during normal operation. Each, however, is capable of providing for the station's entire load (redundancy is used to ensure high availability). Bus 2.1 and 2.2 are normally not connected, but can be coupled if one transformer is failing. Normally up to two, in some seldom cases three VSDs are operated, each with a rated load of 6.4 MW.

There are two identical harmonic filters (H5/H7/H11) at bus 2.1 and 2.2, respectively. Each consists of four parallel branches:

- Single-tuned filter, tuned to 238 Hz ($5^{th}$ harmonic filter with -4.8% detuning)
- Single-tuned filter, tuned to 345 Hz ($7^{th}$ harmonic filter with -1.4% detuning)
- $2^{nd}$ order high-pass filter, tuned to 575 Hz ($11^{th}$ harmonic filter with +4.5% detuning)
- Shunt reactor to compensate for reactive power generation of filter circuit if required

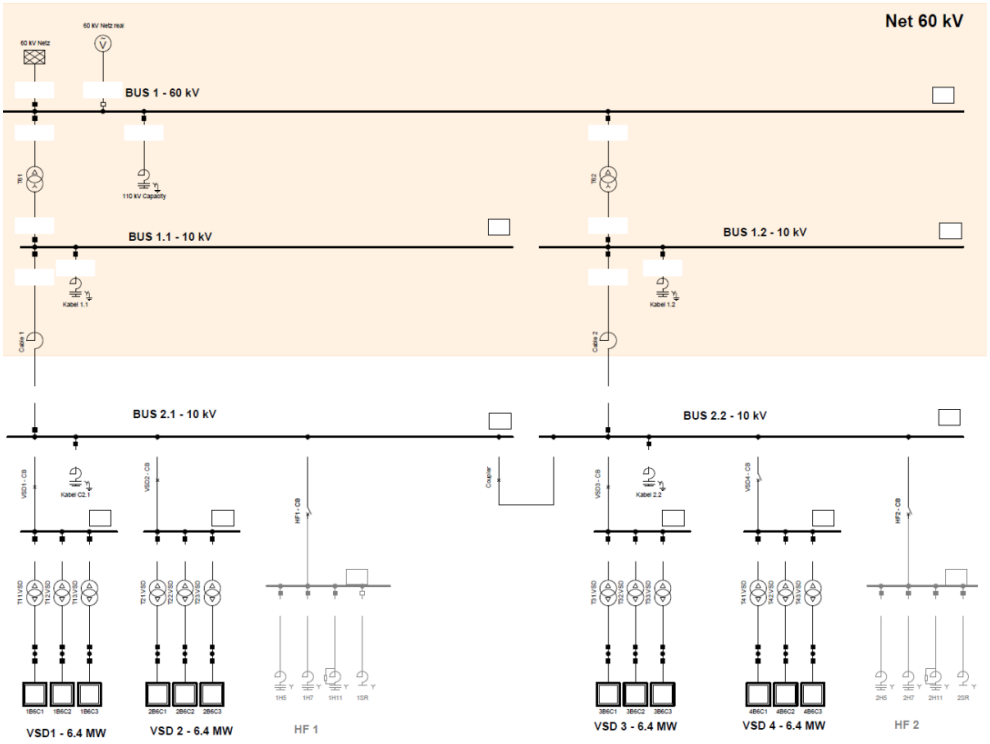


Figure 4.1: Single-Line-Diagram of the Egtved compressor station. [2]

Amplitudes of the $5^{th}$ and $7^{th}$ harmonic were measured by Dr. Walther of MR[3] and are depicted in Figure 4.2.

[3] `http://www.reinhausen.com/en`

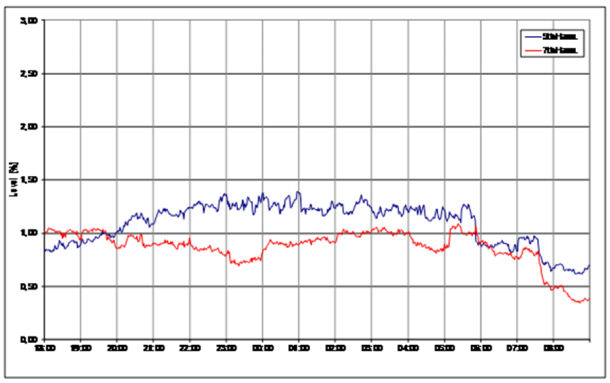

Figure 4.2: $5^{th}$ and $7^{th}$ amplitudes at Egtved 60 kV supply system during one night.

To assure harmonic compliance in all operational states, four different cases were simulated, and are summarized in Table 4.1.

Table 4.1: Harmonic study case overview

| Case | C1 | C2 | C3 | C4 |
|---|---|---|---|---|
| Main Transf. | 1 | 1 | 1 | 2 |
| VSD1 | on | on | on | on |
| VSD2 | off | on | on | on |
| VSD3 | off | off | on | on |
| Coupler | open | open | closed | closed |

The study (see p.2 of [2]) indicates that harmonic distortion limits are violated in all cases expect case 1. Case 4 (with parallel feed-in, closed coupler and three VSDs in operation) is discussed in the following.

In order to judge harmonic compliance it is sufficient to consider the harmonic situation at Bus 2.1 as it has the highest harmonic content. System upwards, at Bus 1.1 the harmonics are damped by the cable connection marked as "Kabel 1.1" and "Kabel 1.2", respectively. Therefore, if the harmonic limits are fulfilled at Bus 2.1 it is reasonable to assume that they are fulfilled at Bus 1.1.

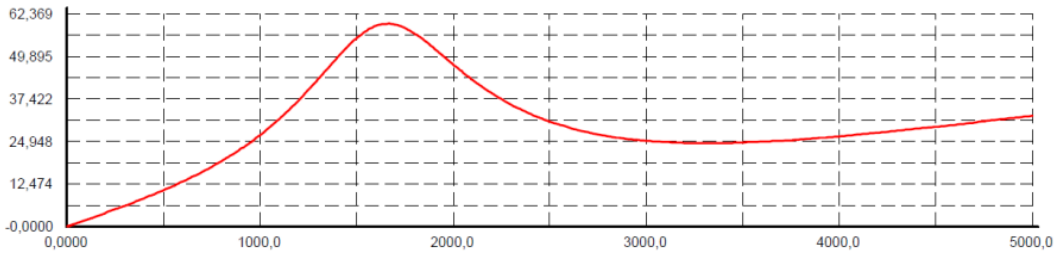


(a) No harmonic filters (Base: $Z_b = Z_1$=0.58 Ω)

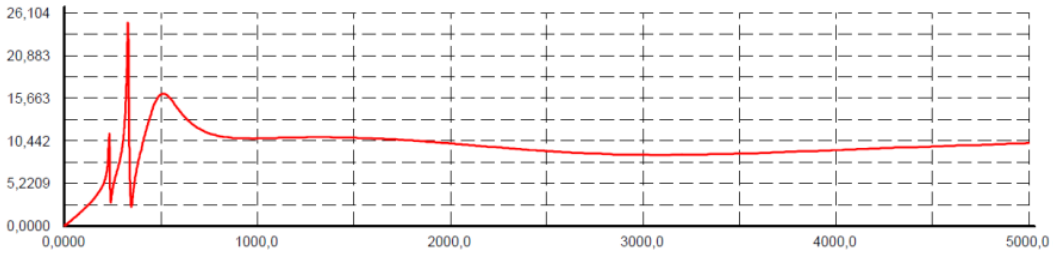


(b) Harmonic filters: H5/H7/H11 (Base: $Z_b = Z_1$=0.59 Ω)

Figure 4.3: Frequency sweep case 4 at Bus 2.1 - 10 kV, x-axis: Frequency [Hz], y-axis: Impedance [p.u.] [2].

As mentioned before, the impedance scan is commonly represented in two different manners. The impedance versus frequency plot, also referred to as frequency sweep, is used to identify minima and maxima and the resulting danger of harmonic amplification. It is shown in Figure 4.3 where as the corresponding maxima and minima are listed in Table 4.2.

The frequency response locus is used to identify series and parallel resonance and is shown in Figure 4.4. The solid black line in the diagram indicates the zero line of the reactance (y-axis). Its intersection with the locus curve thus determines all points where resonance, either parallel or series, occurs. In Figure 4.4a no resonance can be found as there is no filter connected. Figure 4.4b reveals four resonance points, which are summarized in Table 4.3.

Table 4.2: Impedance maxima and minima for case 4, with and without filter

| | Freq. [Hz] | Z [Ω] | Z [p.u.] | Type |
|---|---|---|---|---|
| No Filter | 1665 | 34.5 | 59.4 | local maximum |
| | 3294 | 14.8 | 24.4 | local minimum |
| With Filter | 232 | 6.6 | 11.3 | local maximum |
| | 239 | 1.7 | 44.7 | local minimum |
| | 328 | 14.6 | 30.3 | local maximum |
| | 346 | 1.4 | 2.3 | local minimum |
| | 508 | 9.5 | 16.2 | local maximum |
| | 972 | 6.4 | 10.7 | local minimum |
| | 1356 | 5.9 | 10.9 | local maximum |
| | 3116 | 5.1 | 8.7 | local minimum |

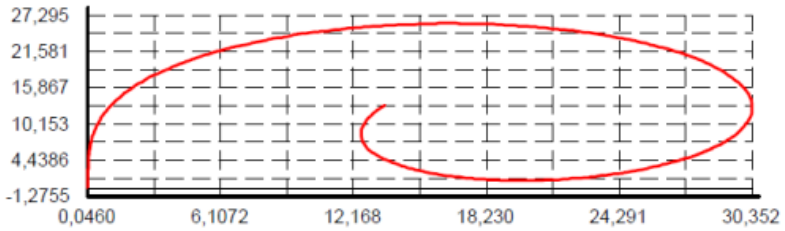


(a) No harmonic filters

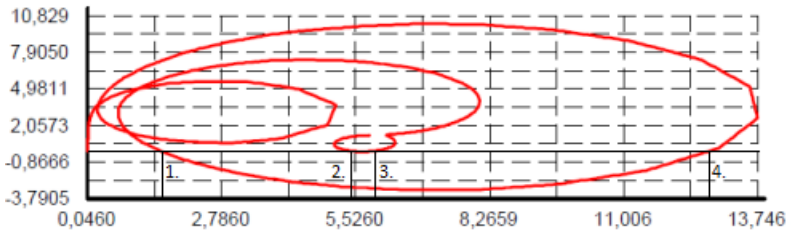


(b) Harmonic filters: H5/H7/H11

Figure 4.4: Frequency response locus case 4, x-axis: Resistance [Ω], y-axis: Reactance [Ω] [2].

Table 4.3: Resonance frequency with H5/H7/H11 filter

| Freq. [Hz] | Z [Ω] | Z [p.u.] | Type |
|---|---|---|---|
| 331 | 13 | 22.1 | parallel resonance |
| 343 | 1.7 | 2.92 | series resonance |
| 2028 | 5.9 | 10 | parallel resonance |
| 2432 | 5.4 | 9.29 | series resonance |

The harmonic spectrum of case 4 with and without filters is depicted in Figure 4.5 and listed in Table 4.4. The red, horizontal line in Figure 4.5 indicates the total harmonic distortion (THD). Harmonic amplification due to the changed impedance trajectory can clearly be observed for the $11^{th}$ harmonic. All other harmonics are attenuated or entirely canceled by the filter circuit. The amplification becomes obvious if one looks again at Table 4.2 or Figure 4.3b where a local maxima can be found as a part of an impedance plateau at the frequency of 508 Hz. The harmonic current at 550 Hz thus causes a high voltage distortion. In the case with no harmonic filter the voltage distortion lays at 0.36% whereas it rises to 0.41% if the harmonic filter is connected. This is a classical example of unwanted harmonic amplification that can lead to high distortion. It indicates the importance of an appropriate filter design.

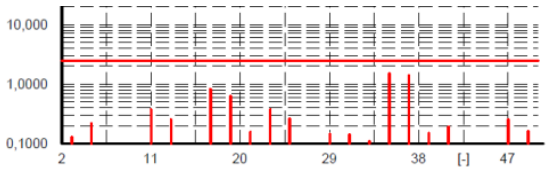


(a) No harmonic filters

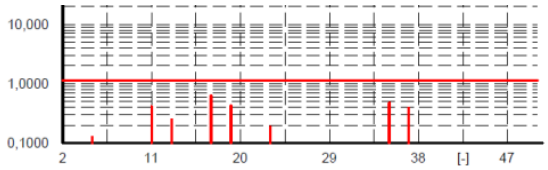


(b) Harmonic filters: H5/H7/H11

Figure 4.5: Voltage spectrum at 10 kV bus [%], case 4 [2].

Table 4.4: Voltage harmonic limits and values at 10 kV bus for case 4

| h | Limits [%] | C4 [%] | C4 with HF [%] |
|---|---|---|---|
| THD | 8.00 | 2.36 | 1.09 |
| 5 | 6.00 | 0.13 | 0.10 |
| 7 | 5.00 | 0.06 | 0.03 |
| 11 | 3.50 | 0.36 | 0.41 |
| 13 | 3.00 | 0.25 | 0.25 |
| 17 | 2.00 | 0.87 | 0.63 |
| 19 | 1.76 | 0.72 | 0.40 |
| 23 | 1.41 | 0.38 | 0.18 |
| 25 | 1.27 | 0.31 | 0.10 |
| 29 | 1.06 | 0.14 | 0.05 |
| 31 | 0.97 | 0.11 | 0.02 |
| 35 | 0.83 | **1.42** | 0.46 |
| 37 | 0.77 | **1.34** | 0.35 |

## 4.2 Impedance Scan Implementation

In this section the impedance scan of the feeding Medium Voltage (MV) system of the gas compressor station in Egtved is implemented in Matlab and discussed.

Based on Figure 10.1 (Appendix A) an equivalent circuit as shown in Figure 4.6 is assumed, representing the medium voltage (MV) system of the compressor station.

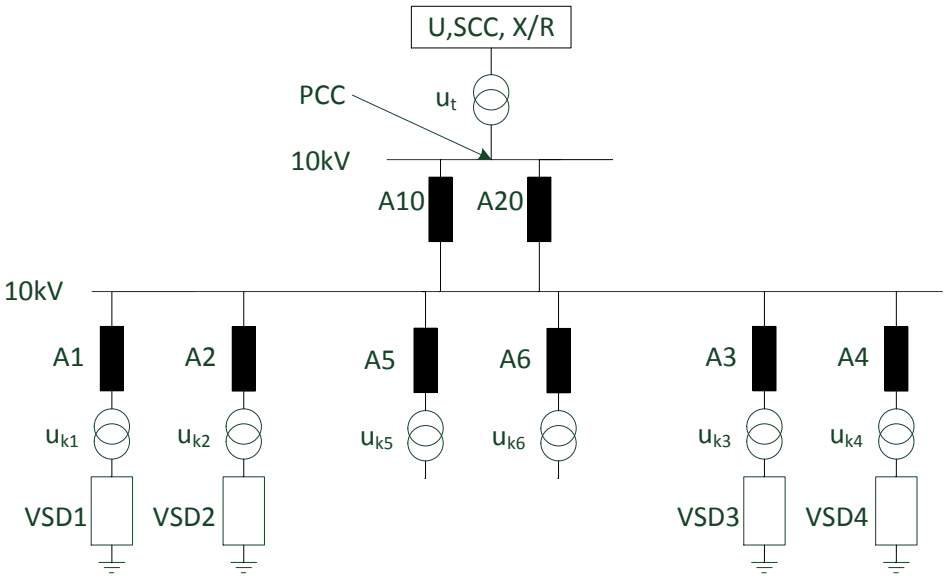


Figure 4.6: Assumed equivalent circuit of the MV system of the Egtved gas compressor station.

The high voltage (HV) system is represented as an equivalent impedance based on the short circuit capacity (SCC) at the HV/MV transformer and an assumed X/R ratio. In a first implementation, the impedance of cables with a length smaller than 150m are neglected, following the guidelines presented above. This means only the impedances of cable A10 and A20 are considered. They are represented as T-models. However, the shunt capacitance of all cables are taken into account in order to achieve accuracy in resonance representation. The VSD impedance and

the low voltage (LV) distribution system is neglected in this first representation. In order to be able to use the system representation for the harmonic current injection method, all harmonic sources were lumped into a single source. All of these simplifications lead to an equivalent circuit according Figure 4.7.The values used for the implementation and its origins are summarized in Tables 10.1-10.3 in Appendix A. The Matlab code for the implementation can be found in Appendix B.

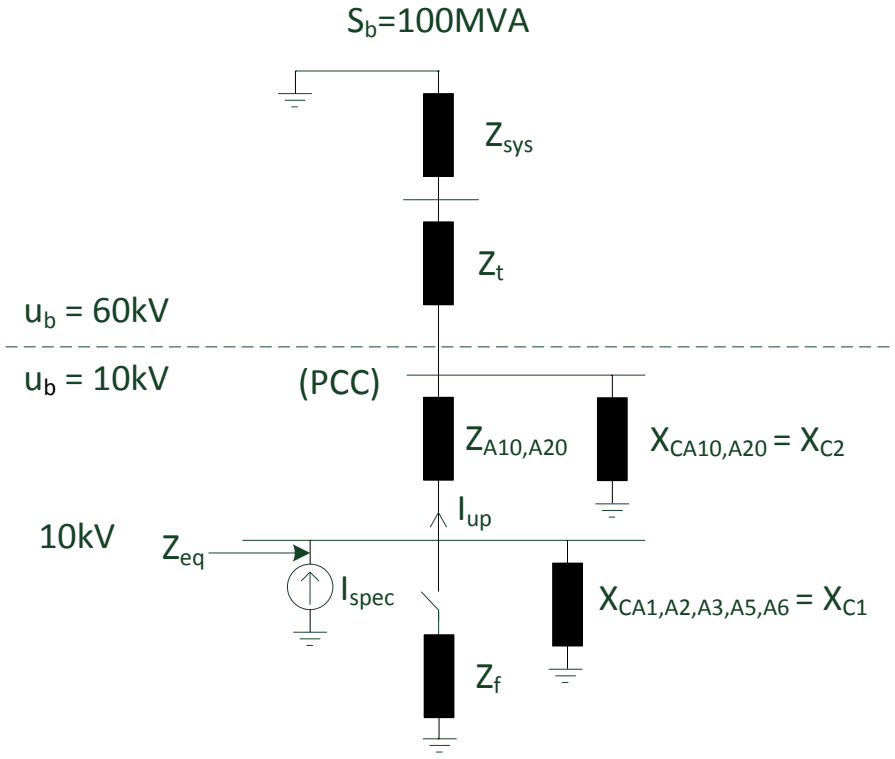


Figure 4.7: Equivalent circuit of Egtved MV system with lumped harmonic source.

The system impedance from the lumped harmonic source terminal as function of frequency is plotted in Figure 4.8. By comparing it to Figure 10.2 in Appendix A - which is taken form GE's harmonic study for the Egtved system - it can be concluded

that this first system approximation reveals valuable results. However, no peaks of minima and maxima impedance occur with this approximated representation. The representation is time consuming and the equations specific to a particular network configuration.

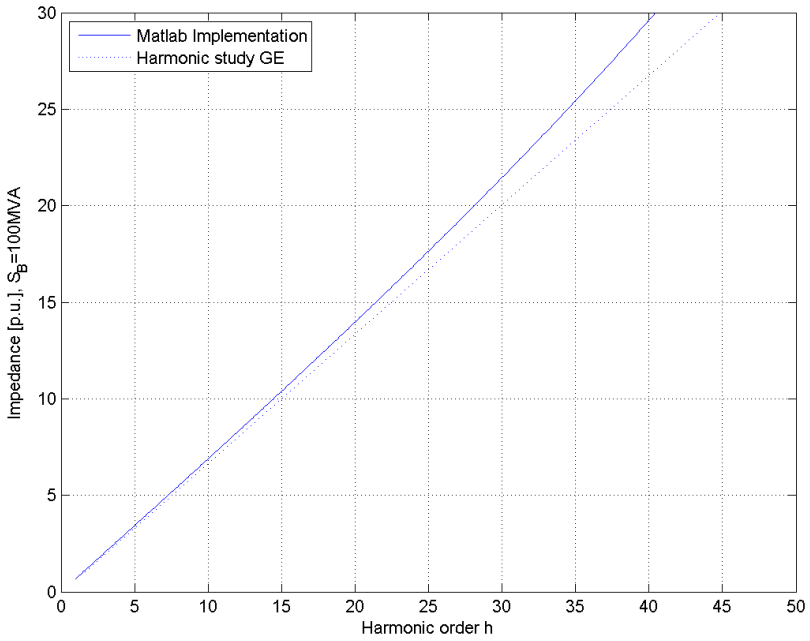


Figure 4.8: Frequency scan Egtved system

To further improve the system representations' accuracy, the VSD impedance should be modeled too. The transformer impedance depends on the harmonic source configuration and could be approximated based on the data of Figure 10.4 in Appendix A. An additional levier for accuracy improvement is to represent the HV system in more detail. The transmission lines could be represented as T-models based on the system configuration according to Figure 10.3in Appendix A.

# Chapter 5

# Harmonic Mitigation

This chapter provides an overview of harmonic mitigation measures. The presented methods can be broadly categorized as either being preventative or corrective in nature. Preventive methods directly reduce the harmonic content created by harmonic sources. In the case of passive front-end VSDs the most common preventive method is the creation of a p-pulse rectifier. This method's principles are introduced together with the therefore needed multiple winding transformers in the first two parts of the chapter. The phase-shifting mitigation approach, another preventive method which opens up due to the use of multiple winding transformers, according GE's patent [24], is discussed in a next section. Corrective methods, by contrast, aim to reduce already generated harmonic distortion. Passive filters are the most common measure in industrial VSD applications and are introduced in the last section of this chapter.

## 5.1 p-pulse Rectifier

Multi-pulse rectifiers with $p > 6$ are commonly used in high power VSDs because of their superior harmonic performance compared to six-pulse rectifiers . Common series-type rectifiers are 12-,18- and 24-pulse topologies that consist of two, three, or four 6-pulse diode rectifiers. Each rectifier connected to a phase-shifted "secondary" winding at its input and in series with the other rectifiers at its output (see Figure

5.1). The phase shift between the "secondary" windings is given by

$$\delta = \frac{360°}{p} \tag{5.1}$$

where $p$ is the pulse-number. As will be shown later, the higher the pulse number, the more harmonics are canceled in the transformer primary winding. Nevertheless, pulse-numbers exceeding 24 are seldom used due to prohibitive transformer size and cost.

Figure 5.1 shows a 12-pulse rectifier with a Y-connected primary and Y- and Δ-connected secondary and tertiary winding, respectively. The secondary Y-winding voltage $v_{ab}$ is in phase with the primary voltage $v_{AB}$ while the tertiary Δ-winding voltage lags $v_{AB}$ by 30°. In order to have the same amplitude at both rectifier outputs, the turn ratio of winding must be

$$\frac{N_3}{N_2} = \sqrt{3} \tag{5.2}$$

which compensates the phase voltage factor of $\sqrt{3}$ between Δ- and Y-connections. Figure 5.1c illustrates the p-peaks per fundamental period that exists in the rectifier output current waveform, $i_d$. As the two 6-pulse rectifier outputs are in series, $i_d$ is the sum of the secondary and tertiary currents. Each rectifier output current has 4 peaks per half-period (Figure 5.1c, where only the secondary current is shown), and are phase-shifter by $30^{\circ}$ from one another. The 12-pulse rectifier input current $I_A$ (see Figure 5.1a) is the sum of the primary side referred secondary and tertiary currents $i'_{aS}$ and $i'_{aT}$,

$$i_A = i'_{aS} + i'_{aT} \quad . \tag{5.3}$$

In the case of the secondary current $i_{aS}$ the transformation to the primary side does not affect the current waveform as primary and secondary quantities are in phase. The magnitude may differ depending on the turn ratio $\frac{N_1}{N_2}$. The tertiary current $i_{aT}$, however, changes waveform due to a phase shift of 30° and its primary side referred waveform $i'_{aT}$ is depicted in Figure 5.1d. The harmonic magnitudes stay the same. In the primary current, the sum of $i'_{aS}$ and $i'_{aT}$ , the $5^{th}$ and $7^{th}$ harmonic are in anti-phase and thus cancel out. This cancellation results in a primary current

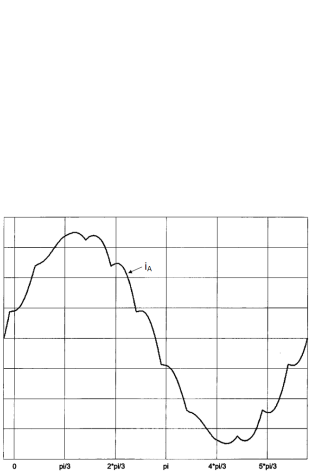


(a) Primary current

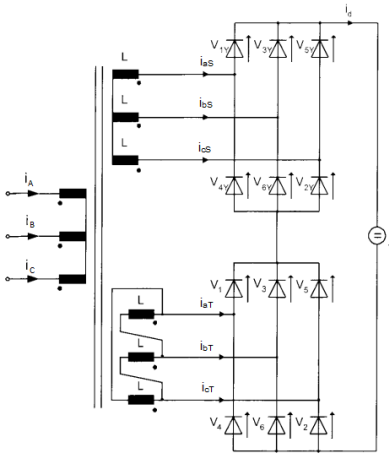


(b) 12-pulse bridge

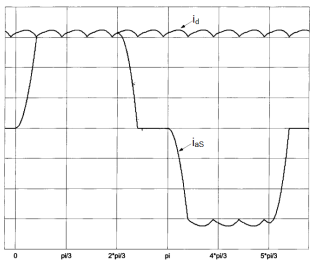


(c) Secondary current $i_{aS}$, output current $i_d$

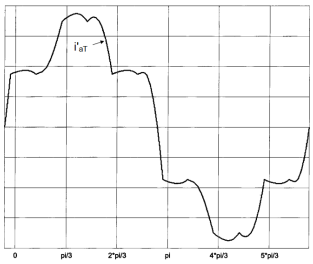


(d) Primary side referred tertiary current $i'_{aT}$

Figure 5.1: 12-pulse diode bridge and current waveforms [3].

which is closer to a sinusoidal waveform as seen in Figure 5.1a.

To illustrate the aforementioned harmonic cancellation of select harmonics, an ideal 6-pulse rectifier current is considered. As detailed in [11], the rectangular waveform of the secondary winding (where instantaneous commutation is assumed) may be represented as:

$$I_{6p} = I_1 \sin \omega t - I_5 \sin 5\omega t - I_7 \sin 7\omega t + I_{11} \sin 11\omega t \pm ... = I_{aS} \quad . \tag{5.4}$$

For harmonic cancellation, the tertiary winding must be phase shifted by $\delta = 30°$ (compare to Equation 5.1) with respect to the secondary winding: The tertiary current can hence be expressed as

$$\begin{aligned} I_{aT} &= I_{6p} \angle \delta \\ &= I_1 \sin(\omega t + \delta) - I_5 \sin(5\omega t + 5\delta) - I_7 \sin(7\omega t + 7\delta) + I_{11} \sin(11\omega t + 11\delta) \pm ... \quad . \end{aligned} \tag{5.5}$$

For simplicity $\frac{N_1}{N_2} = 1$ and $\frac{N_3}{N_2} = \sqrt{3}$ is assumed. If $\theta$ is the phase shift due to the transformer configuration (for the above example $\theta_S = 0°, \theta_T = -30°$) and the IEC notation[1] is used, the primary current of Equation 5.3 can be rewritten as

$$I_A = \begin{cases} I_{aS}\angle\theta_S + I_{aT}\angle\theta_T & h = 1, 4, 7, 10, ... \\ I_{aS}\angle -\theta_S + I_{aT}\angle -\theta_T & h = 2, 5, 8, 11, ... \end{cases} \tag{5.6}$$

where $h$ is the harmonic order.

$I_A$ equals

$$\begin{aligned} I_A =& I_1 \sin(\omega t + \theta_S) - I_5 \sin(5\omega t - \theta_S) - I_7 \sin(7\omega t + \theta_S) \\ &+ I_{11} \sin(11\omega t - \theta_S) \pm ... \\ &+ I_1 \sin(\omega t + \delta + \theta_T) - I_5 \sin(5\omega t + 5\delta - \theta_T) - I_7 \sin(7\omega t + 7\delta + \theta_T) \\ &+ I_{11} \sin(11\omega t + 11\delta - \theta_T) \pm ... \end{aligned} \tag{5.7}$$

which can be re-written to

$$\begin{aligned} I_A =& I_1 \sin(\omega t) - I_5 \sin(5\omega t) - I_7 \sin(7\omega t) \\ &+ I_{11} \sin(11\omega t) \pm ... \\ &+ I_1 \sin(\omega t) - I_5 \sin(5\omega t - 180°) - I_7 \sin(7\omega t - 180°) \\ &+ I_{11} \sin(11\omega t) \pm ... \quad . \end{aligned} \tag{5.8}$$

Note that the $5^{th}$ and $7^{th}$ are in anti-phase and add to zero. The expression thus simplifies to

$$I_A = 2 \cdot (I_1 \sin(\omega t) + I_{11} \sin(11\omega t) \pm ...) \tag{5.9}$$

Accordingly, a 18- or 24-pulse version can be formed which are depicted in Figure 8.5a. In the case of 18-pulse rectifier this leads to the cancellation of the $5^{th}$, $7^{th}$, $11^{th}$ and $13^{th}$ current harmonics. In a 24-pulse version the $5^{th}$, $7^{th}$, $11^{th}$, $13^{th}$, $17^{th}$ and $19^{th}$ harmonics are not present in the input current which results in a nearly

[1] For Y-$\Delta$ transformers, primary side positive sequence lead the "secondary" side by 30° while negative sequence primary quantities lag the "secondary" side by 30 °.

sinusoidal waveform. In general the characteristic harmonics of a p-pulse rectifier are defined as

$$h = np \pm 1 \quad n = 1, 2, 3, ... \quad . \tag{5.10}$$

The above analysis suggests that a p-pulse rectifier can be analyzed by treating each 6-pulse rectifier independently. To compute the line current of the system, all "secondary" currents are refereed to the primary side where they are summed.

## 5.2 Phase shift

As shown above cancellation of the $5^{th}$ and $7^{th}$ input current harmonics occur in series-connected 12-pulse rectifier with a phase shift $\delta = 30°$. Zingel suggests in [24] to use a phase shift $\delta'$ slightly different from the value determined by Equation 5.1, thus in the case of 12-pulse configuration $\delta' \neq 30°$. For example, one can see from evaluating Equation 5.4 to 5.7 with $\delta' = 28°$ that anti-phase harmonic cancellation no longer exists. Compared to $\delta = 30°$, $5^{th}$ and $7^{th}$ harmonics are larger, yet the magnitude of the $11^{th}$, $13^{th}$ harmonics, etc are decreased. In other words, the harmonic energy is distributed more equally along the harmonic spectrum.
If $\delta_{shift}$ is selected appropriately, harmonic suppression requirements can be satisfied without the need of additional filters. The same principal can be applied to any p-pulse rectifier.

## 5.3 Passive Harmonic Filters

Harmonic filters can be categorized as either being active or passive. In addition to passive components (resistors, inductors, capacitors) which are the sole building-blocks of passive filters, active filters incorporate power electronic devices. Active filters are used in low power applications, where they successfully overcome some of the disadvantages of passive filters. In high power applications, however, passive filters are predominately applied. This is due to their low cost-benefit ratio not yet achieved by active designs. Generally, it can be said that for VSDs above 1 MW, passive filters are the most common topology [21]. As a result this chapter focuses

solely on passive filters.

Passive filters can be classified as:

- Series filter (high impedance at tuning frequency), e.g. line reactor in a power electronics converter
- Shunt filter (low impedance at tuning frequency), e.g. single-tuned LC filter

To remove a particular harmonic, series filters are tuned to have a high impedance at the unwanted frequency. If there exist multiple unwanted harmonics, series filters can be cascaded so that each a filter is tuned to a specific harmonic order. The main disadvantages, and reason why series filters are seldom used, is that they have to withstand full current and voltage ratings and that they consume reactive power.

Shunt filters, by contrast, are tuned to provide a low impedance path to ground for a particular range of harmonics. They have to withstand only a fraction of the load current and can provide reactive power. Because of those two advantages, shunt filter topologies are most predominately used in practice. To address the shunt filters more thoroughly, five different topologies are shortly discussed below: single-tuned filter, 1st-3rd order high pass filter, and c-type filter. The design of a passive harmonic filter for VSDs, described extensively in the literature [5, 11, 25–27], is addressed in Chapter 6.

### 5.3.1 Single-tuned filter

The single-tuned (ST) filter topology and its impedance curve as a function of frequency (harmonic order) is shown in Figure 5.2. The impedance curve is determined by

$$Z_f(s) = \frac{LCs^2 + RCs + 1}{Cs} \tag{5.11}$$

where $s = \sigma + i\omega$ the complex operator in the Laplace domain.

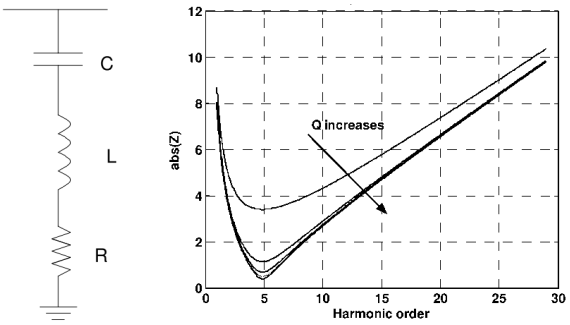


Figure 5.2: Single-tuned filter and its impedance curve [4].

The filter depicted is tuned to eliminate the $5^{th}$ harmonic where one can observe a notch in the impedance curve. From the shape of the impedance curve it becomes clear that this type of filter is suited to eliminate a specific harmonic (narrow notch). The notch frequency is determined by

$$f = \frac{1}{2\pi\sqrt{LC}} \quad . \tag{5.12}$$

Furthermore, the figure indicates that the sharpness of the tuning is determined by the so called quality factor, $Q$, which is defined as

$$Q = \frac{\sqrt{L/C}}{R} \quad . \tag{5.13}$$

Variation in inductance and capacitance values are often on the order of several percent due to component fabrication and aging. The STF's notch frequency is sensitive to parameter variation, thus such deviations in component values can impart a considerable shift of the impedance curve. This can lead to an amplification, instead of suppression, of the targeted harmonic. Figure 5.3 helps to illustrates this risk by depicting the impedance curve of the filter and the power system as seen from the harmonic source. One can see that there exists a parallel- and series-resonance point. The impedance is low close to the series-resonance and consequently, harmonic voltage distortion at similar frequencies is low as well. Close to the parallel-resonance point, however, the impedance is high and harmonic currents cause a high voltage distortion. For inductive systems with one STF, the point of

parallel resonance is given by

$$f = \frac{1}{2\pi\sqrt{(L_s + L)C}} \quad . \tag{5.14}$$

where $L_s$ is the series source inductance.

Comparison of equations 4.24 and 4.26 shows that the parallel-resonance always occurs at a lower frequency than the series-resonance point. Knowing this, harmonic amplification is avoided by detuning the filter to a frequency below the targeted harmonic. This way it is guaranteed - at least if the parameter deviation is within the expected range - that the target harmonic lies at or above the point of series-resonance. Therefore dangerous harmonic amplification is prevented.

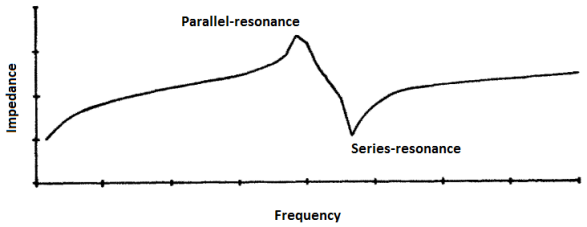


Figure 5.3: Impedance curve of filter and system [5].

### 5.3.2 First-order high-pass filter

The first-order high-pass filter topology and its impedance curve as a function of frequency is shown in Figure 5.4. The impedance curve is determined by

$$Z_f(s) = \frac{RCs + 1}{Cs} \quad . \tag{5.15}$$

Low impedance at high frequencies suggests that the first-order high-pass filter is suitable for a shunt-filter topology where it can provide a low impedance path to ground for harmonics above the tuning frequency.

A quality factor does not exist as there is only a capacitance but no inductance in the filter circuit.

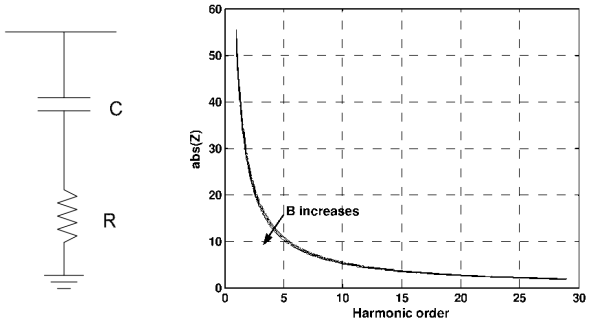


Figure 5.4: First-order high-pass filter and its impedance curve [4]

.

A most significant disadvantage of the first-order high-pass filter is its high losses at the fundamental frequency due to the nearly pure resistive impedance at this frequency. Another disadvantage is the high MVAr filter rating needed to be able to attenuate the wide band of harmonics. Those two disadvantages are the reasons this filter topology is seldom used [4].

### 5.3.3 Second-order high-pass filter

The second-order high-pass filter (HPF2nd) topology and its impedance curve as a function of frequency is show in Figure 5.5. The impedance curve is determined by

$$Z_f(s) = \frac{RLCs^2 + Ls + R}{s(CLs + CR)} \quad . \tag{5.16}$$

One of the advantages of this topology is its shallow notch compared to the single-

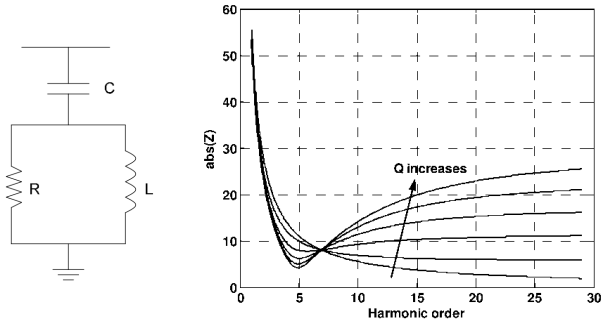


Figure 5.5: Second-order high-pass filter and its impedance curve [4]

.

tuned-filter (compared impedance curve of Figure 5.2 and 5.5), allowing it to be used to filter several high-order harmonics. It also results in a lower parameter deviation sensitivity. Compared to the first-order high-pass filter, it convinces with lower fundamental losses. Because of these superior characteristics, the HP2nd is the most popular filter topology for industrial applications such as high power VSDs [4].

### 5.3.4 Third-order high-pass filter

The third-order high-pass filter topology and its impedance curve as a function of frequency is shown in Figure 5.6. The impedance curve is determined by

$$Z_f(s) = \frac{RLC_1C_2s^3 + (C_1 + C_2)Ls^2 + C_2Rs + 1}{sC_1(C_2Ls^2 + C_2Rs + 1)} \quad . \tag{5.17}$$

When compared to the HPF2nd, the third-order high-pass filter yields even fewer

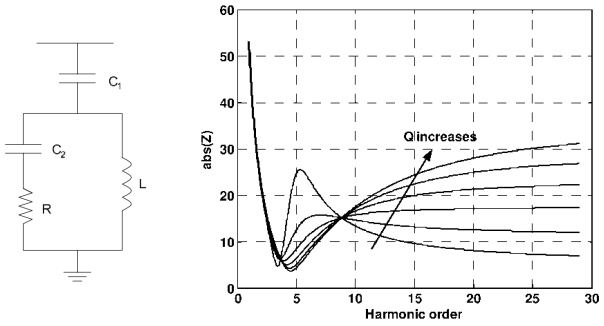


Figure 5.6: Third-order high-pass filter and its impedance curve [4]

.

losses at the fundamental frequency due to the added capacitor $C_2$ which increases the impedance of the resistive branch at low frequencies. It is, however, less effective in filtering high-order harmonics than the second-order type. Due to cost and complexity reason it is seldom used in industry [4].

### 5.3.5 C-type filter

The c-type filter topology and its impedance curve as a function of frequency is show in Figure 5.7. The impedance curve is determined by

$$Z_f(s) = \frac{LRC_1C_2s^3 + LC_2s^2 + (C_1 + C_2)Rs + 1}{sC_1(LC_2s^2 + RC_2s + 1)}. \tag{5.18}$$

The C-type filter is a second-order high-pass filter with an additional auxiliary

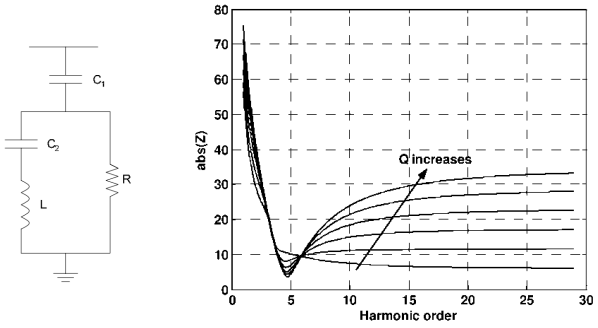


Figure 5.7: C-Type high-pass filter and its impedance curve [4]

.

capacitor $C_2$ added in series with the inductance. The auxiliary capacitor is tuned so that its reactance compensates the inductive reactance at the fundamental frequency which results in a low impedance branch for the fundamental current thus avoiding high losses in the resistive branch. The low fundamental losses are the main advantage of C-type filters. Furthermore, a superior harmonic attenuation at the tuned frequency is reached compared to high-pass filters. Additionally, C-type filters can be tuned to lower harmonic orders then high-pass filters [28]. Its harmonic attenuation for high-order frequencies is, however, less effective than for second-order high-pass filters. In general the C-type filter can thus be categorized to have an intermediate behavior between second- and third-order high-pass filters.

In general, SFT, HPF2nd and parallel combination of the two types are commonly used for industry applications. The reason for this will be further discussed in Chapter 6. Third-order high-pass and type C filter are mostly used in mitigation on a transmission system level [21].

## 5.4 Impedance Scan implementation including Harmonic filter

The system representation of Section 4.2 is now extend with a harmonic filter at the harmonic sources terminal. A standard harmonic filter consisting of a STF branch (tuned to the 3rd harmonic) and two HPF2nd branches (tuned to the 5th and 7th harmonic, respectively) is implemented. The detailed filter parameters for this $H3/H5/H7$ are listed in Table 5.1

Table 5.1: Parameters of H3/H5/H7 filter

| h | Q | Qr [MVAr] | R [Ω] | Xl [Ω] | Xc [Ω] | L [mH] | C [$mu$ F] | Topology |
|---|---|---|---|---|---|---|---|---|
| 3 | 400 | 8.8 | 0.1 | 1.26 | 11.36 | 4 | 280 | STF |
| 5 | 23 | 18.9 | 24.34 | 0.21 | 5.3 | 0.67 | 601 | HP2nd |
| 7 | 9 | 13.9 | 9.25 | 0.15 | 7.19 | 0.47 | 442 | HP2nd |

Figure 5.4 shows the frequency scan of the new impedance including the filter. The introduction of three resonance points in the impedance scan can clearly be observed.

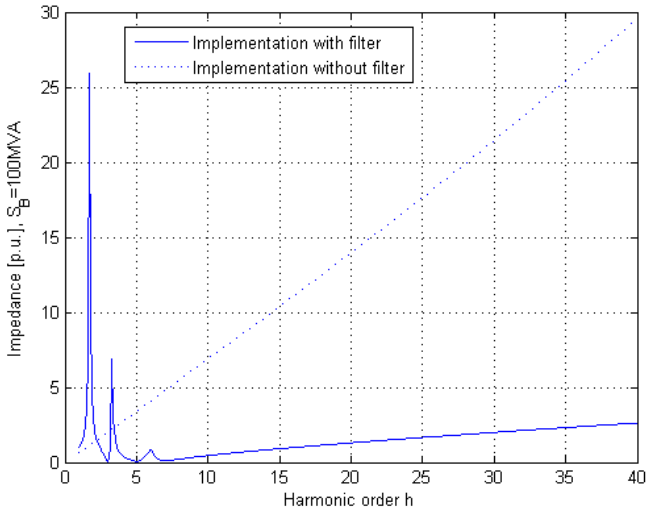


Figure 5.8: Frequency Scan including harmonic filter H3/H5/H7.

# Chapter 6

# Harmonic Filter Design

This chapter presents the fundamentals needed to understand and judge a harmonic filter design. From the considerations in the Section above, it is clear that a harmonic filter must be designed for a specific supply system configuration and that poor design or detuning may lead to harmonic amplification instead of attenuation. The present chapter discusses an iterative filter design process that avoids these problems.

Harmonic filter design methods can be categorized in two groups: Iterative process, discussed in [5, 17, 21, 29] and optimization problem formulation, discussed in [30]. The method of optimization problem formulation is out of the scope of this thesis.

Figure 6.1 shows a possible iterative process of passive filter design. It can be summarized in the following steps, [5, 17, 21, 29]:

*1*) Input data
The VSDs harmonic current spectrum and the power factor must be calculated (see Section 2.3 and Chapter 8) based on the VSDs working point. The system of interest has to be defined and the relevant components to be modeled (see Chapter 4).

*2*) Define min and max capacitor size

As discussed in Chapter 5.3, shunt harmonic filters can be used to supply reactive power in order to improve the power factor of the load. In cases in which the power factor is sufficient, a filter only for harmonic standard fulfillment - a so-called minimum filter - has to be designed. In cases where the filter is designed to improve the power factor, the required reactive power is calculated as

$$Q = P(\tan\theta_1 - \tan\theta_2) \tag{6.1}$$

where $Q$ is the reactive power which the filter has to supply, the initial power factor $PF_1$ equals $\cos\theta_1$ and the required power factor $PF_2$ equals $\cos\theta_2$. Based on the bus voltage, the capacitor reactance is calculated as

$$X_c = \frac{kV^2}{Q} \quad . \tag{6.2}$$

If a power factor range is given, a minimal and maximal reactive power, and consequently a minimal and maximal reactance, can be calculated.

A common practice is to distribute the required capacity evenly among the branches [31].

It shall be noted that a minimum filter design does not necessarily result in a lower kVAr rating. It is possible that the kVAr requirement for harmonic standard fulfillment is higher than the one needed for a certain power factor compensation, or vice versa. Thus, the term is somewhat deceptive.

*3*) Start with STF5, STF7 and HP2nd11 topology

The simplest filter topology would be a single broad band-pass configuration designed to keep all harmonics below required limits. Such a configuration would - in most cases - require a very high capacitance. A more economical configuration is to mitigate lower harmonics with single-tuned filters [17]. In industrial systems, three branch configurations are often applied [29]. Nassif showed in [31] that a configuration with two STF and a HPF2nd can be expected to have superior filter performance in terms of harmonic standard fulfillment, price, components stress and frequency response than all other three-branch topologies. Based on the above publication, it is suggested to

start the design process with a three-branch filter configuration consisting of two single-tuned and a high-pass filter, tuned to the $5^{th}$, $7^{th}$ and $11^{th}$ harmonic, respectively. The same topology is successfully in operation in the EGTVED gas compressor station planned by ILF.

*4*) Decide on detuning

As mentioned in Section 5.3, single tuned filters are often detuned in order to avoid harmonic amplification cause by component's tolerances and aging. A common practice is to detune them to 1-10% below the intended frequency [5].

*5*) Select minimal capacitor size

*6*) Dimension $L$, $R$ according the following equations:

**Single-tuned filter** [11]

The rector is given by

$$X_L = \frac{X_C}{h_n^2} \tag{6.3}$$

where $h_n^2$ is the harmonic order to which the filter should be tuned. The characteristic impedance $X_n$ is defined as

$$X_n = \sqrt{X_L X_C} \quad . \tag{6.4}$$

The reactor resistance is given by

$$R = \frac{X_n}{Q} \tag{6.5}$$

where $Q$ is the quality factor of the filter and normally lies between 30 and 100 [5]. The filter size is calculated as

$$Q_{Filter} = \frac{kV^2}{X_C - X_L} \quad . \tag{6.6}$$

**$2^{nd}$ order high-pass filter** [11]

The rector is given by

$$X_L = \frac{X_C}{h_n^2} \tag{6.7}$$

where $h_n^2$ is the harmonic order to which the filter should be tuned. The characteristic impedance $X_n$ defined as

$$X_n = \sqrt{X_L X_C} \quad . \tag{6.8}$$

The reactor resistance is given by

$$R = X_n Q \tag{6.9}$$

where $Q$ is the quality factor of the filter and normally lays between 0.5 and 2 [5]. The filter size is calculated as

$$Q_{Filter} = \frac{kV^2}{X_C - X_L} \quad . \tag{6.10}$$

*7*) Perform harmonic study, see Chapter 4 and calculate filter components voltages and currents

*8*) Overloaded?
According to [32] a power shunt capacitor can withstand the following ratings in continuous operation, which consequently must not be exceeded in any filter capacitor:

- 110% of rated RMS voltage
- 120% of rated peak voltage, i.e., peak voltage not exceeding $1.2\sqrt{2}V_{ratedRMS}$, including harmonics, but excluding transients
- 135% of nominal RMS current based on rated kVAr and rated voltage
- 135% of rated kVAr

Another commonly used standard is [33].
A reactor should be design to at least withstand the RMS current under which it is operated [11] (based on the withdrawn IEC Standard 60289).
The same holds through for the resistor, thus $I_{rated} \leq I_{RMS}$.

*9*) Harmonic standard, see Chapter 3, fulfilled?

*10*) Is parallel resonance and the resulting harmonic amplification the cause?

*11*) Is there another topology or tuning frequency to be investigated in order to compare different designs?

While the above described filter design process should lead to a suitable harmonic attenuation for the system parameters and working points defined in input data, a designer should also evaluate his design upon possible changes in working points and system configuration, i.e. planned system extensions, in order to verify the effectiveness of it. Once an initial design has been found, several well chosen cases should be tested by performing a harmonic study for each of them.

Particular importance should be paid to the shift in harmonic spectrum under different loading conditions of certain VSDs, such as Line Commutated Inverters (LCIs). A system with a LCI which has a pronounced harmonic current occurring around the $6^{th}$ harmonic when the VSD is at full load and around the $4^{th}$ harmonic for low load operation, is expected to have a pronounced harmonic at the $5^{th}$ order under some intermediate operating conditions. A designer has to consider such a change in harmonic spectrum and design the filter accordingly.

Besides harmonic performance and component stress, filter costs and loss should also be considered.

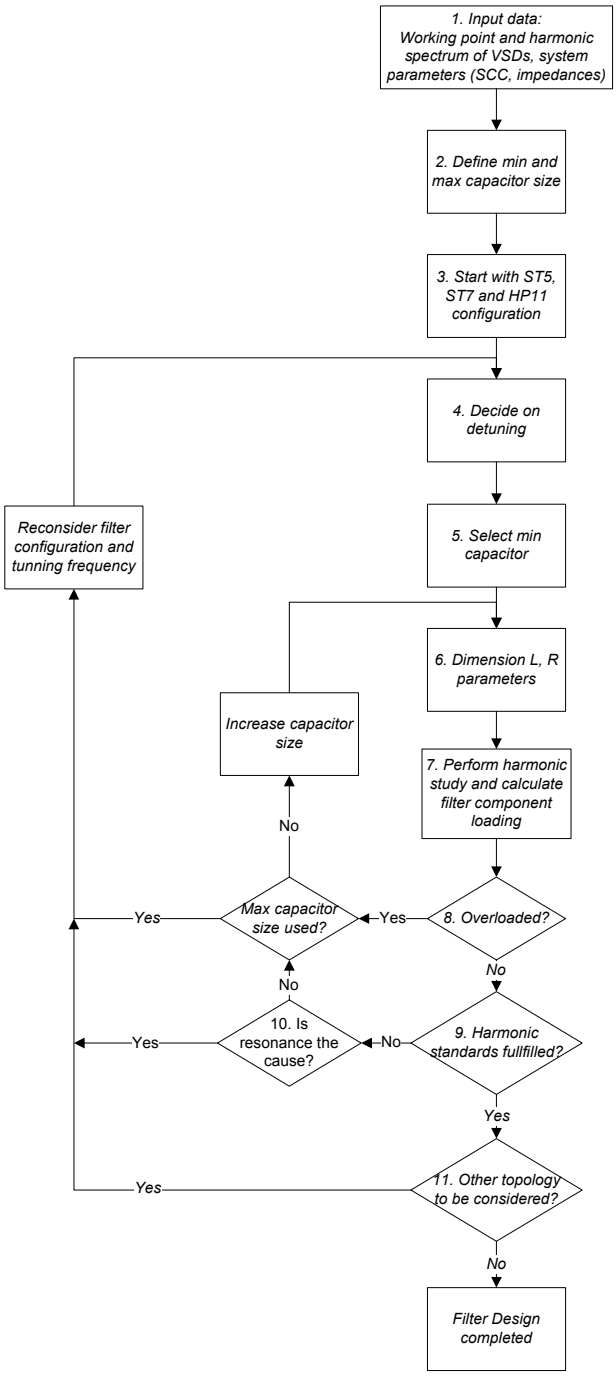


Figure 6.1: Iterative Passive Filter Design Flow Chart.

# Chapter 7

# Conclusion and Outlook - Harmonic Compliance

Harmonic studies of VSDs aim to assess the devices' compliance with harmonic standards. They study well-chosen "worst-case" scenarios that may differ in system configuration and harmonic source configuration. A harmonic study, as defined, consists of: an impedance scan (providing possible parallel or series resonance points), and a calculation of harmonic distortion at a specific point in the network.

The complexity of a harmonic study predominantly depends on the number and the location of the harmonic sources. A simple method to calculate a harmonic study that can be implemented in any numerical computing environment is the current injection method. A simple method to calculate a harmonic study is the current injection method. It is important to be aware of the fact that the supply system itself is a source for harmonic distortion and should be included in the analysis.

An example of a specific network frequency scan has been implemented in Matlab. Its results and limitations were discussed. They can be summarized as following:

- A PI-model of cables with commonly used inductance and capacitance values is sufficient for a first approximation,
- The VSD transformer impedance was neglected in this first representation,

- No peaks of minima and maxima impedance occurred with the simplified representation restricted to the MV system,

- Implementation is time consuming and specific to one network configuration.

In order for a valid assessment of the resonance phenomena, a more detailed network representation including transmission lines has to be implemented. Detailed information regarding network configuration must therefore be available. A further improvement of the system representation's accuracy can be achieved by a detailed model of the VSD multi-winding transformer impedance.

After a detailed enough network representation could be found, the harmonic current injection method can be used to calculate harmonic voltage distortion at any point in the network. The method of current injection is limited to one harmonic source at a specific point in the network. This implies the need for finding a single-lumped-harmonic-source representation that includes the supply system's harmonic distortion and all harmonic sources, taking into account the harmonic cancellations between them.

An appropriate definition of a single-lumped-harmonic current spectrum, together with the aforementioned detailed network representation, are thus the main challenges of this otherwise simple harmonic study approach.

Harmonic mitigation methods can be categorized in preventive and corrective measures. For passive front-end VSDs, the following three measures are most commonly used.

- Creation of p-pulse rectifier (preventive): Examples of commonly used p-pulse configurations are 12-, 18-, 24-pulse rectifiers. Pulse numbers higher than 24 are seldom used due to prohibitive transformer size and cost. In a p-pulse passive rectifier, the following characteristic harmonics are present: $h = np \pm 1 \quad n = 1, 2, 3$

- Phase shift (preventive): Phase shift method (according GE's patent [24]) annuls the harmonic cancellation of p-pulse configuration and distributes the harmonic energy among the spectrum.
- Harmonic filter (corrective): The most commonly used filter topology in VSD applications is a multi-branch filter consisting of a combination of single-tuned and second order high-pass filters. The design of such a filter is commonly done in an iterative process to find a solution that complies with all constraints.

There are no hard-and-fast rules on how to design harmonic measures. A filter design process illustrating a possible design strategy was presented. In practice, filters are often used in combination with the other mitigation measures.

The harmonic impedance scan of the MV system representation was reevaluated, this time with a standard harmonic filter (a parallel combination of the 3rd harmonic, single-tuned filter and two second order, high-pass filters tuned to the 5th and 7th harmonic, respectively) at the VSD terminal. The new impedance scan clearly shows resonance points introduced by the filter.

# Part III

# Harmonic Modeling of Variable Speed Drives

# Chapter 8

# Harmonic Source Modeling

This chapter focuses on the modeling of harmonic sources in order to calculate their harmonic current spectrum. This spectrum is needed to calculate a harmonic study based on the current injection method. First, the scope of interest of this thesis in terms of harmonic sources is defined. Next, two commonly used high power VSD topologies are presented, for each of which a suitable harmonic model is discussed.

Power system harmonic sources take the form of

- Transformers ($I = f(U) = f(BIH)$)
- Rotating machines (winding harmonics)
- Power electronic devices (topology, modulation)

As the topic of this thesis is the analysis of power system harmonics VSDs, only power electronic devices shall be examined.

Numerous VSD topologies are used for high power industrial applications. An overview is provided in [6, 8, 34] and summarized in Figure 8.1. Literature research was carried out for both a voltage and current source converter VSD, LCI and 3-level Neutral Point Clamped VSC, respectively and is summarized below.

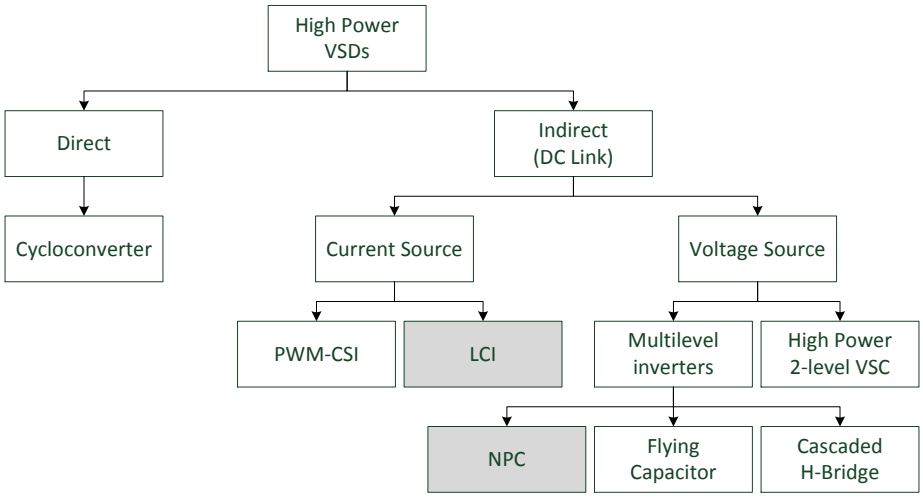


Figure 8.1: Overview of converter topologies used for high power drives.

## 8.1 Line Commutated Inverter Variable Speed Drives

The structure and operation of the LCI is quite simple, as it does not allow for the use of pulse width modulation. These two inherent simplicities allow a rather simple derivation of a model, which turns out to be very insightfull in terms of interharmonic generation.

Line Commutated Inverters are predominantly used in very high power applications up to 100 MW [35]. The main reason for this choice is LCI's semiconductor device, the thyristor, is both less expensive than competing devices and has high voltage and power capabilities, high efficiency and reliability [34]. The basic structure of an LCI is shown in Figure 8.2. It consists of two identical thyristor-based converters connected back-to-back via a DC link inductance. The inductive DC link is the reason for it is classified as current source topology. As the name Line Commutated Inverter indicates, both converters' commutation is dependent on an external AC voltage. The grid-side converter is commutated by the line-voltage while the machine-side converter is commutated by the back e.m.f. of the machine. The current can flow in only one direction (an inherent characteristic of thyristor).

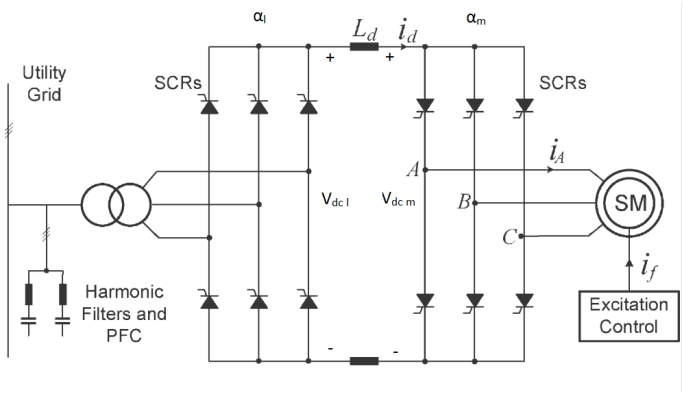


Figure 8.2: Diagram of a LCI VSD. [6]

Nevertheless, power transfer is possible in both directions and depends on voltage polarity across the DC link inductance. It is defined by the DC voltages, $V_{dc_l}$ on the line-side and $V_{dc_m}$ on the machine side. They themselves are dependent on the firing angles, $\alpha_l$ and $\alpha_m$ respectively, as shown in Figure 8.3a and defined below

$$V_{dc_{l/m}} = V_{dcmax} \cos \alpha_{l/m}; \qquad \begin{aligned} \alpha_{l/m} &= 0° \quad \rightarrow \quad +V_{dcmax} \\ \alpha_{l/m} &= 180° \quad \rightarrow \quad -V_{dcmax} \end{aligned} \quad . \tag{8.1}$$

In motor operation, the line-side converter operates as a rectifier (firing angle $\alpha_l < 90° \Rightarrow V_{dc_l} = positive$) and the machine side converter as an inverter (firing angle $90° < \alpha_m < 180° \Rightarrow V_{dc_l} = negative$). The voltage $V_d = V_{dc_l} - V_{dc_m}$ across the inductor is thus positive in the direction of current flow. A positive power transfer from the grid to the synchronous machine results. Conditions are reversed when machine is operated as a generator.

The VSD operation scheme minimizes reactive power flow and thus allows the converter ratings to be used for active power transfer. In motor operation, it keeps $\alpha_m$ constant at 180° ($\Rightarrow V_{dc_m} = -V_{dcmax}$) which means voltage and current are in anti-phase and the machine-side displacement factor is $DPF_m = 1$ (see Figure 8.3b). At the same time an excitation system is used to assure a good magnetic utilization of the machine by keeping the flux linkage at its nominal value [34]. To achieve this, the stator voltage is varied with varying speed. The scheme thus results in

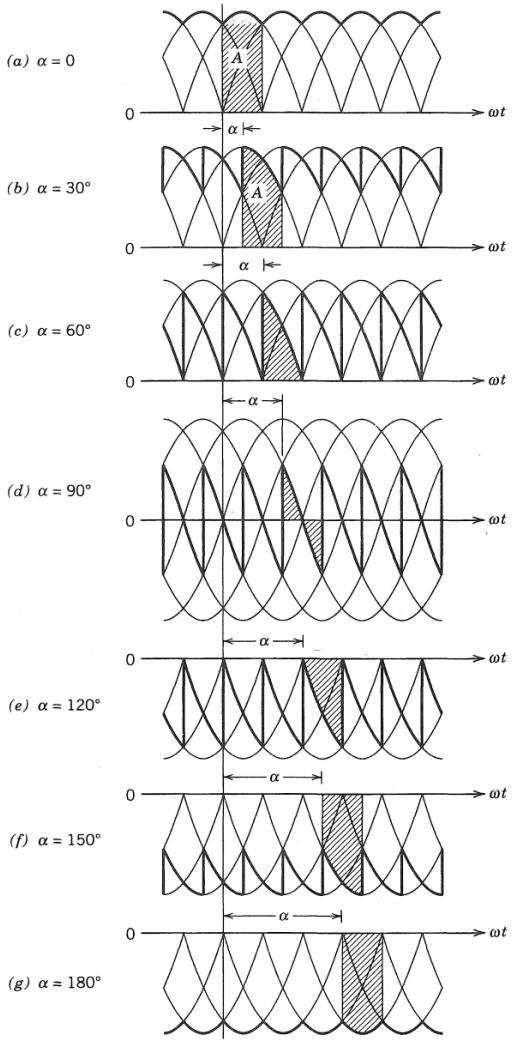


(a) DC-side voltage

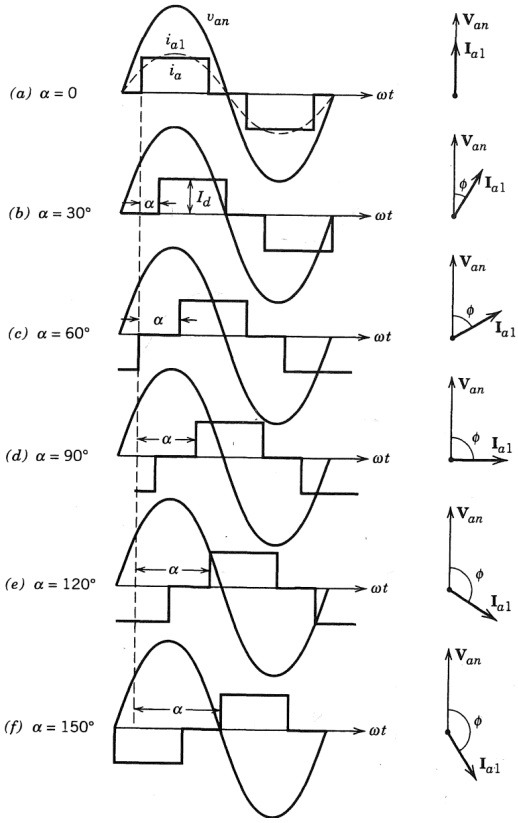


(b) Line-side current

Figure 8.3: 3-phase thyristor converter quantities as a function of $\alpha$ [1].

a proportionality between the machine's speed and the DC link voltage $V_{dc_m}$. In order to keep the current set-value $I_{d\ \ set}$, $\alpha_l$ is varied from $\alpha_l = 90° \Rightarrow V_{dc} = 0$ at stand still to $\alpha_l = 0° \Rightarrow +V_{dcmax}$ at full speed. In breaking operation, $\alpha_m$ is set to zero (rectifier mode) and kept constant ($\Rightarrow V_{dc_m} = +V_{dcmax}$). The line-side angle $\alpha_l$, on the other hand, is now varied between $90° \rightarrow 180°$ (inverter mode). The DC link voltage polarity is thus inversed, which leads to a reversed power flow from the

machine to the grid. In both operations, i.e. motor and breaking, this operation scheme implies that the line-side displacement power factor $DPF_l$ is a function of motor speed, which is one of the disadvantages of an LCI.

The above described working principle is now used to derive an analytical harmonic model for the LCI, which follows that of [7]. Line-side harmonics are caused by two phenomena: First of all, by the non-linear line-side current drawn by LCI, and machine harmonics transferred through the DC link. In superposition, those two phenomena cause not only harmonics at integer multiples of the fundamental frequency but also harmonics at non-integer values. As discussed in Chapter 2 they are referred to as interharmonics. In [7] the following simplifications for the harmonic model are assumed and adpoted for this presentation:

- Balanced line voltage
- No harmonic distortion in line voltage
- Equally spaced thyristor firing angles
- Large DC link inductance

In a thyristor converter two operation states, conduction and commutation, have to be distinguished. The differences between the two states are clear when analyzing the input impedance from the line side.: During the conduction phase, the DC link and machine circuit impedance is seen, while during commutation two lines are shorted, causing the impedance to reduce to the thyristor short circuit impedance. This leads to two different line-side current parts:
On one hand, there is the conduction current that is the product of the conduction function current $I_{l,cf}$ and the DC link current $I_d$. Together they represent the current in the conduction state $I_{l,c} = I_{l,cf} \cdot I_d$. On the other hand, there is the commutation current $I_{l,com}$ representing the commutation state. The line-side current $I_l$ is the sum of the two, depicted in Figure 8.4, and can be represent as:

$$I_l = I_{l,com} + (I_{l,cf} \cdot I_d) \quad . \tag{8.2}$$

Observe that $I_d$ will be zero in case of an infinite large DC link inductance, the

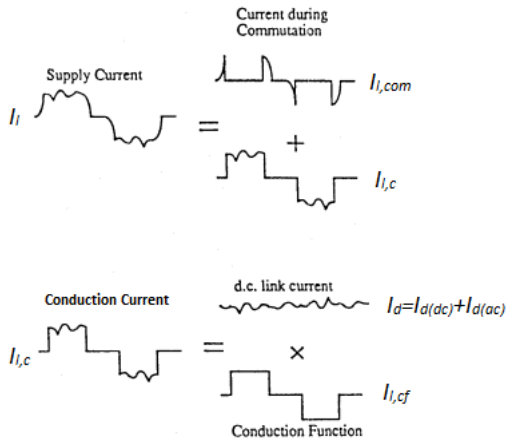


Figure 8.4: Supply current composition. [7]

above assumption, however, only assumes a large inductance and thus $I_d$ is finite. Both $I_{l,com}$ and $I_{l,cf}$ are periodic functions that are connected to the converter valves' switching. Their sum is non-zero during two 120° intervals in each period, once positive and once negative, and they can be represented as Fourier series in the following manner:

$$I_{l,com} = \sum_{n=1}^{\infty} \{A_{l,com_n} \cos n\omega_1 t + B_{l,com_n} \sin n\omega_1 t\} \tag{8.3}$$

$$I_{l,cf} = \sum_{n=1}^{\infty} \{A_{l,cf_n} \cos n\omega_1 t + B_{l,cf_n} \sin n\omega_1 t\} \tag{8.4}$$

where $n = 1, 3, 5, 7....$ For $A_{l,com_n}$, $B_{l,com_n}$, $A_{l,cf_n}$ and $B_{l,cf_n}$ coefficient development refer to [36].

The DC link is represented by an inductance connected between two rectified AC voltages ($V_{dc,l}$ and $V_{dc,m}$), as shown in Figure 8.2, which themselves consists of a DC part and periodic AC components. They can thus be represented as a Fourier series as shown below:

$$V_{dc,l} = \frac{A_{dc,l_0}}{2} + \sum_{m=6}^{\infty} \{A_{dc,l_m} \cos m\omega_1 t + B_{dc,l_m} \sin m\omega_1 t\} \tag{8.5}$$

$$V_{dc,m} = \frac{A_{dc,m_0}}{2} + \sum_{m=6}^{\infty} \{A_{dc,m_m} \cos m\omega_2 t + B_{dc,m_m} \sin m\omega_2 t\} \tag{8.6}$$

where $m = 6, 12, 18, 24...$, $\omega_1$ is the line-side angular frequency and $\omega_2$ the machine-side angular frequency. For $A_{dc,l_n}$, $B_{dc,l_n}$, $A_{dc,m_n}$ and $B_{dc,m_n}$ coefficient development refer to [17].

The DC link current $I_d$ is the sum of an AC part $I_{d_{(ac)}}$ and a DC part $I_{d_{(dc)}}$ and can be written as

$$I_d = I_{d_{(ac)}} + I_{d_{(dc)}} \quad . \tag{8.7}$$

The two components can be determined by again considering Figure 8.2 in which the two rectified voltages are coupled by an inductance. If one neglects the resistance of the inductance for AC quantities, the above components may be expressed as

$$I_{d_{(dc)}} = \frac{A_{dc,m_0} + A_{dc,l_0}}{2R_d} \tag{8.8}$$

$$I_{d_{(ac)}} = \frac{1}{L_d} \int \left( V_{dc,l_{(ac)}} - V_{dc,m_{(ac)}} \right) \mathrm{d}t, \tag{8.9}$$

where $R_d$ is the DC resistance of the inductor $L_d$, $V_{dc,l_{(ac)}}$ and $V_{dc,m_{(ac)}}$ are the AC components of $V_{dc,l}$ and $V_{dc,m}$, respectively.

Equation 8.9 can thus be rewritten as

$$\begin{aligned} I_{d_{(ac)}} = \frac{1}{L_d} \sum_{m=6}^{\infty} & \left\{ \frac{A_{dc,l_m}}{m\omega_1} \cos m\omega_1 t - \frac{B_{dc,l_m}}{m\omega_1} \sin m\omega_1 t \right\} \\ & + \left\{ \frac{A_{dc,m_m}}{m\omega_2} \cos m\omega_2 t - \frac{B_{dc,m_m}}{m\omega_2} \sin m\omega_2 t \right\} \end{aligned} \quad . \tag{8.10}$$

The line-side current $I_l$ of Equation 8.2 can be reformulated as:

$$I_l = I_{l,com} + I_{l,cf} \cdot I_{d_{(dc)}} + I_{l,cf} \cdot I_{d_{(ac)}} \tag{8.11}$$

and by using Equations 8.3, 8.4 and 8.10 it follows

$$I_l = \sum_{n=1}^{\infty} \{A_{l,com} \cos n\omega_1 t + B_{l,com} \sin n\omega_1 t\} \tag{8.12a}$$

$$+I_{d_{dc}} \cdot \sum_{n=1}^{\infty} \{A_{l,cf_n} \cos n\omega_1 t + B_{l,cf_n} \sin n\omega_1 t\} \tag{8.12b}$$

$$+ \sum_{m=6}^{\infty} \left\{ \frac{A_{dc,l_m}}{m\omega_1 L_d} \cos m\omega_1 t - \frac{B_{dc,l_m}}{m\omega_1 L_d} \sin m\omega_1 t \right\} \cdot \tag{8.12c}$$

$$\sum_{n=1}^{\infty} \{A_{l,cf_n} \cos n\omega_1 t + B_{l,cf_n} \sin n\omega_1 t\}$$

$$+ \sum_{m=6}^{\infty} \left\{ \frac{A_{dc,m_m}}{m\omega_2 L_d} \cos m\omega_2 t - \frac{B_{dc,m_m}}{m\omega_2 L_d} \sin m\omega_2 t \right\} \cdot \tag{8.12d}$$

$$\sum_{n=1}^{\infty} \{A_{l,cf_n} \cos n\omega_1 t + B_{l,cf_n} \sin n\omega_1 t\} .$$

Analyzing each component of equation 3.12 provides insight into LCIs harmonic content. Part 8.12a of equation 8.12 represents the harmonics caused by the commutation phase. Part 8.12b represents the harmonics caused by the DC component of $I_d$. One can show that the triple harmonics of part 8.12a and part 8.12b cancel if a very large DC inductance is assumed [7]. Part 8.12c represents the harmonics generated by the modulation of current harmonics resulting from the DC link voltages and the current harmonics of the conduction phase. Part 8.12d is the term of interharmonics and consists of two groups: The first of which are the characteristic interharmonics (modulation of $n = 1, 5, 7, ... \times \omega_1$ of the $I_{l,cf}$ with $m = 6, 12, 18, ... \times \omega_2$ of the $I_{d_{ac}}$) and the other which are small triplen related interharmonics (modulation of $n = 3, 9, 15, ... \times \omega_1$ of the $I_{l,cf}$ with $m = 6, 12, 18, 24, ... \times \omega_2$ of the $I_{d_{ac}}$).

As it can be seen from Equations 8.5, 8.6 and 8.9 and was mentioned earlier, the DC link current is dependent on the two DC side voltages of the line and machine-side converter, respectively. The machine-side voltage magnitude and its frequency, however, are a function of the machine speed. It can therefore be concluded that interharmonics are dependent on the machine's operation point and that they change frequency as the machine is operated at different speeds. This in turn makes it difficult to size components when employing passive harmonic mitigation schemes.

It further creates the danger of exciting resonant oscillations with other components in the power system such as power factor compensation capacitors.

A more advanced model is described in [37]. It uses switching functions apadpted from modulation theory. Carbone highlights in [38] that models as the one above that do not take unbalanced conditions in account may lead to a harmonic underestimation and thus should be utilized with care.

## 8.2 3-level Voltage Source Converter Variable Speed Drive

A passive front-end, 3-level, neutral-point-clamped (NPC), pulse-width-modulated (PWM), voltage source converter (VSC) VSD will be analyzed [1] To develop a suitable harmonic model for the aforementioned VSD, the present section first introduces the converter topology, then provides an overview of different models found in literature, before a suitable model is developed by combining several of the existing concepts.

Figure 8.5 depicts the converter topology. It consists of a passive front-end (diode rectifier), a PWM inverter and a capacitive DC link that connects the two converters. The rectifier converts the AC power to an unregulated DC voltage which is smoothened by the DC link capacitance. The PWM-Inverter modulates the DC voltage to create a magnitude and frequency adjustable three-phase voltage used to control the machine. Figure 8.5a displays three possible passive front-end configurations for which several 6-pulse rectifiers are connected in series to form a higher pulse number rectifier (12-, 18-, 24-pulse, respectively) for a 3 phase input. Figure 8.5b presents the DC link and 3-level NPC PWM Inverter.

For both converters, rectifier as well as the PWM inverter, a wide variety of analytical harmonic models are available. For the rectifier, on the one hand, it should

[1] Most of ILF Consulting Engineers' projects, e.g. gas compressor station in Egtved (DK), Neustift (AU) and Baumgarten (AU), apply a 12/18/24 pulse version of this converter topology.

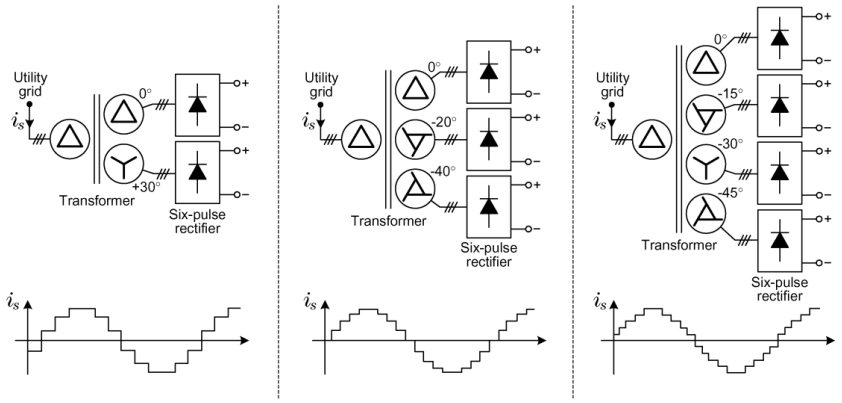


(a) Passive front-end, 12-, 18- and 24-pulse rectifier

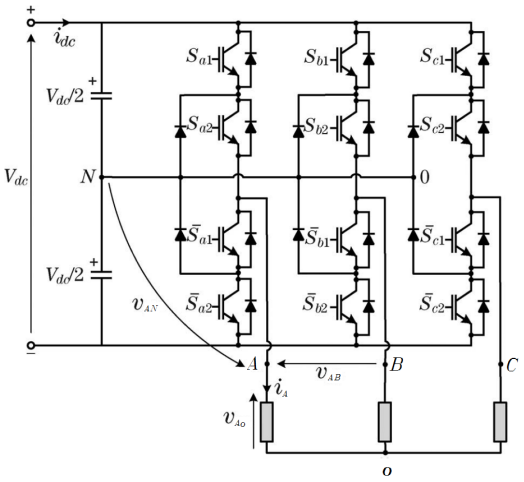


(b) DC link and 3-level NPC PWM inverter

Figure 8.5: Diagram of passive front-end 3-level NPC PWM VSC VSD [8].

be noted that even though the circuit seems rather trivial, its harmonic modeling is not a simple task. The most basic analytic model is the so called ideal model "1/h" which assumes perfect current pulse trains, i.e. infinite slew rate and constant magnitude, during a $\frac{2\pi}{p}$-interval, where $p$ is the rectifiers pulse number [11]. This model is very limited in accuracy, as it neglects commutation and load conditions. It may drastically underestimate the harmonic content, especially the magnitude of $5^{th}$ and $7^{th}$ harmonics [39]. More advanced analytical models, such as presented

in [40, 41], represent the diode bridge by its voltage switching functions. Switching functions relate the AC side voltage to the DC voltage as they define the conducting states of the diodes. Other models, such as [19], represent the rectifier circuit by differential equations. The modeling of the PWM-Inverter, on the other hand, is even more complex, as the harmonic content additionally depends on the applied modulation strategy, e.g. naturally sampled PWM, Direct Torque Control (DTC) PWM or Harmonic Elimination PWM to mention a few. Holmes [10] and Evans [42] describe two different approaches based on switching functions.

Publications which present models of the entry drive system - rectifier, DC link and inverter - often focus solely on the rectifier and DC link and neglect the inverter as a source of line-side harmonic distortion. This simplification is justified by the fact that the DC link represents a shunt filter for harmonics of higher orders and is legitimate in many applications. In such models the inverter and DC link can be represented as single series-impedance [19], or as a series-impedance with a constant back-emf [43], or a current source [44]. This simplification, however, goes along with the negligence of interharmonics as they are predominately caused by the modulation of rectifier and inverter harmonics [15].

If interharmonics have to be taken into account - which [19] suggests in case of high power drives - the inverter stage and possible unbalanced conditions should also be modeled [20, 38].

No reasearch on a 3-level VSD topology was found.

A model based on Jiang's approach of space vector representation that also incorporates unbalanced motor conditions is presented in [45]. The rectifier is modeled by its switching functions, the DC link as a parallel impedance, and the converter as a parallel connected harmonic current source. The current source spectrum is computed based on switching functions of the PWM Inverter and an assumed unbalanced three-phase load current.

The most advanced model encountered includes model refinements as non-ideal commutation, unbalanced supply voltages and a state-space representation of the induction machine, described in [9]. Both rectifier and inverter are modeled by its voltage and current switching functions. The DC link is represented as simple shunt impedance.

In order to assess of the effects on the harmonic content of each of those model refinements (Unbalanced supply conditions, state-space representation of the induction machine, and non-ideal rectifier commutation), the cases discussed in [9] can be compared to each other and also to [15] - for the case of commutation modeling, as both papers analyze the same VSD. THD and TIHD indices are used to evaluate the refinements' influence on the harmonic and interharmonic spectrum, respectively. For each refinement, a case with and without the refinement is listed. To benchmark the improvement across refinements, a relative change,

$$\frac{THD_{refinemant} - THD_{no-refinement}}{THD_{refinement}}$$

is calculated for each case.

For the model refinement supply voltage representation, Table 8.1 (based on values of model "Proposed approach" of Figure 12 of [9]) presents THD and TIHD for a balanced supply voltage ($d_2$[2]$= 0\%$) and an unbalanced voltage ($d_2 = 5\%$). From Table 8.1, it can be seen that an unbalanced supply voltage can severely increase THD as well as TIHD. Neglecting unbalanced supply voltage conditions would thus lead to a significant underestimation of the harmonic spectrum.

For the model refinement state-space representation, the case of a simplified model (motor represented as back-emf and series impedance) is compared to a state-space model. The results are presented in Table 8.2. A state-space representation of the

[2] $d_2$ is the ratio of negative-sequence component to the positive-sequence component with zero relative phase angle, $d_2 = \frac{V^-}{V^+}$ì00%

machine generally increases the harmonic and interharmonic distortion as it provides less damping than the simplified model [9]. The change, however, is minor (THD increase by 4.8%, increase of TIHD by 7.9%). The relative change of this refinement is small compared to the refinement of voltage supply.

Also in the case of non-ideal commutation, a model including commutation effects [9] and a model neglecting it [15] was chosen for comparison. For [15], there are no THD and TIHD values available. In order to compare the models, an underestimation index[3] Neglecting commutation leads to a difference in underestimation of 1.9% of the $5^{th}$ and 0.4% of $7^{th}$ order harmonic for the specified simulation conditions.

Table 8.1: Influence of supply voltage representation on THD and TIHD, based on "Proposed model", Figure 12 of [9].

| | Balanced Supply | Unbalanced Supply ($d_2$=5%) | Relative change [%] |
|---|---|---|---|
| THD | 60.3 | 160.4 | 62.4 |
| TIHD | 1.4 | 7.4 | 80.7 |

Table 8.2: Influence of machine model on THD and TIHD, based on comparisson of "Proposed model" with "Proposed model (w/o)" of Figure 17.a and 17.b. of [9].

| | Simplified Model | State-Space Model | Relative change [%] |
|---|---|---|---|
| THD | 86.0 | 90.4 | 4.8 |
| TIHD | 3.6 | 3.9 | 7.9 |

Based on the above comparison, a model that takes unbalanced supply conditions and commutation effect into account, but neglects the state-space machine representation, is chosen for this thesis. The choice for the simpler machine model is

[3]Based on a difference between the model's prediction and a reference laboratory measurement, normalized by the measurement, the underestimation index is defined as $underest. = \frac{I_{h,Meas.} - I_{h,Model}}{I_{h,Meas.}}$ .

Table 8.3: Influence of commutation phenomenon of rectifier on harmonic spectrum, values from ”Proposed model (w/o)” of Figure 16.a of [9] and "Proposed approach" of Figure 8 of [15].

| | Without commutation | | | With commutation | | |
|---|---|---|---|---|---|---|
| h | Model [p.u] | Meas. [p.u] | underest. | Model [p.u] | Meas. [p.u.] | underest. |
| $5^{th}$ | 58.3 | 66.2 | 12.0 | 48.6 | 54.1 | 10.1 |
| $7^{th}$ | 31.1 | 33.9 | 8.0 | 33.7 | 36.5 | 7.6 |
| $11^{th}$ | 7.4 | 8.1 | 7.9 | 7.6 | 8.2 | 7.9 |

justified by the the state-representation’s small improvement in accuracy and also by the unavailability of detailed machine parameters needed to implement this refinement.

The model’s main parts are the Rectifier, DC link, Inverter and Machine (see Figure 8.6). The rectifier and Inverter are represented in terms of their current and voltage switching functions. The DC link is modeled solely as a capacitor and the simplified machine model with a back-emf and series impedance is used for the induction machine. It is thus a combination of [15], [9] and [10]. In the following each model

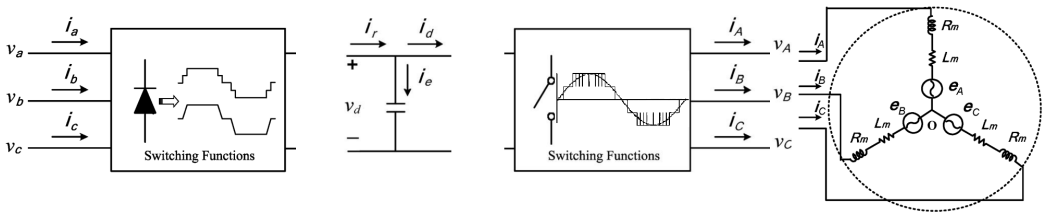


(a) Rectifer (b) DC Link (c) Inverter (d) Machine

Figure 8.6: VSD Model [9].

part is discussed in detail.

### 8.2.1 Rectifier Model

This subsection assumes a 6-pulse rectifier. It is modeled by its voltage and current switching functions. They relate the input voltage $(v_a, v_b, v_c)$ and current $(i_a, i_b, i_c)$ quantities to the corresponding output quantities $v_d$ and $i_r$, respectively:

$$v_d = \sum_k S_v k \cdot v_k, \quad k = a, b, c \tag{8.13}$$

$$i_k = S_{ik} \cdot i_r, \quad k = a, b, c. \tag{8.14}$$

Figure 8.7 shows the voltage $S_{va}$ and current $S_{ia}$ switching functions for phase a when the source resistance, $R_s$, is negligable and a smooth DC current is assumed. The switching functions can be represented in terms of its Fourier coefficients as [9]

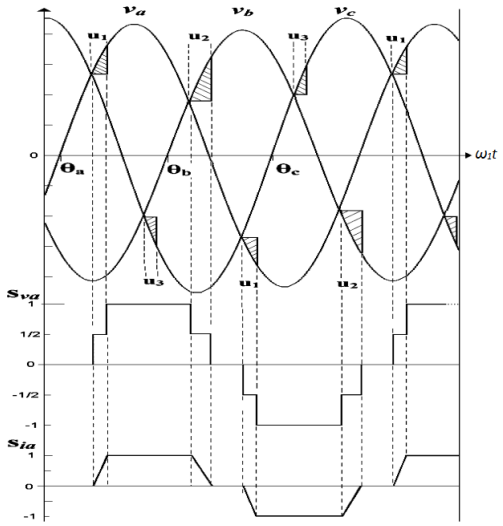


Figure 8.7: 6-pulse rectifier voltage and current switching functions [9].

$$S_{va} = \sum_{\substack{n \in odd \\ n>0}} (A^n_{va} \cos n\omega_1 t + B^n_{va} \sin n\omega_1 t) \tag{8.15}$$

$$S_{ia} = \sum_{\substack{n=6p\pm1 \\ P=1,2,...}} (A^n_{ia} \cos n\omega_1 t + B^n_{ia} \sin n\omega_1 t) \tag{8.16}$$

where the voltage Fourier coefficients can be found as [9]:

$$A^n_{va} = \frac{-1}{n\pi}[\sin(n\sigma_1 + nu_1) - \sin(n\sigma_2 + nu_2) + \sin n\sigma_1 - \sin n\sigma_2] \tag{8.17}$$

$$B_{va}^{n} = \frac{1}{n\pi}[\cos(n\sigma_1 + nu_1) - \cos(n\sigma_2 + nu_2) + \cos n\sigma_1 - \cos n\sigma_2] \tag{8.18}$$

with

$$u_1 = \cos^{-1}\left\{1 - \frac{2X_s I_d}{[V_a^2 + V_c^2 - 2V_a V_c \cos(\theta_c - \theta_a)]^{\frac{1}{2}}}\right\} \tag{8.19}$$

$$u_2 = \cos^{-1}\left\{1 - \frac{2X_s I_d}{[V_a^2 + V_b^2 - 2V_a V_b \cos(\theta_a - \theta_b)]^{\frac{1}{2}}}\right\} \tag{8.20}$$

$$\sigma_1 = tan^{-1}\left(\frac{V_a \sin\theta_a - V_c \sin\theta_c}{V_a \cos\theta_a - V_c \cos\theta_c}\right) \tag{8.21}$$

$$\sigma_2 = tan^{-1}\left(\frac{V_b \sin\theta_b - V_a \sin\theta_a}{V_b \cos\theta_b - V_a \cos\theta_a}\right) \tag{8.22}$$

where $X_s$ is the supply reactance.

The current Fourier coefficients are defined by [9]

$$\begin{aligned}
A_{ia}^{n} =& \frac{2}{\pi}\left\{\frac{1}{n}[\sin n(\sigma_2 + u_2) - \sin n(\sigma_1 + u_1)]\right\} \\
&+ \frac{1}{1 - \cos u_1} \\
&\cdot \left[\frac{1}{n}(\sin n(\sigma_1 + u_1) - \sin n\sigma_1)\right. \\
&\quad - \frac{1}{2(n+1)}(\sin(n\sigma_1 + (n+1)u_1) - \sin n\sigma_1) \\
&\quad \left. - \frac{1}{2(n-1)}(\sin(n\sigma_1 + (n-1)u_1) - \sin n\sigma_1)\right] \\
&+ \frac{1}{1 - \cos u_2} \\
&\cdot \left[\frac{1}{n}(\sin n\sigma_2 - \sin n(\sigma_2 - u_2))\right. \\
&\quad \cdot (\sin(n\sigma_2 + (n+1)u_2) - \sin n\sigma_2) - \frac{1}{2(n-1)} \\
&\quad \left. \cdot (\sin(n\sigma_2 + (n-1)u_2) - \sin n\sigma_2)\right]
\end{aligned} \tag{8.23}$$

$$
\begin{aligned}
B_{ia}^{n} =& \frac{2}{\pi}\left\{\frac{1}{n}[\cos n(\sigma_1+u_1)-\cos n(\sigma_2+u_2)]\right\} \\
&+\frac{1}{1-\cos u_1} \\
&\cdot\left[\frac{1}{n}\left(\cos n\sigma_1+\cos n(\sigma_1+u_1)\right)\right. \\
&\quad -\frac{1}{2(n+1)}(\cos(n\sigma_1+(n+1)u_1)+\cos n\sigma_1) \\
&\quad \left.-\frac{1}{2(n-1)}(\cos(n\sigma_1+(n-1)u_1)+\cos n\sigma_1)\right] \\
&+\frac{1}{1-\cos u_2} \\
&\cdot\left[\frac{-1}{n}\left(\cos n\sigma_2+\cos n(\sigma_2+u_2)\right)\right. \\
&\quad +\frac{1}{2(n+1)}(\cos(n\sigma_2+(n+1)u_2)+\cos n\sigma_2) \\
&\quad \left.+\frac{1}{2(n-1)}(\cos(n\sigma_2+(n-1)u_2)-\cos n\sigma_2)\right] \quad .
\end{aligned}
\tag{8.24}
$$

The Fourier coefficients for phase b and c are the same and the switching functions $S_{vb}, S_{vc}, S_{ib}$ and $S_{ic}$ are obtained by replacing $\omega_1 t$ in Equations 8.15 and 8.16 by $(\omega_1 t - \frac{2\pi}{3})$ for phase b and $(\omega_1 t - \frac{4\pi}{3})$ for phase c, respectively.

### 8.2.2 DC link Model

The DC link is modeled as shunt capacitor, as shown in Figure 8.6b), where the current into the capacitor is expressed as

$$i_c = C_d \frac{\mathrm{d}v_d}{\mathrm{d}t} \quad . \tag{8.25}$$

The relation of the three currents $i_r, i_c$ and $i_d$ at the node is

$$i_r = i_d + i_c \quad . \tag{8.26}$$

### 8.2.3 Inverter Model

The inverter is assumed to be naturally modulated (comparison of a reference signal with a carrier signal) with a phase disposition (PD) carrier arrangement.

The inverter is modeled by its voltage and current switching function, while relate the DC link quantities ($v_d$ and $i_d$) to the corresponding output quantities ($v_{AN}, v_{BN}, v_{CN}$ and $I_A, I_B, I_C$).

$$v_{UN} = S_{UN} \cdot v_d, \quad U = A, B, C \tag{8.27}$$

$$i_d = \sum_U S_{iU} \cdot i_U, \quad U = A, B, C \tag{8.28}$$

The voltage switching functions are derived based on Holmes' analytic representation of modulated waveforms [10]. The most important steps of derivation are shown in the following. A complete derivation is presented in [10], p. 469-481.

Any periodically modulated voltage can be expressed by

$$\begin{aligned} f(t) = \frac{A_{00}}{2} &+ \sum_{n=1}^{\infty} [A_{0n} \cos(n[\omega_1 t + \theta_1]) + B_{0n} \sin(n[\omega_1 t + \theta_1])] \\ &+ \sum_{m=1}^{\infty} [A_{m0} \cos(m[\omega_c t + \theta_c]) + B_{m0} \sin(m[\omega_c t + \theta_C])]) \\ &+ \sum_{m=1}^{\infty} \sum_{\substack{n=\infty \\ (n \neq 0)}}^{\infty} \Big[ A_{mn} \cos(m[\omega_c t + \theta_c] + n[\omega_1 t + \theta_1]) \\ &\qquad + B_{mn} \sin(m[\omega_c t + \theta_c] + n[\omega_1 t + \theta_1]) \Big] \end{aligned} \tag{8.29}$$

where

$$C_{mn} = A_{mn} + jB_{mn} = \frac{1}{2\pi^2} \int_{-\pi}^{\pi} \int_{-\pi}^{\pi} f(x, y) e^{j(mx+ny)} \mathrm{d}x \mathrm{d}y \tag{8.30}$$

and where $x = \omega_c t$, $y = \omega_1 t$. Here, $\omega_c$, and $\omega_1$ are carrier and reference signal angular frequency, respectively.

To find the Fourier coefficients of Equation 8.30, the two dimensional function $f(x, y)$ must be defined. This definition can be visualized by a so called unit cell which depicts the boarders in the $x$,$y$ - plane in which the function is constant. The unit cell of a naturally sampled 3-level inverter with phase disposition (PD) carriers is shown in Figure 8.8.

In case of a 3-level inverter the function $f(x, y)$ can have three voltage levels, i.e

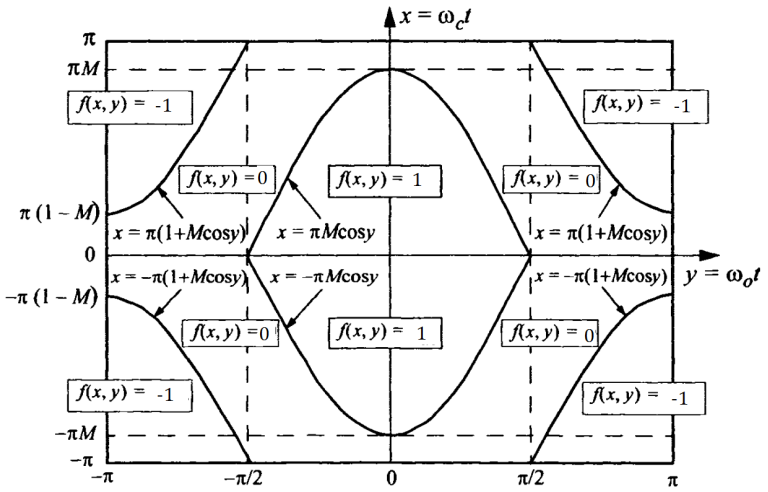


Figure 8.8: Unit cell of a 3-level naturally sampled PWM-Inverter with phase disposition carriers. [10]

$+1(=+V_{dc})$, 0, and $-1(=-V_{dc})$. The boarders of the area in the $x$,$y$ - plane in which the function takes each of those values is defined in the unit cell. Equation 8.30 can thus be rewritten as

$$
\begin{aligned}
C_{mn} = \frac{1}{2\pi^2}\Bigg[ & \int_{-\frac{\pi}{2}}^{\frac{\pi}{2}} \int_{-\pi M\cos y}^{\pi M\cos y} e^{j(mx+ny)}\mathrm{d}x\mathrm{d}y \\
& - \int_{-\pi}^{-\frac{\pi}{2}} \left\{ \int_{-\pi}^{-\pi(1+Mcosy)} e^{j(mx+ny)}\mathrm{d}x + \int_{\pi(1+Mcosy)}^{\pi} e^{j(mx+ny)}\mathrm{d}x \right\}\mathrm{d}y \qquad (8.31) \\
& - \int_{\frac{\pi}{2}}^{\pi} \left\{ \int_{-\pi}^{-\pi(1+Mcosy)} e^{j(mx+ny)}\mathrm{d}x + \int_{\pi(1+Mcosy)}^{\pi} e^{j(mx+ny)}\mathrm{d}x \right\}\mathrm{d}y \Bigg]
\end{aligned}
$$

which may be further reduced to

$$
C_{mn} = \frac{1}{2\pi^2}\{1-\cos([n+m]\pi)\} \int_{-\frac{\pi}{2}}^{\frac{\pi}{2}} \int_{-\pi(1+Mcosy)}^{\pi(1+Mcosy)} e^{j(mx+ny)}\mathrm{d}x\mathrm{d}y \quad . \qquad (8.32)
$$

Evaluating Equation 8.32 for $m = n = 0$ results in

$$
C_{00} = 0 \qquad (8.33)
$$

which represents the DC component, for $m = 0, n = 1$ in

$$C_{01} = M \tag{8.34}$$

which represents the fundamental component. For $m > 0, n = 0$ it results in

$$C_{m0} = -\frac{4}{m\pi^2}(1 - \cos m\pi) \sum_{k=1}^{\infty} \frac{J_{2k-1}(m\pi M)}{[2k-1]} \tag{8.35}$$

where $J_{2k-1}$ is the Bessel function of $(2k-1)^{th}$ order and that represents the carrier harmonics. For $m > 0, n \neq 0$ it results in

$$\begin{aligned} C_{mn} =& \frac{1}{m\pi}\{1 - \cos([n+m]\pi)\} \\ & \cdot \Bigg[ J_n(m\pi M)\sin(n\frac{pi}{2}) \\ & \quad + \frac{4}{\pi}\sum_{k=1}^{\infty} J_{2k-1}(m\pi M)\frac{[2k-1]\cos n\frac{\pi}{2}}{[2k-1+n][2k-1-n]}\Big|_{|n|\neq 2k-1} \Bigg] \end{aligned} \tag{8.36}$$

which represents the sideband harmonics.

By combining Equation 8.33-8.36 with Equation 8.29, the voltage switching function of phase leg $A$ $S_{AN}$ may be expressed as:

$$\begin{aligned} S_{AN} =& M\cos(\omega_1 t) \\ & + \frac{8}{\pi^2}\sum_{m=1}^{\infty}\frac{1}{2m-1}\sum_{k=1}^{\infty}\frac{J_{2k-1}([2m-1]\pi M)}{[2k-1]}\cos([2m-1]\omega_c t) \\ & + \frac{2}{pi}\sum_{m=1}^{\infty}\frac{1}{2m}\sum_{n=-\infty}^{\infty} J_{2n+1}(2m\pi M)\cos(n\pi)\cos(2m\omega_c t + [2n+1]\omega_1 t) \\ & + \frac{8}{\pi^2}\sum_{m=1}^{\infty}\frac{1}{2m-1}\sum_{\substack{n=\infty \\ (n\neq 0)}}^{\infty}\sum_{k=1}^{\infty}\frac{J_{2k-1}([2m-1]\pi M)[2k-1]\cos n\pi}{[2k-1+2n][2k-1-2n]} \\ & \qquad \cdot \cos([2m-1]\omega_c t + 2n\omega_1 t) \quad . \end{aligned} \tag{8.37}$$

The corresponding switching functions for phase $B$ and $C$ are obtained by setting $\theta_1$ in Equation 8.29 to $-\frac{2\pi}{3}$ and $-\frac{4\pi}{3}$, respectively.

The phase-midpoint voltage $v_{AN}(t)$ (see Figure 8.5b) can now be calculated by Equation 8.27. The line-to-line voltage of the converter is obtained by the subtrac-

tion of two phase-to-midpoint voltages, e.g. $v_{AB}(t) = v_{AN}(t) - v_{BN}(t)$.

Next, the current switching function shall be derived based on the assumption of a lossless inverter and balanced load conditions, which, following Kirchoff's voltage law, requires the following equality to hold true:

$$v_d i_d = v_{Ao} i_A + v_{Bo} i_B + v_{Co} i_C. \tag{8.38}$$

Here, $v_{Ao}, v_{Bo}$ and $v_{Co}$ are the inverter output phase voltages with respect to the load mid-point and are defined in Equation 8.46. It can be rewritten as

$$i_d = \frac{v_{Ao}}{v_d} i_A + \frac{v_{Bo}}{v_d} i_B + \frac{v_{Co}}{v_d} i_C \tag{8.39}$$

$$= S_{iA} i_A + S_{iB} i_B + S_{iC} i_C \tag{8.40}$$

$$= \sum_U S_{iU} \cdot i_U, \qquad U = A, B, C \tag{8.41}$$

where $S_{iA}, S_{iB}$ and $S_{iC}$ are the current switching functions of the inverter and thus are defined as

$$S_{iU} = \frac{v_{Uo}}{v_d}. \tag{8.42}$$

.

### 8.2.4 Machine Model

As depicted in Figure 8.6d the induction machine is modeled as a back-emf with a series impedance ($e_A$ and $Z_m$). Assuming balanced machine operation, the three-phase voltages must sum to zero

$$v_{Ao} + v_{Bo} + v_{Co} = 0. \tag{8.43}$$

The relation of inverter output voltage $v_{AN}, v_{BN}$ and $v_{CN}$ to the load mid-point voltage $v_{Ao}, v_{Bo}$ and $v_{Co}$ is given by

$$v_{Uo} = V_{UN} - V_{nN}, \qquad U = A, B, C. \tag{8.44}$$

Manipulation of Equations 8.2.4 and eq:safran2allows the inverter mid-point to load mid-point voltage, $V_{nN}$, to be expressed as a function of the inverter output

voltages as:

$$V_{nN} = \frac{1}{3}(V_{AN} + V_{BN} + V_{CN}) \quad . \tag{8.45}$$

The phase A voltage $v_{Ao}$ applied to the machine is thus be found to be

$$v_{Ao} = \frac{2}{3}v_{AN} - \frac{1}{3}(v_{BN} + V_{CN}). \tag{8.46}$$

The other phase voltages are similarly derived. The machine currents are given by

$$\begin{aligned} i_A &= \frac{v_{Ao} - e_A}{Z_m} \\ i_B &= \frac{v_{Bo} - e_B}{Z_m} \\ i_C &= \frac{v_{Co} - e_C}{Z_m} \quad . \end{aligned} \tag{8.47}$$

### 8.2.5 Model analysis

After each model part has been defined, the analysis of the line-side harmonics can be summarized in the following eight steps:

*1*) Specify the source voltages $v_a, v_b, v_c$ (balanced or unbalanced) and the back-emf of the machine $e_a, e_b, e_c$

*2*) Calculate the DC link voltage $v_d$ by applying the rectifier voltage switching functions to the sources voltages, Equation 8.13 and 8.15.

*3*) Calculate the inverter output voltages $v_A, v_B, v_C$ by applying the inverter voltage switching functions to the DC link voltage, Equation 8.37 and 8.27

*4*) Calculate the machine currents $i_A, i_B, i_C$ by using the simplified machine model, Equation 8.47

*5*) Calculate the DC link current $i_d$ by applying the inverter current switching functions to the machine currents, Equation 8.39

*6*) Calculate the front-end output current $i_r$ by the use of the DC link model, Equation 8.26 and 8.25

*7*) Calculate the line currents $i_a, i_b, i_c$ by applying the rectifier current switching functions to front-end output current, Equation 8.14 and 8.16

*8*) Calculate the line current harmonic content by the use of a Fast Fourier Transform (FFT) algorithm

# Chapter 9

# Harmonic Transformer Modeling

To make the above discussion of harmonic source modeling valuable for high power VSDs applications, a mean to transfer the 6-pulse spectrum to a p-pulse spectrum has to be found. This chapter therefore discusses multi-winding transformer harmonic modeling.

The phase shift of multi-winding transformer, according Equation 5.1, is achieved by an appropriate configuration of primary and "secondary" windings. A phase shift of 30°, for example, can be achieved by a combination of a $\Delta$- and Y-winding. This and other winding configurations are denoted by so called transformer vector groups, which consist of two letters and a number. The first letter indicates the connection of the primary (HV) winding and is capitalized, the second letter describes the secondary (LV) winding configuration and is lower-case. Possible letters are Y,D,Z (or y,d,z accordingly) and indicate wye (or Y), delta (or $\Delta$) and zigzag configurations, respectively. The number indicates the phase shift between HV- and LV-side-voltage and stands for the multiple of 30 ° by which the LV-side- is lagging the HV-side-voltage in an anticlockwise direction. The vector group Yd1 thus refers to a transformer with a Y-connected primary and a $\Delta$-connected secondary winding where the secondary voltage is lagging the primary voltage by 30 °. All Y/$\Delta$, $\Delta$/Y, Y/Y and $\Delta$/$\Delta$ vector groups that comply with this standard are shown in Figure 9.1.

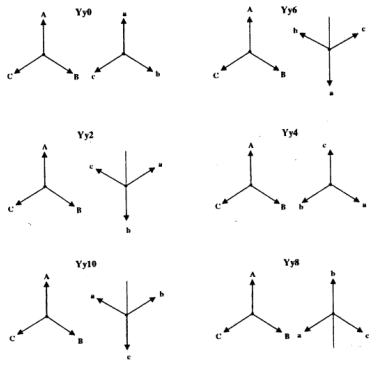


(a) Yy vector groups

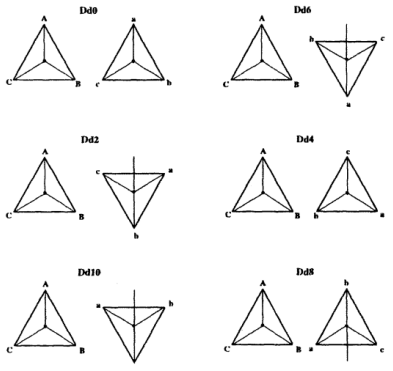


(b) Dd vector groups

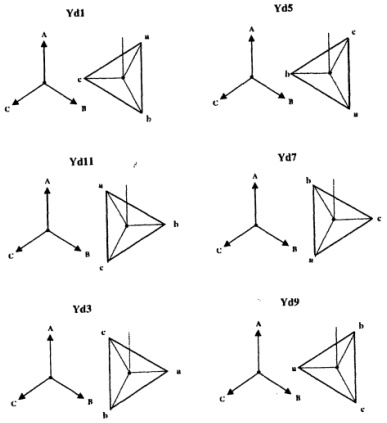


(c) Yd vector groups

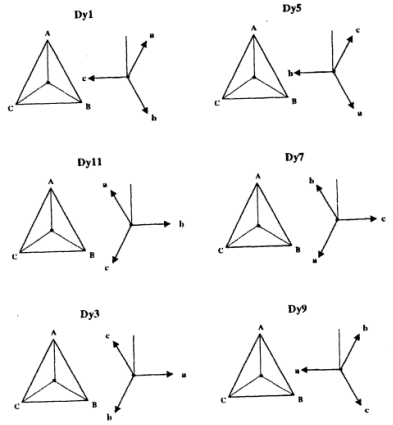


(d) Dy vector groups

Figure 9.1: Vector groups of Y/$\Delta$ configurations [11]

Depending on the vector group, there are different relations between primary and secondary quantities. For each vector group a transformation matrix can be derived that, together with the transformation ratio $\alpha$, fully determines the relation of primary and secondary quantities of an ideal transformer [11]. The transformation ratio $\alpha$ is the ratio of secondary to primary voltage and is defined as

$$\alpha = kN \tag{9.1}$$

where $N$ is the turn ratio of secondary to primary winding and k is defined as

$$k = \begin{cases} \sqrt{3}, & \Delta - Y - \text{transformers} \\ \frac{1}{\sqrt{3}}, & Y - \Delta - \text{transformers} \\ 1, & \Delta - \Delta - or Y - Y - \text{transformers} \end{cases} . \tag{9.2}$$

In the following, the transformation matrix for a Dy1 two-winding transformer is derived. For a Dy1 transformer, the primary currents are

$$\begin{aligned} I_A &= I_{AC} - I_{BA} \\ I_B &= I_{BA} - I_{CB} \\ I_C &= I_{CB} - I_{AC} \end{aligned} \tag{9.3}$$

or in matrix form as

$$\begin{aligned} \boldsymbol{I}_{ABC} = \begin{pmatrix} I_A \\ I_B \\ I_C \end{pmatrix} &= \begin{pmatrix} 1 & -1 & 0 \\ 0 & 1 & -1 \\ -1 & 0 & 1 \end{pmatrix} \begin{pmatrix} I_{AC} \\ I_{BA} \\ I_{CB} \end{pmatrix} \\ &= \frac{\alpha}{\sqrt{3}} \begin{pmatrix} 1 & 0 & -1 \\ -1 & 1 & 0 \\ 0 & -1 & 1 \end{pmatrix} \begin{pmatrix} I_a \\ I_b \\ I_c \end{pmatrix} . \end{aligned} \tag{9.4}$$

The transformation can be generalized to

$$\boldsymbol{I}_{ABC} = \alpha \cdot \boldsymbol{T} \cdot \boldsymbol{I}_{abc} \tag{9.5}$$

where $\boldsymbol{T}$ is the transmission matrix and thus, in case of a Yd1 vector group, defined as

$$\boldsymbol{T} = \frac{1}{\sqrt{3}} \begin{pmatrix} 1 & -1 & 0 \\ 0 & 1 & -1 \\ -1 & 0 & 1 \end{pmatrix} . \tag{9.6}$$

Through similar techniques, all other Y/$\Delta$ vector group transformation matrices can be derived. The transformation of primary and secondary quantities for two winding Y/$\Delta$ transformers are shown in Figure 9.2. The arrow in the Figure indicates the transformation direction, either primary to secondary transformation, or vice versa.

The number above the arrow refers to vector group number and thus is related to the phase shift of the winding configuration.

The transformation matrices for Δ-Δ and Y-Y configurations are now derived.

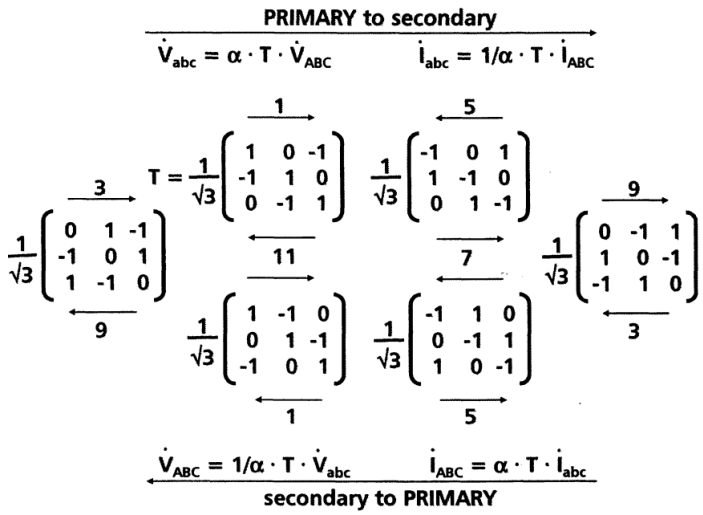


Figure 9.2: Voltage and current transformation for Δ/Y vector groups of two winding transformers [11].

For a Yy0 transformer, Kirchoff's current law requires that one can write

$$I_A + I_B + I_C = 0, \tag{9.7}$$

which leads to

$$\begin{aligned} 2I_A - I_B - I_C &= 3I_A \\ 2I_B - I_C - I_A &= 3I_B \\ 2I_C - I_A - I_B &= 3I_C \quad . \end{aligned} \tag{9.8}$$

If represented in matrix form this can be re-written to

$$\begin{pmatrix} I_A \\ I_B \\ I_C \end{pmatrix} = \frac{1}{3}\begin{pmatrix} 2 & -1 & -1 \\ -1 & 2 & -1 \\ -1 & -1 & 2 \end{pmatrix}\begin{pmatrix} I_A \\ I_B \\ I_C \end{pmatrix} \quad . \tag{9.9}$$

In the case of a Yy0 transformer $k = 1$ and thus $\alpha = N$. Therefore from Equation 9.9 it follows

$$\begin{pmatrix} I_A \\ I_B \\ I_C \end{pmatrix} = \frac{\alpha}{3} \begin{pmatrix} 2 & -1 & -1 \\ -1 & 2 & -1 \\ -1 & -1 & 2 \end{pmatrix} \begin{pmatrix} I_a \\ I_b \\ I_c \end{pmatrix} \quad . \tag{9.10}$$

The transformation can be generalized to

$$\boldsymbol{I}_{ABC} = \alpha \cdot \boldsymbol{T_e} \cdot \boldsymbol{I}_{abc} \tag{9.11}$$

where $\boldsymbol{T_e}$ is the transmission matrix and thus in case of a Yy0 vector group defined as

$$\boldsymbol{T_e} = \frac{1}{\sqrt{3}} \begin{pmatrix} 2 & -1 & -1 \\ -1 & 2 & -1 \\ -1 & -1 & 2 \end{pmatrix} \quad . \tag{9.12}$$

By similar derivations, all other Y/Y and $\Delta/\Delta$ vector group transformation matrices can be derived. The transformation of primary and secondary quantities for two winding these transformers can be summarized as shown in Figure 9.3.

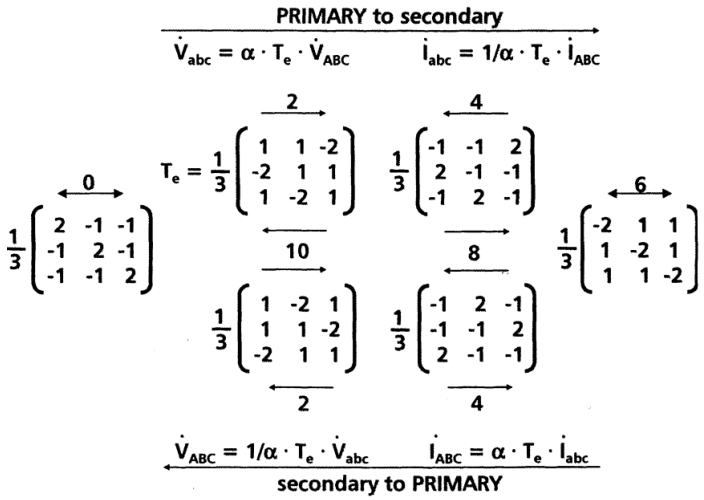


Figure 9.3: Voltage and current transformation for Y/Y and $\Delta/\Delta$ vector groups [11].

Figure 9.4 shows the results of the application of this modeling approach to an harmonic spectrum of unity amplitude for harmonics $h = 1, 5, 11, 17, 23, 29, 35$. In

case of a phase shift according Equation 5.1, the $5^th$ / $7^th$ and $5^th$ / $7^th$, $11^th$ / $13^th$ for 12-pulse- and 18-pulse-rectifiers, respectively, cancell entierly. Is the phase shift $\delta'$ decreased, the characteristic harmonics decrease too while non-characterisitc harmonics increase. The proposed model is thus capable of modeling multi-winding transformers as well as representing the phase shift mitigation measure as described earlier in this thesis. The analysis underlying Matlab code can be found in Appendix B.

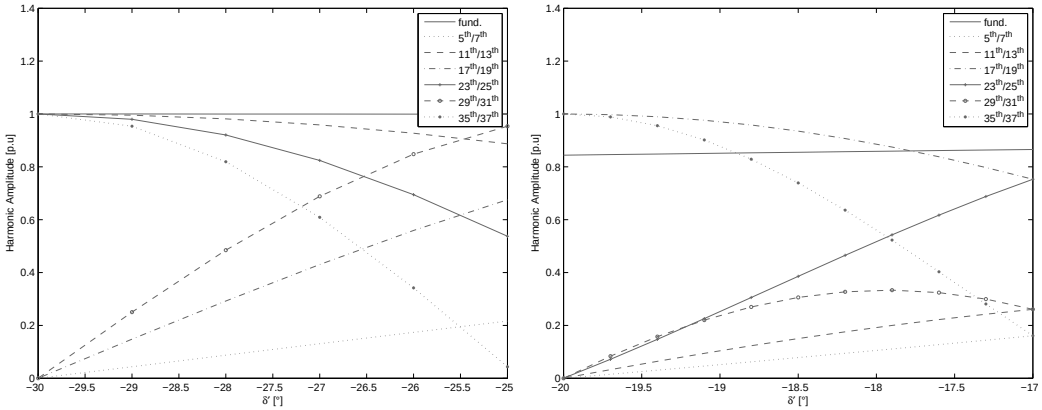


(a) 12-pulse rectifier

(b) 18-pulse rectifier

Figure 9.4: Harmonic amplitudes as a function of phase shift angle $\delta'$

As discussed in Section 5.1, in order to find the harmonic current spectrum of the VSD as an entire system, each 6-pulse current spectrum (see Subsection 8.2) has to be transferred to the transformer's primary side. A imaginable process of generating a p-pulse spectrum is thus the following:

*1*) Chose the turn ratio of the winding $Nn$ that is in phase with the primary winding $N1$ as $\frac{N1}{Nn} = \frac{p}{6}$ and all other "secondary" winding ratios so that their secondary voltage levels are the same as the one of $Nn$.

*2*) Calculate harmonic spectrum of VSD with a 6-pulse rectifier according Section 8.2 while using partial nominal load $P_{6,VSD,partial} = \frac{P_{p,VSD}}{(p/6)}$.

*3*) Add the according phase shift to the "secondary" winding spectra to fulfill Equation 5.1.

*4*) Use the transformation matrices to transform the spectra to the primary side

*5*) Add all to the primary referred currents in order to get the primary current.

The validity and accuracy of it has to be verified.

# Chapter 10

# Conclusion and Outlook - Harmonic Modeling of Variable Speed Drives

To perform a harmonic study based on current injection, the harmonic spectrum of the VSD input currents must be known. A harmonic model of the VSD, which depends on its topology, must therefore be formulated. A wide variety of analytical models for 6-pulse passive front-end VSDs are described in literature. The most accurate analytical models use current and voltage switching functions adapted from modulation theory.

An evaluation of passive front-end VSC VSD harmonic models was presented. It was determined that a state-space representation of the machine only slightly improves the prediction accuracy of harmonic content. Load side harmonics have to be included for high power VSDs as they are the main reason for interharmonic generation. The commutation effect of the front-end was found to have a significant influence on low-order harmonic amplitudes and thus should be included in a harmonic model. Finally, no research on 3-level VSC PWM inverters influence on the harmonic content was found.

Based on the aforementioned findings, a model for 6-pulse, passive front-end, two-level VSC VSD was adapted to a 3-level topology. This was done under the assump-

tion that the harmonic spectrum of a 3-level VSD differs from a 2-level spectrum, mainly in terms of interharmonics.

In order to be valuable for high-power VSD harmonic studies, a 6-pulse harmonic model has been adapted to a p-pulse model. To enable this modification, a multi-winding transformer model was discussed in this work. This model enables for an arbitrary inter-winding phase shift to exist, which makes it suitable to also model the harmonic mitigation based on the phase shift method. The presented model is applicable to three- and four-winding transformers. A three-winding model was implemented in Matlab and proved the model's value for its intended purpose.

To determine the current spectrum of a p-pulse VSD, it must be verified that a valid spectrum can be obtained by generating a 6-pulse spectrum for a load $P_{6,VSD} = \frac{P_{p,VSD}}{(p/6)}$ and phase shifting it according to the transformer configuration to finally obtain the spectrum of the p-pulse system.

To address the remaining uncertainties, the following work flow is proposed:

- Implementation of 6-pulse 3-level VSC in Matlab,
- Verification of model properties,
- Verification of the significance of 3-level implementation by comparing the results to [9],
- Verification of assumptions concerning the p-pulse spectrum by comparing the obtained spectrum to a measured spectrum, e.g; measurements of Dr. Walther in Egtved.

If the validity of the harmonic current spectrum has been verified, it can be used to calculate a harmonic study in combination with the presented network representation based on the harmonic injection method as described in this thesis.

# Bibliography


[1] N. Mohan, T. Undeland, and W. Robbins, *Power electronics: converters, applications, and design*, ser. Power Electronics: Converters, Applications, and Design. John Wiley & Sons, 2003, no. v. 1.

[2] B. Walther, "Power Quality Management, EGTVED Compressor Station / Denmark, Harmoinc Filter System 10.0 kV 1500kVAr," *Maschinenfabrik Reinhausen GmbH*, 2011.

[3] T. Rechberger, "Analytische Berechnung des Netzstroms einer ungesteuerten B12-Brueckenschaltung mit kapazitiver Glaettung der Zwischenkreisspannung," *e & i Elektrotechnik und Informationstechnik*, vol. 121, no. 3, pp. 111–117, 2004.

[4] A. Nassif and W. Xu, "Passive Harmonic Filters for Medium-Voltage Industrial Systems: Practical Considerations and Topology Analysis," in *Power Symposium, 2007. NAPS '07. 39th North American*, 2007, pp. 301–307.

[5] D. A. Gonzalez and J. C. Mccall, "Design of Filters to Reduce Harmonic Distortion in Industrial Power Systems," *Industry Applications, IEEE Transactions on*, vol. IA-23, no. 3, pp. 504–511, 1987.

[6] B. Wu, J. Pontt, J. Rodriguez, S. Bernet, and S. Kouro, "Current-Source Converter and Cycloconverter Topologies for Industrial Medium-Voltage Drives," *Industrial Electronics, IEEE Transactions on*, vol. 55, no. 7, pp. 2786 –2797, july 2008.

[7] E. Delaney and R. Morrison, "The Calculation Of Harmonic And Interharmonic Distortion In Current Source Converter Systems," in *Harmonics in Power Systems., ICHPS V International Conference on*, sep 1992, pp. 251 –255.

[8] J. Rodriguez, S. Bernet, B. Wu, J. Pontt, and S. Kouro, "Multilevel Voltage-Source-Converter Topologies for Industrial Medium-Voltage Drives," *Industrial Electronics, IEEE Transactions on*, vol. 54, no. 6, pp. 2930–2945, 2007.

[9] G. Chang, S.-K. Chen, H.-J. Su, and P.-K. Wang, "Accurate Assessment of Harmonic and Interharmonic Currents Generated by VSI-Fed Drives Under Unbalanced Supply Voltages," *Power Delivery, IEEE Transactions on*, vol. 26, no. 2, pp. 1083–1091, 2011.

[10] D. Holmes and T. Lipo, *Pulse Width Modulation for Power Converters: Principles and Practice*, ser. IEEE Press Series on Power Engineering. John Wiley & Sons, 2003.

[11] G. Wakileh, *Power Systems Harmonics: Fundamentals, Analysis and Filter Design*, ser. Power Systems. Springer, 2001.

[12] "IEC (1994) Electromagnetic compatibility (EMC) - Part 2: Environement - Section 4: Compability level in industrial plants for low frequency conducted disturbances," *IEC Standard, 61000-2-4*.

[13] "IEEE Recommended Practices and Requirements for Harmonic Control in Electrical Power Systems," *IEEE Std 519-1992*.

[14] "EN 50160 - Voltage Characteristics in Public Distribution Systems," *EN Standard, 50160*, 2004.

[15] G. Chang and S.-K. Chen, "An analytical approach for characterizing harmonic and interharmonic currents generated by VSI-fed adjustable speed drives," *Power Delivery, IEEE Transactions on*, vol. 20, no. 4, pp. 2585–2593, Oct.

[16] P. G.W. Chang, W.Xu, *IEEE Tutorial on Harmonics Modeling and Simulation, Harmonics Theory*. IEEE Press, New York, 1998.

[17] J. Arrillaga, B. Smith, N. Watson, and A. Wood, *Power System Harmonic Analysis*. Wiley, 1997.

[18] A. Testa, M. Akram, R. Burch, G. Carpinelli, G. Chang, V. Dinavahi, C. Hatziadoniu, W. Grady, E. Gunther, M. Halpin, P. Lehn, Y. Liu, R. Langella, M. Lowenstein, A. Medina, T. Ortmeyer, S. Ranade, P. Ribeiro, N. Watson, J. Wikston, and W. Xu, "Interharmonics: Theory and Modeling," *Power Delivery, IEEE Transactions on*, vol. 22, no. 4, pp. 2335–2348, 2007.

[19] G. Carpinelli, F. Iacovone, A. Russo, P. Varilone, and P. Verde, "Analytical modeling for harmonic analysis of line current of VSI-fed drives," *Power Delivery, IEEE Transactions on*, vol. 19, no. 3, pp. 1212–1224, July.

[20] M. Rifai, T. Ortmeyer, and W. McQuillan, "Evaluation of current interharmonics from AC drives," *Power Delivery, IEEE Transactions on*, vol. 15, no. 3, pp. 1094–1098, 2000.

[21] J. Das, "Passive filters - potentialities and limitations," *Industry Applications, IEEE Transactions on*, vol. 40, no. 1, pp. 232–241, 2004.

[22] S. Ranade and W. Xu, "An overview of harmonics modeling and simulation - Task Force on Harmonics Modeling and Simulation," *IEEE Special Publication, 98TP125-0*, 1998.

[23] T. Ortmeyer, M. Akram, and T. Hiyama, "Harmonic Modeling of Networks - Task Force on Harmonics Modeling and Simulation," *IEEE Special Publication, 98TP125-0*, 1998.

[24] Z. Reinhard, "Power converter circuit," Patent EP 1 622 248 A2, 02 1, 2006.

[25] J. Phipps, "A transfer function approach to harmonic filter design," *Industry Applications Magazine, IEEE*, vol. 3, no. 2, pp. 68–82, 1997.

[26] M. McGranaghan and D. Mueller, "Designing harmonic filters for adjustable-speed drives to comply with IEEE-519 harmonic limits," *Industry Applications, IEEE Transactions on*, vol. 35, no. 2, pp. 312–318, 1999.

[27] "IEEE Guide for Application and Specification of Harmonic Filters," *IEEE Std 1531-2003*, pp. 1–60, 2003.

[28] M. Zamani, M. Moghaddasian, M. Joorabian, S. Seifossadat, and A. Yazdani, "C-type filter design based on power-factor correction for 12-pulse HVDC converters," in *Industrial Electronics, 2008. IECON 2008. 34th Annual Conference of IEEE*, 2008, pp. 3039–3044.

[29] T. Thasananutariya and S. Chatratana, "Planning Study of Harmonic Filter for ASDs in Industrial Facilities," *Industry Applications, IEEE Transactions on*, vol. 45, no. 1, pp. 295–302, 2009.

[30] J. Maza-Ortega, J. Churio-Barboza, and M. Burgos-Payan, "A software-based tool for optimal design of passive tuned filters," in *Industrial Electronics (ISIE), 2010 IEEE International Symposium on*, 2010, pp. 3273–3278.

[31] A. Nassif, W. Xu, and W. Freitas, "An Investigation on the Selection of Filter Topologies for Passive Filter Applications," *Power Delivery, IEEE Transactions on*, vol. 24, no. 3, pp. 1710–1718, 2009.

[32] "IEEE Standard for Shunt Power Capacitors," *IEEE Std 18-2012 (Revision of IEEE Std 18-2002)*, pp. 1–39, 2013.

[33] "IEC (2005) Shunt capacitors for A.C. power systems having a rated voltage above 1000 V - Part 1: General," *IEC Standard, 60871-1-1.*

[34] H. Stemmler, "High-power industrial drives," *Proceedings of the IEEE*, vol. 82, no. 8, pp. 1266 –1286, aug 1994.

[35] R. Bhatia, H. Krattiger, A. Bonanini, D. Schafer, J. Inge, and G. Sydnor, "Adjustable speed drive using single 135000 HP synchronous motor," in *Electric Machines and Drives Conference Record, 1997. IEEE International*, may 1997, pp. TC1/9.1 –TC1/9.3.

[36] J.Arrillaga, "Power System Harmonic Models," in *Proceedings of the International Symposium on Energy Conversion in Power Systems*, 1989, pp. 1–12.

[37] L. Hu and R. Yacamini, "Harmonic transfer through converters and HVDC links," *Power Electronics, IEEE Transactions on*, vol. 7, no. 3, pp. 514 –525, jul 1992.

[38] R. Carbone, A. Testa, D. Menniti, R. Morrison, and E. Delaney, "Harmonic and Interharmonic Distortion in Current Source Type Inverter Drives," *Power Delivery, IEEE Transactions on*, vol. 10, no. 3, pp. 1576 –1583, jul 1995.

[39] S. Hansen, L. Asiminoaei, and F. Blaabjerg, "Simple and advanced methods for calculating six-pulse diode rectifier line-side harmonics," in *Industry Applications Conference, 2003. 38th IAS Annual Meeting. Conference Record of the*, vol. 3, 2003, pp. 2056–2062 vol.3.

[40] M. Sakui, H. Fujita, and M. Shioya, "A method for calculating harmonic currents of a three-phase bridge uncontrolled rectifier with DC filter," *Industrial Electronics, IEEE Transactions on*, vol. 36, no. 3, pp. 434 –440, aug 1989.

[41] M. Sakui and H. Fujita, "An analytical method for calculating harmonic currents of a three-phase diode-bridge rectifier with DC filter," *Power Electronics, IEEE Transactions on*, vol. 9, no. 6, pp. 631 –637, nov 1994.

[42] P. Evans and R. Hill-Cottingham, "DClink current in PWM inverters," *Electric Power Applications, IEE Proceedings B*, vol. 133, no. 4, pp. 217–224, 1986.

[43] R. Carbone, F. De Rosa, R. Langella, A. Sollazzo, and A. Testa, "Modelling of AC/DC/AC conversion systems with PWM inverter," in *Power Engineering Society Summer Meeting, 2002 IEEE*, vol. 2, July, pp. 1004–1009 vol.2.

[44] W. Xu, H. Dommel, M. Hughes, G. Chang, and L. Tan, "Modelling of adjustable speed drives for power system harmonic analysis," *Power Delivery, IEEE Transactions on*, vol. 14, no. 2, pp. 595–601, Apr.

[45] D. Basic, "Input Current Interharmonics of Variable-Speed Drives due to Motor Current Imbalance," *Power Delivery, IEEE Transactions on*, vol. 25, no. 4, pp. 2797–2806, Oct.

[46] Nexans, *Power Cables, 1 to 30kV*, 2012. [Online]. Available: http://http://www.nexans.de/Germany/2012/Starkstrom_DuGB_10okt12_klein_1.pdf

# Part IV

# Appendix

# Appendix A - Network Data Egtved

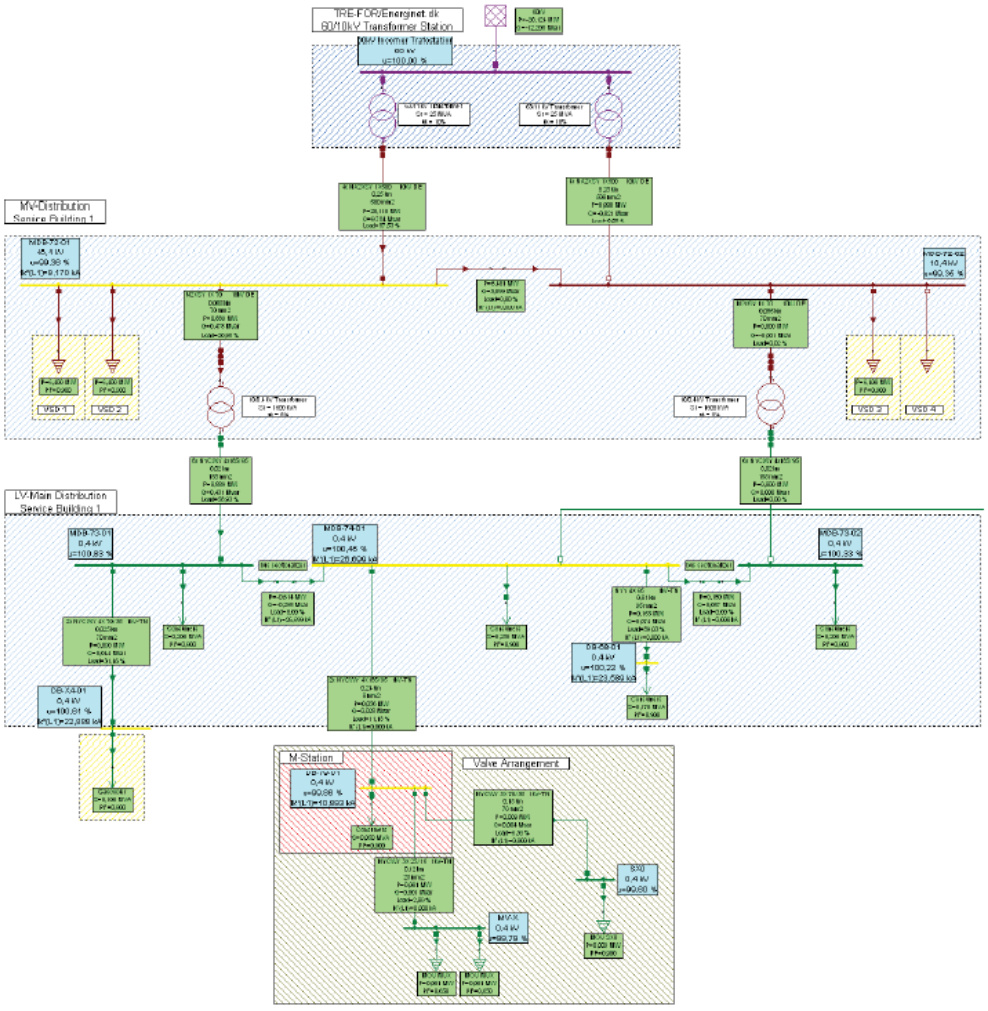


Figure 10.1: Detailed network configuration of MV and LV distribution system at Egtved gas compressor station.

Table 10.1: Cable parameters

| Label | L [km] | Ref. | D [mm$^2$] | Ref. | Z [$\frac{m\Omega}{km}$] | Ref. | C [$\frac{\mu F}{km}$] | Ref. |
|---|---|---|---|---|---|---|---|---|
| A1 | 0.02 | Fig.10.3 | 300 | Fig.10.3 | (77+j*101) | Fig.10.3 | 0.19 | [46] |
| A2 | 0.04 | Fig.10.3 | 300 | Fig.10.3 | (77+j*101) | Fig.10.3 | 0.19 | [46] |
| A3 | 0.08 | Fig.10.3 | 300 | Fig.10.3 | (77+j*101) | Fig.10.3 | 0.19 | [46] |
| A4 | 0.1 | Fig.10.3 | 300 | Fig.10.3 | (77+j*101) | Fig.10.3 | 0.19 | [46] |
| A5 | 0.085 | Fig.10.1 | 70 | Fig.10.1 | (268+j*129) | [46] | 0.19 | [46] |
| A6 | 0.085 | Fig.10.1 | 70 | Fig.10.1 | (268+j*129) | [46] | 0.19 | [46] |
| A10 | 0.2 | Fig.10.3 | 500 | Fig.10.3 | (47+j*90) | 10.3 | 0.40 | [46] |
| A20 | 0.2 | Fig.10.3 | 500 | Fig.10.3 | (47+j*90) | 10.3 | 0.40 | [46] |

Table 10.2: Transformer parameters

| Transformer | Z [p.u] | Vprim [kV] | Vsec [kV] | S base [MVA] | X/R | Ref. |
|---|---|---|---|---|---|---|
| MV Transf. | 10 | 63 | 11 | 25 | 26.6 | Data sheet TR7301 |
| *: Assump. | | | | | | |

Table 10.3: HV system data

| SCC [MVA] | X/R | V base [kV] | MVA base [MVA] | Reference |
|---|---|---|---|---|
| 423 | 12* | 60 | 100 | Fig.10.1 |
| *: Assumption | | | | |

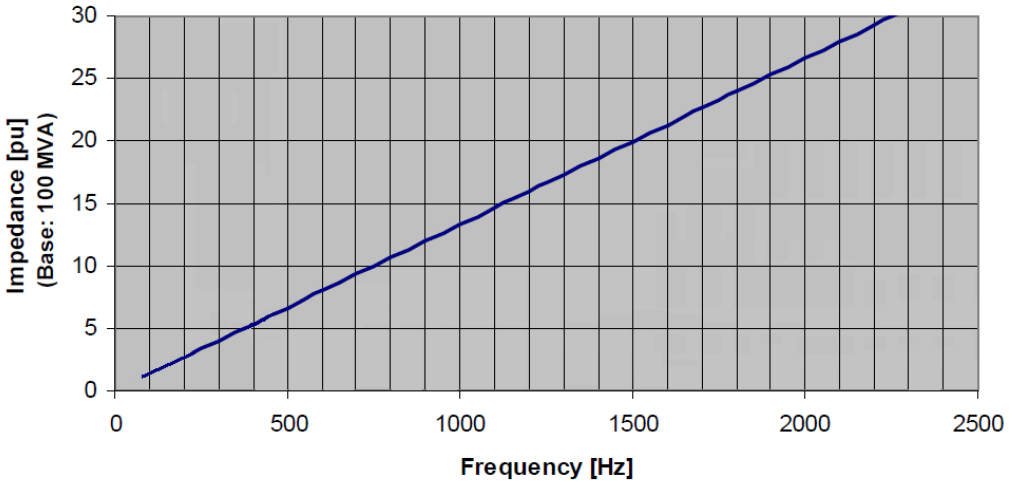


Figure 10.2: Frequency scan of GE harmonic study for EGTVED compressor station, copyright GE

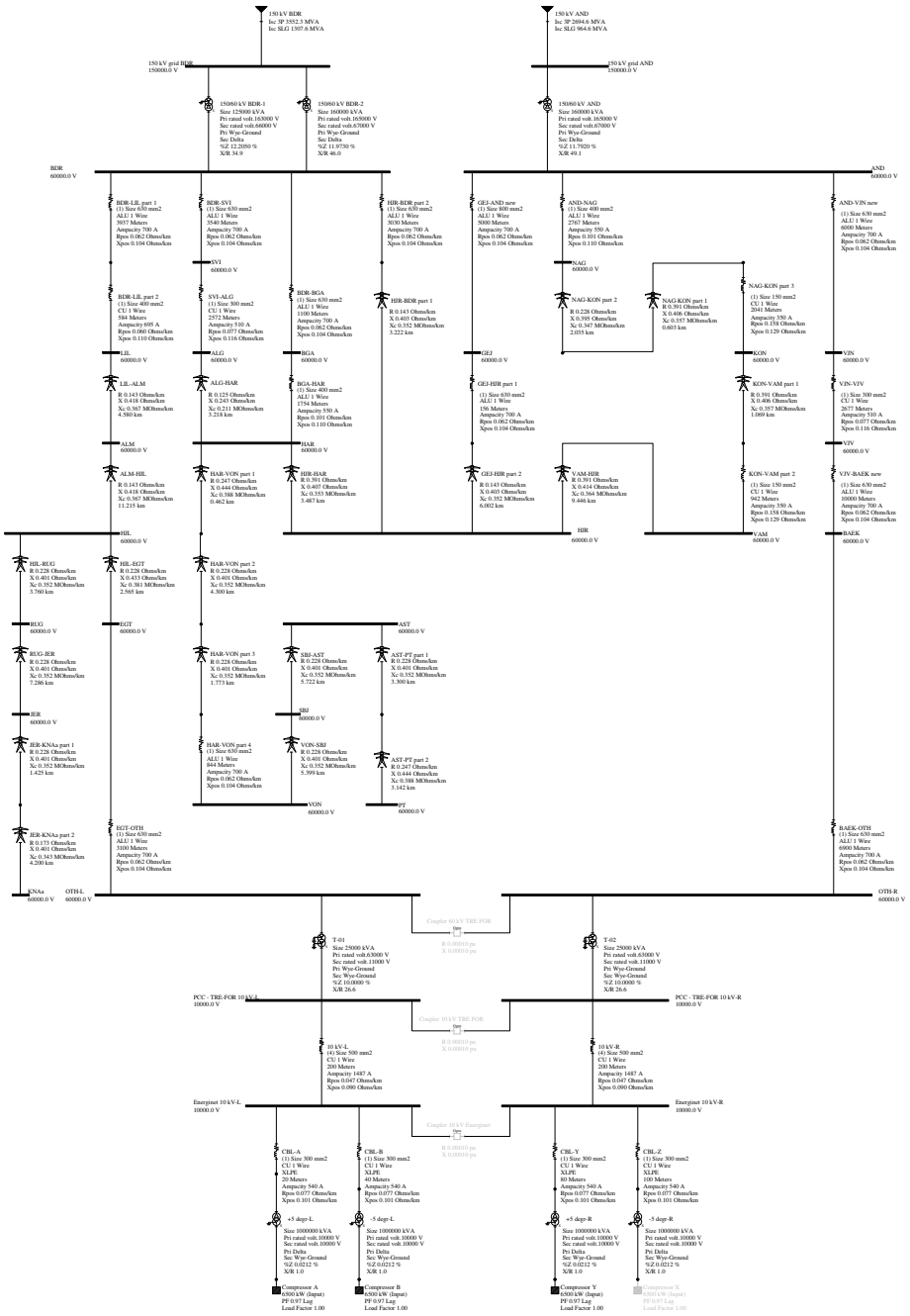

Figure 10.3: Network configuration of the feeding power system of the Egtved compressor station.

## RITZ Instrument Transformers

### TEST-CERTIFICATE TRANSFORMER

| | | | |
|---|---|---|---|
| **Customer:** | Converteam Berlin | **Order-Nr.:** | 10435969.030 |
| **Project:** | EGTVED | **Calc.Sht:** | 56689 |
| **Serial-Nr.:** | 10788277 | | **Sheet 1 of 6** |

| Three Phase Cast Resin Transformer | | | | | | E2 - C2 - F1 |
|---|---|---|---|---|---|---|
| Type: | DTR108000 | Weigth: | 18000 | kg | Insul.cl.: | F / F |
| Year: | 2012 | Capacity: | 7700 | kVA | IL : | LI75AC28 / LI60AC20 |
| Serial-Nr.: | 10788277 | Duty: | Continuous | | | |
| Protection | IP 00 | Frequency: | 50Hz | Standard: | IEC 60076 | |
| Cooling: | AN | | Vector group: | Dd(-20°)0 | Dd0 | Dd(+20°)0 |
| Ambient: | 40 °C | | Impedance voltages: | 7,61% | 7,30% | 7,35% |

| HV | Voltage (V) | Current (A) | LV | Voltage (V) | Current (A) | Capacity: (kVA) |
|---|---|---|---|---|---|---|
| | 10660 | | | | | |
| 1U-1V-1W | 10400 | 427,5 | 2U-2V-2W | 2250 | 658,6 | 2567 |
| | 10140 | | 3U-3V-3W | 2250 | 658,6 | 2567 |
| | 9880 | | 4U-4V-4W | 2250 | 658,6 | 2567 |
| | 9620 | | | | | |

**Power Frequency Test**

| | | | |
|---|---|---|---|
| HV | 28 kV | to LV1+LV2+LV3+Core | Frequency: 50Hz; t: 1min. |
| LV1 | 20 kV | to LV2+LV3+Core | Frequency: 50Hz; t: 1min. |
| LV2 | 20 kV | to LV1+LV3+Core | Frequency: 50Hz; t: 1min. |
| LV3 | 20 kV | to LV1+LV2+Core | Frequency: 50Hz; t: 1min. |

**Inter -Turn - Test**

1U-1V-1W energ. with 20,8 kV Frequency: 200 Hz t: 1min.

**Measurement of Turns-Ratio**

2U-2V-2W

| from | to | rated | meas. U | meas. V | meas. W | Phase shift: |
|---|---|---|---|---|---|---|
| 10660 V | 2250 V | 4,738 | 4,757 | 4,757 | 4,757 | -20,36° |
| 10400 V | 2250 V | 4,622 | 4,646 | 4,645 | 4,645 | -20,36° |
| 10140 V | 2250 V | 4,507 | 4,534 | 4,533 | 4,534 | -20,36° |
| 9880 V | 2250 V | 4,391 | 4,422 | 4,422 | 4,422 | -20,36° |
| 9620 V | 2250 V | 4,276 | 4,288 | 4,288 | 4,288 | -20,36° |

3U-3V-3W

| from | to | rated | meas. U | meas. V | meas. W | Phase shift: |
|---|---|---|---|---|---|---|
| 10660 V | 2250 V | 4,738 | 4,734 | 4,734 | 4,734 | 0° |
| 10400 V | 2250 V | 4,622 | 4,623 | 4,623 | 4,623 | 0° |
| 10140 V | 2250 V | 4,507 | 4,512 | 4,512 | 4,512 | 0° |
| 9880 V | 2250 V | 4,391 | 4,400 | 4,401 | 4,401 | 0° |
| 9620 V | 2250 V | 4,276 | 4,269 | 4,269 | 4,269 | 0° |

4U-4V-4W

| from | to | rated | meas. U | meas. V | meas. W | Phase shift: |
|---|---|---|---|---|---|---|
| 10660 V | 2250 V | 4,738 | 4,757 | 4,757 | 4,757 | +20,36° |
| 10400 V | 2250 V | 4,622 | 4,645 | 4,645 | 4,645 | +20,36° |
| 10140 V | 2250 V | 4,507 | 4,534 | 4,534 | 4,533 | +20,36° |
| 9880 V | 2250 V | 4,391 | 4,422 | 4,422 | 4,422 | +20,36° |
| 9620 V | 2250 V | 4,276 | 4,288 | 4,288 | 4,288 | +20,36° |

**Date:** 16. Mai 12 **Tester:** Florjanski

## RITZ Instrument Transformers

### TEST-CERTIFICATE TRANSFORMER

| | | | |
|---|---|---|---|
| **Customer:** | Converteam Berlin | **Order-Nr.:** | 10435969.030 |
| **Project:** | EGTVED | **Calc.Sht:** | 56689 |
| **Serial-Nr.:** | 10788277 | | **Sheet 2 of 6** |

**Vector-Group and Polarity Check**

| Dd(-20°)0 | Dd0 | Dd(+20°)0 |
|---|---|---|
| System top | System middle | System bottum |

Vector group checked with TETTEX Transformer Turns Ratio Meter TTR2795
Result: Phase shifting see measurment of turns ratio

**Measurement of Winding Resistance** T (°C) 20,9

| 10660 V HV - Tap | | | 10400 V HV - Tap | | |
|---|---|---|---|---|---|
| 1U-1V | 71,437 | mOhm | 1U-1V | 69,604 | mOhm |
| 1U-1W | 71,514 | mOhm | 1U-1W | 69,663 | mOhm |
| 1V-1W | 71,395 | mOhm | 1V-1W | 69,549 | mOhm |
| 10140 V HV - Tap | | | 9880 V HV - Tap | | |
| 1U-1V | 67,760 | mOhm | 1U-1V | 65,909 | mOhm |
| 1U-1W | 67,813 | mOhm | 1U-1W | 65,959 | mOhm |
| 1V-1W | 67,697 | mOhm | 1V-1W | 65,842 | mOhm |
| 9620 V HV - Tap | | | **HV coil numbers** | | |
| 1U-1V | 63,707 | mOhm | U | 10788277/1 | |
| 1U-1W | 63,748 | mOhm | V | 10788277/2 | |
| 1V-1W | 63,628 | mOhm | W | 10788277/3 | |

| LV | Dd(-20°)0 top | | LV | Dd 0 middle | |
|---|---|---|---|---|---|
| 2U-2V | 8,410 | mOhm | 3U-3V | 6,292 | mOhm |
| 2U-2W | 8,379 | mOhm | 3U-3W | 6,293 | mOhm |
| 2V-2W | 8,407 | mOhm | 3V-3W | 6,286 | mOhm |
| LV | Dd(+20°)0 bottum | | | | |
| 4U-4V | 8,364 | mOhm | | | |
| 4U-4W | 8,322 | mOhm | | | |
| 4V-4W | 8,347 | mOhm | | | |

**Date:** 16. Mai 12 **Tester:** Florjanski

## RITZ Instrument Transformers

### TEST-CERTIFICATE TRANSFORMER

| | | | |
|---|---|---|---|
| **Customer:** | Converteam Berlin | **Order-Nr.:** | 10435969.030 |
| **Project:** | EGTVED | **Calc.Sht:** | 56689 |
| **Serial-Nr.:** | 10788277 | | **Sheet 3 of 6** |

**Measurement of No-Load-Losses**

Frequency 50 Hz — Mp=Measuring Neutralpoint

| Energ. | Voltage(V) | Current(A) | Losses(W) | corr(W) | Losses(W) |
|---|---|---|---|---|---|
| 3U - Mp | 1299,6 | 2,694 | 3060 | 22 | |
| 3V - Mp | 1298,0 | 2,763 | 2195 | 24 | |
| 3W - Mp | 1300,8 | 3,638 | 3668 | 10 | |
| Average | 1299,5 | 3,032 | | | |
| Sum | | | 8923 | 56 | 8867 |

**Measurement of Short-Circuit-Losses**

2U-2V-2W 3U-3V-3W 4U-4V-4W short circuited

Frequency 50 Hz — Mp=Measuring Neutralpoir — T (°C) 20,9

| Energ. | Voltage(V) | Current(A) | Losses(W) | corr(W) | Losses(W) |
|---|---|---|---|---|---|
| 1U - Mp | 248,75 | 214,29 | 2910 | | |
| 1V - Mp | 251,45 | 214,30 | 3380 | | |
| 1W - Mp | 250,58 | 214,58 | 3140 | | |
| Average | 250,26 | 214,39 | | | |
| Sum | | | 9430 | 0 | 9430 |

**Calculations for Impedance and Short-Circuit-Losses**

| | measured | calculated for rated power | | | 7700 kVA |
|---|---|---|---|---|---|
| T (°C) | 20,9 | 20,9 | 75 | 120 | 20 |
| U sc (V) | 433,46 | 864,26 | | | |
| I sc (A) | 214,39 | 427,46 | | | |
| P sc (W) | 9430 | 37488 | 44092 | 49724 | 37381 |
| I^2*R (W) | | 34064 | 41266 | 47256 | 33945 |
| P ad (W) | | 3424 | 2826 | 2468 | 3436 |
| U r (%) | | 0,49 | 0,57 | 0,65 | 0,49 |
| U x (%) | | 8,30 | | | |
| U sc (%) | | 8,31 | 8,32 | 8,32 | 8,31 |

**Measurement of Short-Circuit-Losses**

2U-2V-2W short circuited **-20°**

Frequency 50 Hz — Mp=Measuring Neutralpoir — T (°C) 20,9

| Energ. | Voltage(V) | Current(A) | Losses(W) | corr(W) | Losses(W) |
|---|---|---|---|---|---|
| 1U - Mp | 230,01 | 72,40 | 1221 | | |
| 1V - Mp | 232,76 | 72,25 | 1263 | | |
| 1W - Mp | 233,77 | 72,63 | 1151 | | |
| Average | 232,18 | 72,43 | | | |
| Sum | | | 3635 | 0 | 3635 |

**Calculations for Impedance and Short-Circuit-Losses:**

| | measured | calculated for rated power | | | 2567 kVA |
|---|---|---|---|---|---|
| T (°C) | 20,9 | 20,9 | 75 | 120 | 20 |
| U sc (V) | 402,15 | 791,16 | | | |
| I sc (A) | 72,43 | 142,49 | | | |
| P sc (W) | 3635 | 14069 | 16175 | 18018 | 14035 |
| I^2*R (W) | | 11820 | 14319 | 16397 | 11778 |
| P ad (W) | | 2249 | 1856 | 1621 | 2257 |
| U r (%) | | 0,55 | 0,63 | 0,70 | 0,55 |
| U x (%) | | 7,59 | | | |
| U sc (%) | | 7,61 | 7,61 | 7,62 | 7,61 |

Winding resistance
HV upper system

| Tap | R(mOhm) |
|---|---|
| 1U-1V | 208,70 |
| 1U-1W | 208,76 |
| 1V-1W | 208,61 |

Date: 16. Mai 12 Tester: Florjanski

## RITZ Instrument Transformers

### TEST-CERTIFICATE TRANSFORMER

| | | | |
|---|---|---|---|
| **Customer:** | Converteam Berlin | **Order-Nr.:** | 10435969.030 |
| **Project:** | EGTVED | **Calc.Sht:** | 56689 |
| **Serial-Nr.:** | 10788277 | | **Sheet 4 of 6** |

**Measurement of Short-Circuit-Losses**

3U-3V-3W short circuited **0°**

Frequency 50 Hz Mp=Measuring Neutralpoir T (°C) 20,9

| Energ. | Voltage(V) | Current(A) | Losses(W) | corr(W) | Losses(W) |
|---|---|---|---|---|---|
| 1U - Mp | 220,93 | 72,82 | 966 | | |
| 1V - Mp | 225,49 | 72,82 | 1128 | | |
| 1W - Mp | 225,32 | 72,81 | 977 | | |
| Average | 223,91 | 72,82 | | | |
| Sum | | | 3071 | 0 | 3071 |

**Calculations for Impedance and Short-Circuit-Losses**

| | measured | calculated for rated power | | | 2567 kVA |
|---|---|---|---|---|---|
| T (°C) | 20,9 | 20,9 | 75 | 120 | 20 |
| U sc (V) | 387,83 | 758,90 | | | |
| I sc (A) | 72,82 | 142,49 | | | |
| P sc (W) | 3071 | 11759 | 13742 | 15445 | 11727 |
| I^2*R (W) | | 10456 | 12667 | 14506 | 10420 |
| P ad (W) | | 1303 | 1075 | 939 | 1307 |
| U r (%) | | 0,46 | 0,54 | 0,60 | 0,46 |
| U x (%) | | 7,28 | | | |
| U sc (%) | | 7,30 | 7,30 | 7,31 | 7,30 |

Winding resistance HV middle system

| Tap | R(mOhm) |
|---|---|
| 1U-1V | 208,94 |
| 1U-1W | 209,21 |
| 1V-1W | 208,74 |

**Measurement of Short-Circuit-Losses**

4U-4V-4W short circuited **+20°**

Frequency 50 Hz Mp=Measuring Neutralpoir T (°C) 20,9

| Energ. | Voltage(V) | Current(A) | Losses(W) | corr(W) | Losses(W) |
|---|---|---|---|---|---|
| 1U - Mp | 221,90 | 72,76 | 1074 | | |
| 1V - Mp | 227,02 | 72,64 | 1256 | | |
| 1W - Mp | 225,55 | 72,66 | 1140 | | |
| Average | 224,82 | 72,69 | | | |
| Sum | | | 3470 | 0 | 3470 |

**Calculations for Impedance and Short-Circuit-Losses**

| | measured | calculated for rated power | | | 2567 kVA |
|---|---|---|---|---|---|
| T (°C) | 20,9 | 20,9 | 75 | 120 | 20 |
| U sc (V) | 389,41 | 763,35 | | | |
| I sc (A) | 72,69 | 142,49 | | | |
| P sc (W) | 3470 | 13334 | 15552 | 17460 | 13298 |
| I^2*R (W) | | 11777 | 14267 | 16338 | 11736 |
| P ad (W) | | 1557 | 1285 | 1123 | 1563 |
| U r (%) | | 0,52 | 0,61 | 0,68 | 0,52 |
| U x (%) | | 7,32 | | | |
| U sc (%) | | 7,34 | 7,35 | 7,35 | 7,34 |

Winding resistance HV bottom system

| Tap | R(mOhm) |
|---|---|
| 1U-1V | 208,42 |
| 1U-1W | 208,64 |
| 1V-1W | 208,26 |

**Date:** 16. Mai 12 **Tester:** Florjanski

## RITZ Instrument Transformers

### TEST-CERTIFICATE TRANSFORMER

| | | | |
|---|---|---|---|
| **Customer:** | Converteam Berlin | **Order-Nr.:** | 10435969.030 |
| **Project:** | EGTVED | **Calc.Sht:** | 56689 |
| **Serial-Nr.:** | 10788277 | | **Sheet 5 of 6** |

**Measurement of Short-Circuit-Losses**

2U-2V-2W short circuited

Frequency 50 Hz Mp=Measuring Neutralpoir T (°C) 20,9

| Energ. | Voltage(V) | Current(A) | Losses(W) | corr(W) | Losses(W) |
|---|---|---|---|---|---|
| 3U - Mp | 77,75 | 335,85 | 2067 | | |
| 3V - Mp | 76,95 | 335,06 | 2192 | | |
| 3W - Mp | 77,64 | 335,04 | 1934 | | |
| Average | 77,45 | 335,32 | | | |
| Sum | | | 6193 | 0 | 6193 |

**Calculations for Impedance and Short-Circuit-Losses**

| | measured | calculated for rated power | | | 2567 kVA |
|---|---|---|---|---|---|
| T (°C) | 20,9 | 20,9 | 75 | 120 | 20 |
| U sc (V) | 134,14 | 263,47 | | | |
| I sc (A) | 335,32 | 658,61 | | | |
| P sc (W) | 6193 | 23892 | 23410 | 23591 | 23908 |
| I^2*R (W) | | 9557 | 11578 | 13258 | 9524 |
| P ad (W) | | 14334 | 11833 | 10333 | 14385 |
| U r (%) | | 0,93 | 0,91 | 0,92 | 0,93 |
| U x (%) | | 11,67 | | | |
| U sc (%) | | 11,71 | 11,71 | 11,71 | 11,71 |

**Measurement of Short-Circuit-Losses**

2U-2V-2W short circuited

Frequency 50 Hz Mp=Measuring Neutralpoir T (°C) 20,9

| Energ. | Voltage(V) | Current(A) | Losses(W) | corr(W) | Losses(W) |
|---|---|---|---|---|---|
| 4U - Mp | 93,51 | 335,83 | 2374 | | |
| 4V - Mp | 93,18 | 335,51 | 2656 | | |
| 4W - Mp | 93,97 | 335,30 | 2240 | | |
| Average | 93,55 | 335,55 | | | |
| Sum | | | 7270 | 0 | 7270 |

**Calculations for Impedance and Short-Circuit-Losses**

| | measured | calculated for rated power | | | 2567 kVA |
|---|---|---|---|---|---|
| T (°C) | 20,9 | 20,9 | 75 | 120 | 20 |
| U sc (V) | 162,04 | 318,05 | | | |
| I sc (A) | 335,55 | 658,61 | | | |
| P sc (W) | 7270 | 28008 | 27324 | 27449 | 28030 |
| I^2*R (W) | | 10894 | 13197 | 15113 | 10856 |
| P ad (W) | | 17114 | 14127 | 12337 | 17175 |
| U r (%) | | 1,09 | 1,06 | 1,07 | 1,09 |
| U x (%) | | 14,09 | | | |
| U sc (%) | | 14,14 | 14,13 | 14,13 | 14,14 |

**Date:** 16. Mai 12 **Tester:** Florjanski

**RITZ Instrument Transformers**

**TEST-CERTIFICATE TRANSFORMER**

| | | | |
|---|---|---|---|
| **Customer:** | Converteam Berlin | **Order-Nr.:** | 10435969.030 |
| **Project:** | EGTVED | **Calc.Sht:** | 56689 |
| **Serial-Nr.:** | 10788277 | | **Sheet 6 of 6** |

**Measurement of Short-Circuit-Losses**

4U-4V-4W short circuited

Frequency 50 Hz Mp=Measuring Neutralpoir T (°C) 20,9

| Energ. | Voltage(V) | Current(A) | Losses(W) | corr(W) | Losses(W) |
|---|---|---|---|---|---|
| 3U - Mp | 74,19 | 335,91 | 1889 | | |
| 3V - Mp | 73,63 | 335,03 | 2023 | | |
| 3W - Mp | 73,46 | 335,22 | 1764 | | |
| Average | 73,76 | 335,39 | | | |
| Sum | | | 5676 | 0 | 5676 |

**Calculations for Impedance and Short-Circuit-Losses**

| | measured | calculated for rated power | | | 2567 kVA |
|---|---|---|---|---|---|
| T (°C) | 20,9 | 20,9 | 75 | 120 | 20 |
| U sc (V) | 127,76 | 250,88 | | | |
| I sc (A) | 335,39 | 658,61 | | | |
| P sc (W) | 5676 | 21888 | 21743 | 22123 | 21898 |
| I^2*R (W) | | 9522 | 11535 | 13209 | 9489 |
| P ad (W) | | 12366 | 10208 | 8914 | 12410 |
| U r (%) | | 0,85 | 0,85 | 0,86 | 0,85 |
| U x (%) | | 11,12 | | | |
| U sc (%) | | 11,15 | 11,15 | 11,15 | 11,15 |

**Partial Discharge Test**

1U-1V-1W energ. for 30sec with 18720 V

| HV | Voltage(V) | t (min) | Start Value | End Value | Remarks |
|---|---|---|---|---|---|
| 1U-1V | 13520 V | 3 | < 3pC | < 3pC | |
| 1V-1W | 13520 V | 3 | < 3pC | < 3pC | |
| 1W-1U | 13520 V | 3 | < 3pC | < 3pC | |

**Check of temperature control circuits**

| Sensor | Function | Ohm |
|---|---|---|
| PTC 160 | Warning | 245 |
| PTC 180 | Tripping | 221 |
| Sensor | Set place | Ohm |
| PT100 | Winding U | 108,6 |
| PT100 | Winding V | 108,8 |
| PT100 | Winding W | 109,1 |
| PT100 | Core | 109 |

**Guaranted and measured Values**

| | guaranted | Tol. [%] | measured | Diff. [%] |
|---|---|---|---|---|
| No Load -Losses | 10750 W | 15 | 8867 W | -17,5 |
| Short-Circuit-Losses | 44000 W at 75°C | 15 | 44092 W | 0,2 |
| Short-Circuit-Losses | 50750 W at 120°C | 15 | 49724 W | -2,0 |
| Impedance | % at 75°C | +/- 10 | 8,32% | |
| Impedance Dd(-20°)0 | 8 % at 75°C | +/- 10 | 7,61% | -4,8 |
| Impedance Dd0 | 8 % at 75°C | +/- 10 | 7,30% | -8,7 |
| Impedance Dd(+20°)0 | 8 % at 75°C | +/- 10 | 7,35% | -8,2 |

**Date:** 16. Mai 12 **Tester:** Florjanski

Figure 10.4: Test protocol of transformer of VSD1 (copyright Ritz Instruments Transformer), data sheet for other VSD transformers also available

# Appendix B - Matlab Code

```
clc;clear all; close all;
%%%%%%%% Harmonic definitions %%%%%%%%%%%%%%%%%%%
hmax=49; % Harmonics of interest
step=0.1; %Suggested step size for frequency vector in harmonic
    modeling: 2Hz \cite{DasFilterEvaluation} 0.005 / 0.1001
h=[1:step:50];% linspace(1,hmax,nb)

%%%%%%%%%%System Data%%%%%%%%%%%%%%%%%
XR=12; %Assumption
SCC=423; %[MVA] %Reference: 26-441-EC-7001_1A-SCC inc LF
f=50;%[Hz]
%Power base value
S_b=100; %[MVA]
%HV side base values
Ub_HV=60; %%[kV] %Reference: 26-441-EC-7001_1A-SCC inc LF
Ib_HV=S_b/(sqrt(3)*Ub_HV)*1000; %[A]
Zb_HV=Ub_HV/(Ib_HV*sqrt(3))*1000;%[Ohm]
%LV side base values
Ub_LV=10; %[kV] %Reference: 26-441-EC-7001_1A-SCC inc LF
Ib_LV=S_b/(sqrt(3)*Ub_LV)*1000; %[A]
Zb_LV=Ub_LV/(Ib_LV*sqrt(3))*1000; %[Ohm]
%Short-circuit currents
% [x,y]=pol2cart(atan(XR),SCC/(sqrt(3)*Ub_HV));
% I3p=conj((x+i*y)*1000/Ib_HV);
% I1p=I3p*0.9; %Assumption
%System impedances
% Zp=1/I3p;
% Z0=3/I1p-2*Zp;
% Zsys=[(real(Zp)+i*imag(Zp).*h)]; %%h=3*n+-1;h=3,6,9,...
```

```
phi=atan(XR)
Zsys=S_b/(SCC)*(cos(phi)+j.*h*sin(phi))
Ysys=1./Zsys;
%60kV Transformer, Data sheet TR-73-01
S_t=25; %[MVA]
Ut_HV=63; %[kV]
Ut_LV=11; %[kV]
Zt=0.1;%[pu]
XRt=26.6;%
Rt=Zt/sqrt(XRt^2);
Xt=Rt*XRt;
Zt_p=Rt+j*Xt;
Zt_p=Zt_p*S_b/S_t*(Ut_HV/Ub_HV)^2
Zt_0=Zt_p;%Y-Y, both directly grounded -> Z0=Z, with Rg: Zt_0=Zt_p+3*Rg
    /Zb_LV;
Zt=[(real(Zt_p)+i*imag(Zt_p).*h)]; %h=3*n+-1; h=3,6,9,...
Yt=1./Zt;
% VSD Trafo
%Zvsd=1; %Warte auf Antwort von Ritzl, 0.0735
%Zvsd=[(real(Zvsd)+imag(Zvsd.*h));(real(Zvsd)+imag(Zvsd.*h))]/Zb_LV;
%Cables, Reference: nexans.de
%A1-3
Z_a1=(0.077+j*0.101)*0.02;% [Ohm] l=20m
Z_a1=[(real(Z_a1)+i*imag(Z_a1.*h))]/Zb_LV; %h=3*n+-1; h=3,6,9,...
Z_a2=2*Z_a1;%l=40m
Z_a3=2*Z_a2;%l=80m
C_a1=0.19*0.02;%[uF]
C_a2=C_a1*2;
C_a3=C_a2*2;
%A5-A6
C_a5=0.19*0.085;%[uF]
C_a6=C_a5;
Xc_12345=1/(2*pi*f*(C_a1+C_a2+C_a3+C_a5+C_a6)*1e-6);
Zc_12345=[-j*Xc_12345./h]/Zb_LV;
%A10, A20
Z_a10=(0.047+j*0.09)*0.2; %[Ohm], l=20m
Z_a10=[(real(Z_a10)+i*imag(Z_a10.*h))]/Zb_LV;
Z_a20=Z_a10;
```

```
C_a10=0.4*0.2;%[uF]
C_a20=C_a10;
Xc_1020=1/(2*pi*f*(C_a10+C_a20)*1e-6);
Zc_1020=[-j*Xc_1020./h]/Zb_LV; %Impedance of cabel capacitance A10,A20

%Impedances. for Impedance scan (triplen are handeled as positive
    sequence):Z(1,:), for harmonic distortion calculation (triplen
    handeled as zero sequences): Z(2,:)%
%Impedance as seen from harmonic source, without filters
Zup2=Zc_1020.*(Zt+Zsys)./(Zc_1020+(Zt+Zsys));
Zup1=Z_a10.*Z_a20./(Z_a10+Z_a20)+Zup2;
Zeq=(Zup1.*Zc_12345)./(Zup1+Zc_12345);
Yeq=1./Zeq;
%Plot
figure
plot(h,abs(Zeq(1,:))*Zb_LV)
xlabel('Harmonic order h')
ylabel('Impedance [p.u.], S_B=100MVA')
hold on
x1=7;
y1=3.2;
x2=195;
y2=94.2;
xnom=216.4; %=50
ynom=93.8; %=30
x1graph=50/xnom*x1
y1graph=30/ynom*y1
x2graph=50/xnom*x2
y2graph=30/ynom*y2
plot([x1graph x2graph], [y1graph y2graph],:)
grid on
legend('Matlab Implementation','Harmonic study GE','Location','
    NorthWest')
XLIM([0 50])
YLIM([0 30])
saveas(gcf,'HarmonicImplementationFS_withoutFilter.png')
```

src/harmonicimplementation_withoutFilter.m

```
clc;clear all; close all;
%%%%%%%% Harmonic definitions %%%%%%%%%%%%%%%%%%%
hmax=49; % Harmonics of interest
step=0.1; %Suggested step size for frequency vector in harmonic
    modeling: 2Hz \cite{DasFilterEvaluation} 0.005 / 0.1001
h=[1:step:50];% linspace(1,hmax,nb)

%%%%%%%%%System Data%%%%%%%%%%%%%%%%
XR=12; %Assumption
SCC=423; %[MVA] %Reference: 26-441-EC-7001_1A-SCC inc LF
f=50;%[Hz]
%Power base value
S_b=100; %[MVA]
%HV side base values
Ub_HV=60; %%[kV] %Reference: 26-441-EC-7001_1A-SCC inc LF
Ib_HV=S_b/(sqrt(3)*Ub_HV)*1000; %[A]
Zb_HV=Ub_HV/(Ib_HV*sqrt(3))*1000;%[Ohm]
%LV side base values
Ub_LV=10; %[kV] %Reference: 26-441-EC-7001_1A-SCC inc LF
Ib_LV=S_b/(sqrt(3)*Ub_LV)*1000; %[A]
Zb_LV=Ub_LV/(Ib_LV*sqrt(3))*1000; %[Ohm]
%Short-circuit currents
% [x,y]=pol2cart(atan(XR),SCC/(sqrt(3)*Ub_HV));
% I3p=conj((x+i*y)*1000/Ib_HV);
% I1p=I3p*0.9; %Assumption
%System impedances
% Zp=1/I3p;
% Z0=3/I1p-2*Zp;
% Zsys=[(real(Zp)+i*imag(Zp).*h)]; %%h=3*n+-1;h=3,6,9,...
phi=atan(XR)
Zsys=S_b/(SCC)*(cos(phi)+j.*h*sin(phi))
Ysys=1./Zsys;
%60kV Transformer, Data sheet TR-73-01
S_t=25; %[MVA]
Ut_HV=63; %[kV]
Ut_LV=11; %[kV]
Zt=0.1;%[pu]
XRt=26.6;%
```

```
38 Rt=Zt/sqrt(XRt^2);
   Xt=Rt*XRt;
40 Zt_p=Rt+j*Xt;
   Zt_p=Zt_p*S_b/S_t*(Ut_HV/Ub_HV)^2
42 Zt_0=Zt_p;%Y-Y, both directly grounded -> Z0=Z, with Rg: Zt_0=Zt_p+3*Rg
       /Zb_LV;
   Zt=[(real(Zt_p)+i*imag(Zt_p).*h)]; %h=3*n+-1; h=3,6,9,...
44 Yt=1./Zt;
   % VSD Trafo
46 %Zvsd=1; %Warte auf Antwort von Ritzl, 0.0735
   %Zvsd=[(real(Zvsd)+imag(Zvsd.*h));(real(Zvsd)+imag(Zvsd.*h))]/Zb_LV;
48 %Cables, Reference: nexans.de
   %A1-3
50 Z_a1=(0.077+j*0.101)*0.02;% [Ohm] l=20m
   Z_a1=[(real(Z_a1)+i*imag(Z_a1.*h))]/Zb_LV; %h=3*n+-1; h=3,6,9,...
52 Z_a2=2*Z_a1;%l=40m
   Z_a3=2*Z_a2;%l=80m
54 C_a1=0.19*0.02;%[uF]
   C_a2=C_a1*2;
56 C_a3=C_a2*2;
   %A5-A6
58 C_a5=0.19*0.085;%[uF]
   C_a6=C_a5;
60 Xc_12345=1/(2*pi*f*(C_a1+C_a2+C_a3+C_a5+C_a6)*1e-6);
   Zc_12345=[-j*Xc_12345./h]/Zb_LV;
62 %A10, A20
   Z_a10=(0.047+j*0.09)*0.2; %[Ohm], l=20m
64 Z_a10=[(real(Z_a10)+i*imag(Z_a10.*h))]/Zb_LV;
   Z_a20=Z_a10;
66 C_a10=0.4*0.2;%[uF]
   C_a20=C_a10;
68 Xc_1020=1/(2*pi*f*(C_a10+C_a20)*1e-6);
   Zc_1020=[-j*Xc_1020./h]/Zb_LV; %Impedance of cabel capacitance A10,A20
70
   %Filter1: STF
72 h1=3; %ftuned
   Qc1=8.8; %[MVAr]
74 Q1=380;  %Qualitz factor, for STF 30<Q<100
```

```
Xc_1=Ub_LV^2/Qc1
Xl_1=Xc_1/h1^2
Xn1=sqrt(Xl_1*Xc_1);
R1=Xn1/Q1 %[Ohm]
L1=Xl_1/(2*pi*f)%[H]
C1=(Xc_1*(2*pi*f))^-1%[F]
%Filter2: HP2nd
h2=5; %ftuned
Qc2=18.9; %[MVAr]
Q2=23;  %Qualitz factor, for STF 30<Q<100
Xc_2=Ub_LV^2/Qc2
Xl_2=Xc_2/h2^2
Xn2=sqrt(Xl_2*Xc_2);
R2=Xn2*Q2 %[Ohm]
L2=Xl_2/(2*pi*f)%[H]
C2=(Xc_2*(2*pi*f))^-1%[F]
%Filter3: HP2nd
h3=7; %ftuned
Qc3=13.9; %[MVAr]
Q3=9;  %Qualitz factor, for STF 30<Q<100
Xc_3=Ub_LV^2/Qc3
Xl_3=Xc_3/h3^2
Xn3=sqrt(Xl_3*Xc_3);
R3=Xn3*Q3 %[Ohm]
L3=Xl_3/(2*pi*f)%[H]
C3=(Xc_3*(2*pi*f))^-1%[F]
%Filter impedance
Zf_1=(R1+i*(Xl_1.*h-Xc_1./h));
Zf_2=1./(1/R2+1./(i*Xl_2.*h))-(i*Xc_2./h);
Zf_3=1./(1/R3+1./(i*Xl_3.*h))-(i*Xc_3./h);
Yf_1=1./Zf_1;
Yf_2=1./Zf_2;
Yf_3=1./Zf_3;
Yf=Yf_1+Yf_2+Yf_3;
Zf=[1./Yf];
% Filter branches plots in Ohm
plot(h,abs(Zf_1))
xlim([1  49])
```

```
saveas(gcf,'Zf1.png')
figure
plot(h,angle(Zf_1)*180/pi)
xlim([1 49])
saveas(gcf,'Zf1_ang.png')
figure
plot(h,abs(Zf_2))
xlim([1 49])
saveas(gcf,'Zf2.png')
figure
plot(h,angle(Zf_2)*180/pi)
xlim([1 49])
saveas(gcf,'Zf2_ang.png')
figure
plot(h,abs(Zf_3))
xlim([1 49])
saveas(gcf,'Zf3.png')
figure
plot(h,angle(Zf_3)*180/pi)
xlim([1 49])
saveas(gcf,'Zf3_ang.png')
%Filer in total
plot(real(Zf),imag(Zf))
xlim([0 25])
ylim([-40 40])
saveas(gcf,'Zf_locus.png')
figure
plot3(real(Zf(1,:)),imag(Zf(1,:)),h)
grid on
xlim([0 25])
ylim([-40 40])
saveas(gcf,'Zf_3Dlocus.png')
figure
plot(h,abs(Zf))
xlim([1 49])
saveas(gcf,'Zf.png')
figure
plot(h,angle(Zf)*180/pi)
```

```
saveas(gcf,'Zf_ang.png')
%pu conversion
Z_f=Zf/Zb_LV;
Yf=1./Zf;
Yf_0=zeros(1,length(Yf));

%Impedances. for Impedance scan (triplen are handeled as positive
    sequence):Z(1,:), for harmonic distortion calculation (triplen
    handeled as zero sequences): Z(2,:)%
%Impedance as seen from harmonic source, with filters
Zup2=Zc_1020.*(Zt+Zsys)./(Zc_1020+(Zt+Zsys));
Zup1=Z_a10.*Z_a20./(Z_a10+Z_a20)+Zup2;
Zeq_f=1./(1./Zup1+1./Zc_12345+1./Zf);
%Impedance scan
plot(h,abs(Zeq_f(1,:))*Zb_LV)
xlabel('Harmonic order h')
ylabel('Impedance [p.u.], S_B=100MVA')
grid on
saveas(gcf,'HarmonicImplementationFS_withFilter.png')
```

src/harmonicimplementation_withFilter.m

```
%Multi-Winding Transformers
clc;clear all;close all;
set(0,'DefaultAxesLineStyleOrder',{'-',':','--','-.','-+','--o',':*','
    -.x'})
set(0,'DefaultAxesColorOrder',[0.4,0.4,0.4])

stor=0;
phia=0/180*pi+stor;
phib=-120/180*pi;
phic=120/180*pi-stor;
h=[1,5,11,17,23,29,35]

%3 winding transformer -> 12-pulse
shift=25/180*pi:1/180*pi:30/180*pi
shift=-1*shift;
for m=1:length(shift)
for k=1:length(h)
n=h(k);
%Phase currents in Cartesian coordinates
%First 6-pulse rectifier with shift delta
[x,y]=pol2cart((phia+shift(m))*n,1);
I_1a=x+i*y;
[x,y]=pol2cart((phib+shift(m))*n,1);
I_1b=x+i*y;
[x,y]=pol2cart((phic+shift(m))*n,1);
I_1c=x+i*y;
%Second 6-pulse rectifier without shift
[x,y]=pol2cart(phia*n,1);
I_2a=x+i*y;
[x,y]=pol2cart(phib*n,1);
I_2b=x+i*y;
[x,y]=pol2cart(phic*n,1);
I_2c=x+i*y;

%3-phase currents of first and second rectifier
I_abc_1_1=[I_1a;I_1b;I_1c];
I_abc_2_1=[I_2a;I_2b;I_2c];

```

```
%Transformation matrices, alpha
T=1/sqrt(3)*[1,-1,0;0,1,-1;-1,0,1];
T_e=1/3*[2,-1,-1;-1,2,-1;-1,-1,2];
alpha=1/2;

%Refered primary currents
I_ABC_1=alpha*T*I_abc_1_1;
I_ABC_2=alpha*T_e*I_abc_2_1;
%Primary current
I_ABC=I_ABC_1+I_ABC_2;
%Absolut value of I_A
I_A_abs(k,m)=abs(I_ABC(1,1))
end
%I_A(:,m)=[I_A_abs(:,m)]
end
plot(shift/pi*180,I_A_abs,'MarkerSize',3)
legend('fund.','5^{th}/7^{th}','11^{th}/13^{th}','17^{th}/19^{th}','
    23^{th}/25^{th}','29^{th}/31^{th}','35^{th}/37^{th}')
ylabel('Harmonic Amplitude [p.u]')
xlabel('\delta\prime [°]')
saveas(gcf,'12pulsePhaseShift.eps', 'psc2');
figure;

clear I_A_abs;
%4 winding -> 18-pulse Dd0
shift=17/180*pi:0.3/180*pi:20/180*pi
shift=-1*shift;
for m=1:length(shift)
for k=1:length(h)
n=h(k);
%Phase currents in Cartesian coordinates
%First 6-pulse rectifier with shift delta, Dd(-20)0
[x,y]=pol2cart((phia+shift(m))*n,1);
I_1a=x+i*y;
[x,y]=pol2cart((phib+shift(m))*n,1);
I_1b=x+i*y;
[x,y]=pol2cart((phic+shift(m))*n,1);
I_1c=x+i*y;
```

```
%Second 6-pulse rectifier without shift Dd0
[x,y]=pol2cart(phia*n,1);
I_2a=x+i*y;
[x,y]=pol2cart(phib*n,1);
I_2b=x+i*y;
[x,y]=pol2cart(phic*n,1);
I_2c=x+i*y;
%Third 6-pulse rectifier with shift delta Dd(+20)0
[x,y]=pol2cart((phia-shift(m))*n,1);
I_3a=x+i*y;
[x,y]=pol2cart((phib-shift(m))*n,1);
I_3b=x+i*y;
[x,y]=pol2cart((phic-shift(m))*n,1);
I_3c=x+i*y;


%3-phase currents of first, second and third rectifier
I_abc_1=[I_1a;I_1b;I_1c];
I_abc_2=[I_2a;I_2b;I_2c];
I_abc_3=[I_3a;I_3b;I_3c];

%-20°
[x,y]=pol2cart(-20/180*pi,1)
m20degr=x+i*y;
%20°
[x,y]=pol2cart(20/180*pi,1)
p20degr=x+i*y;

I_abc_1=I_abc_1*m20degr
I_abc_3=I_abc_3*p20degr

%Transformation matrices, alpha
%T=1/sqrt(3)*[1,-1,0;0,1,-1;-1,0,1];
T=1/sqrt(3)*[1,0,-1;-1,1,0;0,-1,1];
T_e=1/3*[2,-1,-1;-1,2,-1;-1,-1,2];
alpha=1/3;

%Refered primary currents
```

```
113 I_ABC_1=alpha*T_e*I_abc_1;
    I_ABC_2=alpha*T_e*I_abc_2;
115 I_ABC_3=alpha*T_e*I_abc_3;


117

    %I_ABC_1=I_ABC_1*m20degr
119 %I_ABC_3=I_ABC_3*p20degr

121 %Primary current
    I_ABC=I_ABC_1+I_ABC_2+I_ABC_3;
123 %Absolut value of I_A
    I_A_abs(k,m)=abs(I_ABC(1,1))
125 end
    %I_A(:,m)=[I_A_abs(:,m)]
127 end
    plot(shift/pi*180,I_A_abs,'MarkerSize',3)
129 legend('fund.','5^{th}/7^{th}','11^{th}/13^{th}','17^{th}/19^{th}','
        23^{th}/25^{th}','29^{th}/31^{th}','35^{th}/37^{th}')
    ylabel('Harmonic Amplitude [p.u]')
131 xlabel('\delta\prime [°]')
    saveas(gcf,'18pulsePhaseShift.eps', 'psc2');
```

src/multiwindingtransformer_for.m

```
clc;clear all; close all;
nb=1e5; %number of points

%%%%%%%%%%System Data%%%%%%%%%%%%%%%%
hmax=49; %Harmonics of interest
step=0.1; %Suggested step size for frequency vector in harmonic
    modeling: 2Hz \cite{DasFilterEvaluation}
h=[1:step:50];%linspace(1,hmax,nb)
XR=20;
SCC=10000; %[MVA]
f=50;%[Hz]
%Harmonic source
ispec=[100 2.6 1.9 2.7 17.5 4.2 11 3.9 1 1.3 4.5 3.3 2.9 1.7 2.5 1.7
    1.5 1]/100;
%Transformer
St=190; %[MVA]
U_HV=400; %[kV]
U_LV=33; %[kV]
Zt=0.38+i*11.995; %[%]
Rg=476.3; %[Ohm]
%Filters
%Filter1: STF
h1=3; %ftuned
Qc1=8.9; %[MVAr]
Q1=400;  %Qualitz factor, for STF 30<Q<100
Xc_1=U_LV^2/Qc1;
Xl_1=Xc_1/h1^2;
Xn1=sqrt(Xl_1*Xc_1);
R1=Xn1/Q1; %[Ohm]
L1=Xl_1/(2*pi*f);%[H]
C1=(Xc_1*(2*pi*f))^-1;%[F]
%Filter2: HP2nd
h2=4.3; %ftuned
Qc2=19.2; %[MVAr]
Q2=22.8;  %Qualitz factor, for STF 30<Q<100
Xc_2=U_LV^2/Qc2;
Xl_2=Xc_2/h2^2;
Xn2=sqrt(Xl_2*Xc_2);
```

```
R2=Xn2*Q2; %[Ohm]
L2=Xl_2/(2*pi*f);%[H]
C2=(Xc_2*(2*pi*f))^-1;%[F]
%Filter3: HP2nd
h3=6.5; %ftuned
Qc3=14.4; %[MVAr]
Q3=8.6;  %Qualitz factor, for STF 30<Q<100
Xc_3=U_LV^2/Qc3;
Xl_3=Xc_3/h3^2;
Xn3=sqrt(Xl_3*Xc_3);
R3=Xn3*Q3; %[Ohm]
L3=Xl_3/(2*pi*f);%[H]
C3=(Xc_3*(2*pi*f))^-1;%[F]

%%%%%%%%%%p.u. conversion%%%%%%%%%%%%%%
%Power base value
S_b=100; %[MVA]
%HV side base values
Ub_HV=U_HV; %%[kV]
Ib_HV=S_b/(sqrt(3)*Ub_HV)*1000; %[A]
Zb_HV=Ub_HV/(Ib_HV*sqrt(3))*1000;%[Ohm]
%LV side base values
Ub_LV=U_LV; %[kV]
Ib_LV=S_b/(sqrt(3)*Ub_LV)*1000; %[A]
Zb_LV=Ub_LV/(Ib_LV*sqrt(3))*1000; %[Ohm]

%Short-circuit currents
[x,y]=pol2cart(atan(XR),SCC/(sqrt(3)*Ub_HV));
I3p=conj((x+i*y)*1000/Ib_HV);
I1p=I3p*0.9;

%System impedances
Zp=1/I3p;
Z0=3/I1p-2*Zp; %Verstehe ich nicht...
Zsys=[real(Zp)+i*imag(Zp).*h;real(Z0)+i*imag(Z0).*h]; %%h=3*n+-1;h
    =3,6,9,...
Ysys=Zsys.^-1;
```

```
%Transformer impedance
Zt_p=Zt/100*S_b/St;
Zt_n=Zt_p;
Zt_0=Zt_p+3*Rg/Zb_LV;
Zt=[real(Zt_p)+i*imag(Zt_p).*h;real(Zt_0)+i*imag(Zt_0).*h]; %h=3*n+-1;
    h=3,6,9,...
Yt=Zt.^-1;

%Filter impedance
Zf_1=(R1+i*(Xl_1.*h-Xc_1./h));
Zf_2=1./(1/R2+1./(i*Xl_2.*h))-(i*Xc_2./h);
Zf_3=1./(1/R3+1./(i*Xl_3.*h))-(i*Xc_3./h);
Yf_1=1./Zf_1;
Yf_2=1./Zf_2;
Yf_3=1./Zf_3;
Yf=Yf_1+Yf_2+Yf_3;
Zf=1./Yf;

%Filter branches plots in Ohm
plot(h,abs(Zf_1))
xlim([1 49])
saveas(gcf,'Zf1.png')
figure
plot(h,angle(Zf_1)*180/pi)
xlim([1 49])
saveas(gcf,'Zf1_ang.png')
figure
plot(h,abs(Zf_2))
xlim([1 49])
saveas(gcf,'Zf2.png')
figure
plot(h,angle(Zf_2)*180/pi)
xlim([1 49])
saveas(gcf,'Zf2_ang.png')
figure
plot(h,abs(Zf_3))
xlim([1 49])
saveas(gcf,'Zf3.png')
```

```
figure
plot(h,angle(Zf_3)*180/pi)
xlim([1 49])
saveas(gcf,'Zf3_ang.png')
%Filer in total
plot(real(Zf),imag(Zf))
xlim([0 25])
ylim([-40 40])
saveas(gcf,'Zf_locus.png')
figure
plot3(real(Zf),imag(Zf),h)
grid on
xlim([0 25])
ylim([-40 40])
saveas(gcf,'Zf_3Dlocus.png')
figure
plot(h,abs(Zf))
xlim([1 49])
saveas(gcf,'Zf.png')
figure
plot(h,angle(Zf)*180/pi)
saveas(gcf,'Zf_ang.png')
%pu conversion
Zf=Zf/Zb_LV;
Yf=1./Zf;


%Impedances. for Impedance scan (triplen are handeled as positive
    sequence):Z(1,:), for harmonic distortion calculation (triplen
    handeled as zero sequences): Z(2,:)%
%Impedance from 33kV Bus, series connection of Zsys and Zt
Z33=[Zsys(1,:)+Zt(1,:);Zsys(2,:)+Zt(2,:)];
Y33=1./Z33;
%Impedance from harmonic source, parallel connection of Z33 and Zf
Yeq=Y33+[Yf;Yf];
Zeq=1./Yeq;

SCC33=1/conj(Z33(1,1));
```

```
XR33=tan(angle(SCC33));
148
150 %Impedance scan
figure
152 plot(h,abs(Zeq(1,:))*Zb_LV)
hold on
154 plot(h,abs(Z33(1,:))*Zb_LV)
xlim([1 19])
156 saveas(gcf,'Z33_scan.png')

158 %Time domain harmonic current waveform
wt=[0:0.0000001:1];
160 i=zeros(1,length(wt));
for n=1:length(ispec)
162     for k=1:length(wt)
        i(k)=sin(2*pi*n*wt(k))*ispec(n)+i(k);
164     end
end
166 figure
plot(wt,i)
168 saveas(gcf,'Currentwaveform.png')

170 %Harmonic distortion results
ispec=ispec(1,2:end);
172 HD=[transp(ispec),zeros(length(ispec),1),zeros(length(ispec),1),zeros(
    length(ispec),1),zeros(length(ispec),1)];
Iconv=1000 %[A] provided from a load flow study
174 ispec=ispec*Iconv/Ib_LV;
h=[1:1/step:length(h)];
176 for k=2:length(ispec)
    if mod(k,3)==0
178         s=2
    else
180         s=1
    end
182     HD(k,2:end)=[abs(Zeq(s,h(k)))*ispec(k),abs(Y33(s,h(k)))*abs(Zeq(s,h
        (k)))*ispec(k),abs(Yf(h(k)))*abs(Zeq(s,h(k)))*ispec(k),abs(Zsys
```

```
        (s,h(k)))*abs(Yf(h(k)))*abs(Zeq(s,h(k)))*ispec(k)];
end
HD
[h;Zeq]
```

src/ex10_11.m